Pacific Northwest
NATIONAL LABORATORY

PNNL-38953, Rev. 0
EWG-RPT-058, Rev. 0

Glass Property-Composition Models Update for use in Direct Feed High-Level Waste Flowsheet Development: EWG3.0

February 2026

Xiaonan Lu
John D Vienna
Pavel Ferkl
Dongsang Kim
José Marcial
Jincheng Bai
Dewei Wang
Jarrod V Crum
James J Neeway
Nicholas A Lumetta

U.S. DEPARTMENT of ENERGY

Prepared for the U.S. Department of Energy
under Contract DE-AC05-76RL01830

DISCLAIMER

PACIFIC NORTHWEST NATIONAL LABORATORY
operated by
BATTELLE
for the
UNITED STATES DEPARTMENT OF ENERGY
under Contract DE-AC05-76RL01830

Printed in the United States of America

Available to DOE and DOE contractors from
the Office of Scientific and Technical Information,
P.O. Box 62, Oak Ridge, TN 37831-0062
www.osti.gov
ph: (865) 576-8401
fax: (865) 576-5728
email: reports@osti.gov

Available to the public from the National Technical Information Service
5301 Shawnee Rd., Alexandria, VA 22312
ph: (800) 553-NTIS (6847)
or (703) 605-6000
email: info@ntis.gov
Online ordering: http://www.ntis.gov

PNNL-38953, Rev. 0
EWG-RPT-058, Rev. 0

Glass Property-Composition Models Update for use in Direct Feed High-Level Waste Flowsheet Development: EWG3.0

February 2026

Xiaonan Lu
John D Vienna
Pavel Ferkl
Dongsang Kim
José Marcial
Jincheng Bai
Dewei Wang
Jarrod V Crum
James J Neeway
Nicholas A Lumetta

Prepared for
the U.S. Department of Energy
under Contract DE-AC05-76RL01830

Pacific Northwest National Laboratory
Richland, Washington 99354

Abstract

A set of preliminary glass property models and constraints were developed and augmented by models from literature for use in design of direct feed high-level waste glasses for flowsheet evaluation, testing, and design of the High-Level Waste Facility at the Waste Treatment and Immobilization Plant located at the Hanford site. These models and constraints are meant to be used as a placeholder while glass property-composition data gaps are filled and final plant operating models are developed. This report describes the motivation and intended use of the models, the compilation of data, model fitting and selection, and methods to apply the models and constraints in glass design and offers example calculations demonstrating their intended use.

Quality Assurance

This work was performed in accordance with the Pacific Northwest National Laboratory (PNNL) Nuclear Quality Assurance Program (NQAP). The NQAP complies with DOE Order 414.1D, *Quality Assurance*, and 10 CFR 830, *Nuclear Safety Management*, Subpart A, *Quality Assurance Requirements*. The NQAP uses NQA-1-2012, *Quality Assurance Requirements for Nuclear Facility Application*, as its consensus standard and NQA-1-2012, Subpart 4.2.1, as the basis for its graded approach to quality.

The NQAP works in conjunction with PNNL's laboratory-level Quality Management Program, which is based on the requirements as defined in DOE Order 414.1D and 10 CFR 830, Subpart A.

The work of this report was performed to a technology readiness level of 6 and is appropriate for nuclear facility design activities within the constraints identified in this report.

Acknowledgments

The authors gratefully acknowledge the financial support provided by the U.S. Department of Energy Hanford Field Office, Waste Treatment and Immobilization Plant Project, with technical oversight by AA Kruger. The following Pacific Northwest National Laboratory staff members are acknowledged for their contributions: T Jin for technical review of the report; CE Curry and M Diaz Acevedo for assistance with the data reviewing; BJ Riley for making Figures 1.1 and 3.1; M Willburn for technical editing of the report; DB MacPherson, AM Sachs, CE Charron, and CA Martin for quality assurance and programmatic support during the conduct of this work; RL Russell, V Gervasio, and WC Eaton for project management. We thank DL Bauer, SM Barnes, R Peters, and S Voss from Bechtel National Inc., and GV Smith and AJ Schubick from Hanford Tank Waste Operations & Closure for helpful discussions and inputs.

Acronyms and Abbreviations

3TS	three times saturation (method)
Alt-18	(Analysis of Alternatives) alternative 18
APPS	Aspen Process Performance Simulation (WTP steady-state flowsheet model)
AMPS	Advanced Modular Pretreatment System
BOF	balance of facilities
CCC	canister centerline cooling
CCP	Calculation Control Package
CI	confidence interval
DFHLW	Direct Feed High-Level Waste
DOE	U.S. Department of Energy
DWPF	Defense Waste Processing Facility
EA	Environmental Assessment (glass)
EC	electrical conductivity
ELG	enhanced LAW glass (models)
EWG	enhanced waste glass
EWG2	second iteration of enhanced waste glass
GFC	glass-forming chemical
HFO	Hanford Field Office
HLW	high-level waste
INEEL	Idaho National Engineering and Environmental Laboratory
INL	Idaho National Laboratory
LAB	WTP Laboratory
LAW	low-activity waste
MC	Monte Carlo
MdAE	median average error
MFPV	melter feed preparation vessel
MV	model validity
NC	normalized concentration by 7-day PCT
NC_{Ave}	average normalized concentration
NL	normalized loss by 7-day PCT
NP	nepheline
NQAP	Nuclear Quality Assurance Program
PCT	product consistency test
PERT	Program Evaluation and Review Techniques
PNNL	Pacific Northwest National Laboratory
PQM	partial quadratic mixture

PT	pretreatment
PTHLW	pretreated high-level waste
QA	quality assurance
RMSE	root mean squared error
SD	standard deviation
SRNL	Savannah River National Laboratory
SUCI	simultaneous upper confidence interval
TCLP	toxicity characteristic leaching procedure
TOC	total organic carbon
TSCR	Tank Side Cesium Removal
VFT	Vogel-Fulcher-Tammann (viscosity-temperature equation)
VSL	Vitreous State Laboratory
WL	waste oxide loading
WTP	Waste Treatment and Immobilization Plant

Symbols

A	preexponential term in VFT viscosity- or EC-temperature equation
B	temperature effect term in VFT viscosity- or EC-temperature equation
B_i	temperature effect coefficient for i^{th} component viscosity or EC model
C_{950}-Sp	a spinel volume percent concentration at 950°C
c_α	concentration of element α in PCT test solution (α = B, Na, Li)
C_{Cd}	calculated Cd release by TCLP
C_{Cr}	calculated Cr release by TCLP
c_{ele}	measured TCLP elemental release in the unit of mg/L
$c_{ij}^{oxide\ in\ waste}$	concentration of the i^{th} component measured in the j^{th} waste (g/g)
C_V	calculated V release by TCLP
f_α	concentration of element α in glass (α = B, Na, Li)
f_{ele}	mass fraction of the element in glass
g_F	concentration of F in glass
g_i	concentration of i^{th} component in glass, mass basis
g_{P2O5}	concentration of P_2O_5 in glass
g_{SO3}	concentration of SO_3 in glass
g_{ThO2}	concentration of ThO_2 in glass
g_{ZrO2}	concentration of ZrO_2 in glass
$g_{ik}^{oxide\ in\ GFC}$	mass fraction of the i^{th} oxide in the k^{th} GFC (g/g)
k_{neck}	K-3 refractory neck corrosion extent
k_{bubb}	K-3 refractory neck corrosion at 1208°C using bubbled method
k_i	the i^{th} component coefficient for ln[k]
k_{ii}	the i^{th} component quadratic coefficient for ln[k]
k_{ij}	the i^{th} and j^{th} components crossproduct coefficient for ln[k]
k_{stat}	K-3 refractory neck corrosion at 1200°C using static method
k_{s1200}	an offset coefficient for data measured under static conditions at 1200 °C for 6 or 7 d
$k_{s1150\text{-}3}$	an offset coefficient for data measured under static conditions at 1150 °C for 3 d
$k_{s1150\text{-}7}$	an offset coefficient for data measured under static conditions at 1150 °C for 7 d
$k_{s1200\text{-}3}$	an offset coefficient for data measured under static conditions at 1200 °C for 3 d
L_α^L	lower limit on transformed property α [$t(P_\alpha)$]
L_α^U	upper limit on transformed property α [$t(P_\alpha)$]
M_j^{waste}	mass of the j^{th} waste (kg)
M_k^{GFC}	mass of the k^{th} GFC (kg)
M_G	glass mass

$M_{GFC,\alpha}$	mass of the GFC α
M_{WOx}	ratio of mass of waste oxides (g) per volume of waste (L) in a campaign
n	number of datapoints used to fit a model
n^{wastes}	number of wastes mixed
n^{GFCs}	number of GFCs added
N_{ALK}	normalized alkali content in glass = g_{Na2O} + 0.66 g_{K2O} + 2.07 g_{Li2O}
N_{NaLi}	normalized soda and lithia content in glass = g_{Na2O} + 2.07 g_{Li2O}
N_{SiAl}	normalized silica-alumina content in glass = g_{SiO2} + 1.697 g_{Al2O3}
NL_α	normalized loss of component α during 7-day PCT (α = B, Na, Li)
NP P	distance from nepheline formation boundary line
p	number of terms in a model
p_i	i^{th} component model coefficient
p_{ii}	i^{th} component quadratic term model coefficient
p_{ij}	i^{th} and j^{th} components cross-product term model coefficient
$Q_{CL\%}^{prop}$	CL% percentile of the distribution of property value realizations
$Q_{50\%}^{prop}$	median predicted property value or CL% = 50% percentile of the distribution of 10,000 property value realizations
R^2	coefficient of determination
r_B	TCLP normalized boron release
r_i	the i^{th} component renormalized mass fraction in glass after excluding SO_3 (r_i = $g_i/(1\text{-}g_{SO3})$)
r_{ele}	normalized elemental TCLP release
q_i	the i^{th} component renormalized mole fraction in glass after excluding Cl (q_i = $x_i/(1\text{-}x_{Cl})$)
S	glass surface area in PCT
$S_{0/1}$	a static method counter (= 1 for k_{stat}, = 0 for k_{bubb})
S_{1200}	a static method counter (= 1 for static at 1200 °C and 6 or 7 days and = 0 for other conditions)
$S_{1150\text{-}3}$	a static method counter (= 1 for static at 1150 °C and 3 d and = 0 for other conditions)
$S_{1150\text{-}7}$	a static method counter (= 1 for static at 1150 °C and 7 d and = 0 for other conditions)
$S_{1200\text{-}3}$	a static method counter (= 1 for static at 1200 °C and 3 d and = 0 for other conditions)
T	temperature
T_0	infinite viscosity or EC temperature value in VFT equation
$T_{1\%}$	temperature at 1 vol% spinel
$T_{2\%}$	temperature at 2 vol% spinel
T_M	melting temperature

T_L	liquidus temperature (temperature at 0 vol% crystal)
T_L-P	liquidus temperature for phosphate phases
T_L-Zr	liquidus temperature for zirconium-containing phases
$t(P_\alpha)$	transformed property α
U_{comp}^{prop}	composition uncertainty of a property
U_{comp}	composition uncertainty
U_{pred}	prediction uncertainty
U_α^{pred}	uncertainty in prediction of $t(P_\alpha)$
U_α^{comp}	expression of composition uncertainty expressed in units of $t(P_\alpha)$
V	PCT solution volume
V_{Batch}	a melter feed preparation vessel (MFPV) batch volume
V_{DCW}	dust control water volume
V_{Dil}	dilution water volume
V_{Flush}	the sum of flush water volume
V_{GFC}	glass-forming chemical volume
v_i	fraction of i^{th} oxide retained in the glass (g/g)
V_{heel}	heel volume
$V_{Working}$	MFPV working volume
V_{Wtrf}	waste transfer volume
w_i	i^{th} component w_{SO3} model coefficient
wt%	weight percent
w_{SO3}	sulfur solubility
$w_{SO3\text{-}MT}$	sulfur solubility by melter tolerance method
$w_{SO3\text{-}bub}$	sulfur solubility by bubbling method
$w_{SO3\text{-}sat}$	sulfur solubility by (one time) saturation method
$w_{SO3\text{-}3TS}$	sulfur solubility by three times saturation method
x_i	concentration of i^{th} component in glass, mole basis
ε	electrical conductivity
ε_{1100}	electrical conductivity at 1100°C
ε_{1150}	electrical conductivity at 1150°C
ε_{1200}	electrical conductivity at 1200°C
η_{1100}	viscosity at 1100°C
η_{1150}	viscosity at 1150°C
η_T	viscosity at temperature, T
ρ	density at room temperature
$\rho_{P,\,\alpha}$	GFC α particle density
Y	glass yield in grams of glass per liter of melter feed

Contents

Figures

Tables

1.0 Introduction

The U.S. Department of Energy (DOE) Hanford Field Office (HFO) is responsible for the safe storage, treatment, and immobilization of nuclear waste stored in underground tanks at the Hanford Site. The Waste Treatment and Immobilization Plant (WTP) is the cornerstone of the tank waste cleanup strategy at Hanford. This plant includes, as primary components, the Low-Activity Waste (LAW) Facility, the High-Level Waste (HLW) Facility, the Pretreatment (PT) Facility, the Laboratory (LAB), and the balance of facilities (BOF). The current strategy is to stage the startup of the LAW, HLW, and PT facilities (DOE 2013; Bernards et al. 2020). The LAW Facility along with the needed components of the LAB and the BOF started treating LAW in 2025. To facilitate the startup of the LAW Facility prior to the PT Facility, a Tank Side Cesium Removal (TSCR) system was constructed to remove solids and cesium-137 (^{137}Cs) from the tank waste supernate, thereby removing much of the radioactivity of the supernatant liquid to feed to the LAW Facility (Westesen et al. 2022). The TSCR began operations on January 26, 2022, and continues today.

By 2013 (Kruger and Vienna 2013) advances in glass formulation for HLW had matured to the point that it was apparent that pursuing a path circumventing PT and directly feeding the HLW Facility was plausible. The concept was matured and in 2015 the framework for Direct Feed-HLW a team of DOE and site contractor staff submitted a Grand Challenge (“Making a Significant Difference Through Creativity and Innovation”) proposal. It was selected as the “Winner” (Vienna et al. 2015).

An analysis of alternatives for startup and operations of the PT and HLW facilities was conducted to identify the most likely alternatives along with the upper-level implications (Parsons 2023). Seventeen alternatives were considered, including concurrent startup of the HLW and PT facilities and HLW Facility operations without the PT Facility. Based on the results of these options, HFO requested an 18th alternative (Alt-18), in which the annual budget for Hanford was constrained (Bernards et al. 2021). This scenario includes a Waste Transfer Vault that couples the HLW Facility with tank farms using a waste feed transfer vessel and an effluent collection vessel, as shown in Figure 1.1.

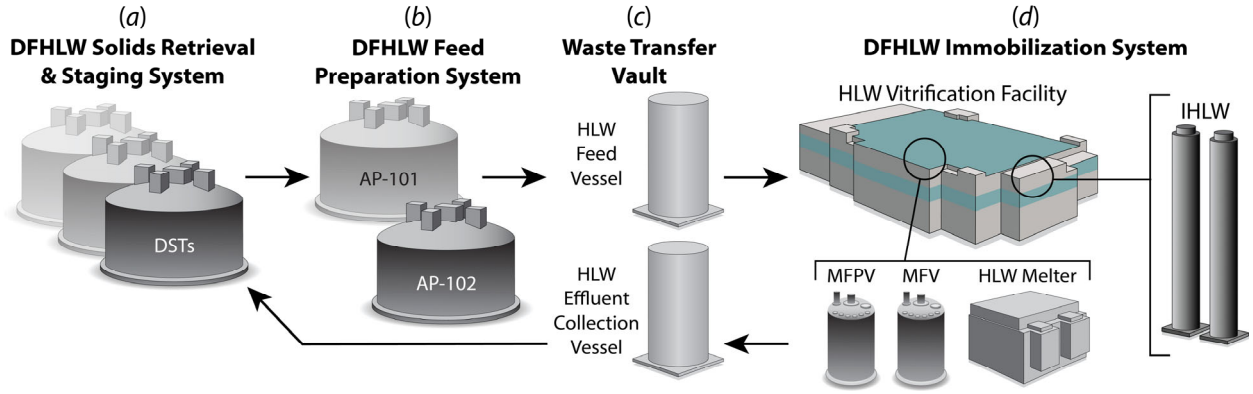

Figure 1.1. DFHLW vitrification flowchart.

A holistic agreement between HFO and Washington State Department of Ecology includes milestones for the construction and commissioning of additional pretreatment capabilities after startup of the HLW Facility. Consent Decree milestones for PT Facility are now “asterisked” and will be revisited and revised, as appropriate, after HLW treatment begins (US District Court 2025). HFO empowered a team of experts from the WTP contractor (Bechtel National Inc.),

Tank Farm Contractor (currently Hanford Tank Waste Operations & Closure), Pacific Northwest National Laboratory (PNNL), and HFO to develop a more detailed Direct Feed High-Level Waste (DFHLW) flowsheet based on the Alt-18 concept. Through this effort, the team identified the need to formulate glass using the enhanced waste glass (EWG) method, which results in reasonable waste processing rates (Vienna et al. 2023).

To support the DFHLW flowsheet evaluations and ultimately HLW Facility operations, an iterative process for EWG glass development was adopted, including the following steps:

1. Conduct DFHLW glass formulation (generating waste loadings and glass compositions) with existing property modeling and constraints using the latest feed vectors.
2. Evaluate the processing rates.
3. Select representative glasses (e.g., cluster analysis) to conduct experimental validation.
4. Compare measured vs. predicted data.
5. Design matrices to systematically cover composition gaps and test glasses.
6. Develop property models with additional data and update formulation constraints.

The glass property testing and modeling efforts are performed under direction from the DOE according to a schedule agreed upon by WTP contractor staff. This is consistent with the division of scope between PNNL and WTP contracts. This report documents the current iteration of this work.

Table 1.1 summarizes the iterations performed to date. A total of five full iterations is planned for the EWG models (EWG1 through EWG5). However, two partial iterations were also added for programmatic reasons (EWG2.5 and EWG2.6). Table 1.2 lists the timeline, objectives, data used, and additions for DFHLW glass formulation algorithms.

Table 1.1. Summary of reports for DFHLW glass formulation algorithm, process rate evaluation and experimental validation.

Algorithm	Property Models/Formulation	Process Rate Evaluation	Experimental Validation
WTP Baseline	Vienna and Kim (2014) (24590-HLW- RPT-RT-05-001, Rev. 1)	Chapman (2007) (24590-HLW-RPT-PE-07-001)	Kot et al. (2006a) (VSL-06R1240-1)
		Vienna et al. (2022a) (PNNL-32866, Rev. 1)	Matlack et al. (2008a) (VSL-08R1220-1)
EWG1	Vienna et al. (2016) (PNNL-25835, Rev. 0)	Vienna et al. (2022a) (PNNL-32866, Rev. 1)	--
EWG2	Lu and Vienna (2023), DFHLW Example Glass Selection Memo (CCN-335241, PNNL-SA-187966)	Lu et al. (2024a), DFHLW Process Control Chemical Limits Memo (PNNL-SA-199714)	Gervasio et al. (2024) (PNNL-35503, Rev. 0)
EWG2.5	Vienna et al. (2024) (PNNL-35884, Rev. 1)	Lu et al. (2024b) (PNNL-36196, Rev. 0)	Russell et al. (2025a) (PNNL-37506, Rev. 0)
EWG2.6	Vienna et al. (2025) (PNNL-37762, Rev. 0)	Lu et al. (2025) (PNNL-38134, Rev. 0)	--
EWG3.0	This report	Future	Future

Table 1.2. Summary of the timeline, objectives, data used, and additions for DFHLW glass formulation algorithms.

Version:	EWG1	EWG2	EWG2.5	EWG2.6	EWG3.0	EWG4	EWG5	GlassApp
Timeline:	2016	2022	2024	2025	2026	2028	2030	2032
Objectives	Mission projections with pretreated high-level waste (PTHLW)	Mission projections with DFHLW	Initial estimate of DFHLW for flowsheet evaluation	Refined estimate of DFHLW for flowsheet evaluation	Refined estimate of DFHLW for flowsheet evaluation	Waste qualification report and initial integrated plant version	Cold and hot commissioning, initial operations	Plant operations interface
Number of DFHLW glasses	0	0	15	81	215	400-500	450-550	No change
Data additions	PTHLW	No new models or data were generated under EWG2. LAW and PTHLW models were combined to calculate properties	+APPS1 (Gervasio et al. 2023)	+APPS2 (Russell et al. 2025a), +HAL24 (Russell et al. 2025b)	+HS24 (in progress), +P-Sol (Bai et al. 2025), +LAWHNK (Gervasio et al. 2026)	+HNA25 (in progress), +HFE25 (in progress), +HAL25 (in progress), +HFO-ML (in progress), *+Na10, +S10, +APPS3, +K3M1, +M2 +MCM1 +MCM2 +Melter data, +Gap M +VSLglasses*	*+V&V-crucible, +V&V-melter*	None
Plant data	None	None	None	None	Baseline design	Updated design	+Equip testing	+Plant interfaces

Glasses in italic font are future planned glasses.
APPS = Aspen Process Performance Simulation

The current report documents the EWG3.0 models and constraints. These models and constraints are not final models and were not designed to operate the plant efficiently for the mission. Rather, they are intended to supply a reasonable estimate of ultimate glass compositions and waste loading to allow design support flowsheet calculations to be confirmed for final HLW design with a DFHLW feed.

2.0 Property Models

Table 2.1 summarizes EWG2.6 (most recent past model set) and EWG3.0 (current report) model developments and recommendations of future property model developments. Each of the EWG3.0 model updates are discussed in this section. Model evaluation techniques include predicted versus measured property plots, standardized residual, outlier diagnostics, coefficient of determination, R^2 statistics (R^2, R^2adjust, R^2press), and root mean squared error (RMSE). Equations and details of these statistical methods for model evaluation can be found in Appendix B of Vienna et al. (2022b). Pooled standard deviation (SD) was calculated using the duplicate set glasses (e.g., glasses with the same chemical compositions but measured at different time periods and/or laboratories) to access the uncertainty from experimental measurements. Section 3.0 presents glass formulation constraints, overall model validity (MV) constraint, composition and process uncertainties, optimization criteria, and example calculations using these property models.

Table 2.1. Summary of EWG2.6 and EWG3.0 model developments and recommendations of future property model developments.

Property	EWG2.6 (Vienna et al. 2025)	EWG3.0 (this report)	Future
Viscosity	New model with combined LAW and HLW glass data	New model with additional data. Section 2.1	New model including crystal impact and additional data
Electrical conductivity (EC)	New model with combined LAW and HLW glass data	New model with additional data. Section 2.1	New model including crystal impact and additional data
Melter SO_3 tolerance	New model with three times saturation (3TS) SO_3 solubility ($w_{SO3\text{-}3TS}$).	New model with a broader database. Section 2.2	New model to include additional data
K-3 refractory corrosion	New model with additional data	New model with expanded composition range and reduced uncertainty. Section 2.3	New model to include additional data
Isothermal crystallinity – P_2O_5 liquidus temperature (T_L)	New model for phosphate phase T_L	New model with additional data. Section 2.4	New model to include additional data
Isothermal crystallinity – ZrO_2 liquidus temperature	New T_L-Zr model incorporating all data since 2009	No change to zirconia-containing phase model because only two data points can be added and the EWG2.6 model predicts well for these data. Section 2.5	New model to include additional data
Isothermal crystallinity – spinel	New model for spinel 1 vol% ($T_{1\%}$) $\leqslant$ 950°C	New model for spinel concentration at 950 °C, allowing for variable crystal fraction estimates. Section 2.6	New model for spinel concentration as functions of composition and temperature
Product consistency test (PCT)	Vienna and Crum (2018) model with prediction uncertainty	New model with additional data. Section 2.7	New model to include additional data
Toxicity Characteristic Leaching Procedure (TCLP)	Kim and Vienna (2003)	New model with additional data and additional constraints. Section 2.8	New model to include additional data
Nepheline formation	Modify the nepheline model p threshold to 0.031	No change since the current model and threshold predicts well for new data recently collected. Section 2.9	New model to include additional data
Metal corrosion	Not applied	Preliminary limit on F concentration. Section 2.10	A composition property model
Prediction uncertainty	99% confidence intervals (CIs) to processing and regulatory constraints and 99% simultaneous CIs for repository constraints.	99% CIs to processing and regulatory constraints and 99% simultaneous CIs for repository constraints. Section 3.1	90% confidence intervals to processing and regulatory constraints and 95%/95% simultaneous CIs for repository constraints.
Composition and process uncertainty	Not applied.	Applied with Monte Carlo simulation method. Section 3.3	Apply analytical solution(s) from Gunnell et al. (2025). Include compositional impact from heel.
GFC rules	Rules for V_2O_5, and Cr_2O_3 addition.	Updated the rules for V_2O_5 addition. Section 3.4	Replace V_2O_5 with V_2O_3. Improved optimization criteria to eliminate undesired GFC additions.

GFC = glass-forming chemical

2.1 Viscosity and Electrical Conductivity

Constraints on viscosity (η) at the processing temperature ensure sufficient processing rate and flow of glass, reducing the likelihood of discharge and container-filling issues, while minimizing corrosion of melter construction materials. Constraints on EC (ε) at the processing temperature ensure sufficient energy can be supplied by the power source without exceeding current density limits of the power system.

2.1.1 Database

In addition to the data used in the EWG2.6 models, data from several other glass matrices (LAWML2, HAIG, DHW, HFG, HS24, LAWHNK, and HAL24) were added. Data points with $\log_{10}[\eta$ (Pa s)] > 3.5 (η > 3162 Pa s) or $\log_{10}[\varepsilon$ (S m^{-1})] < 0.75 (ε < 5.62 S m^{-1}) were excluded. For both properties, 20% of quality assurance (QA)-qualified glasses were selected for model testing while the remaining 80% of QA-qualified glasses and all non-QA-qualified glasses were used for model training. Figure 2.1 shows training and testing data vs. inverse temperature. The data for viscosity and EC are summarized in Table 2.2 and Table 2.3. In this context, QA-qualified data was generated under an accepted NQA-1 program as applied technology or technology readiness level ≥ 4.

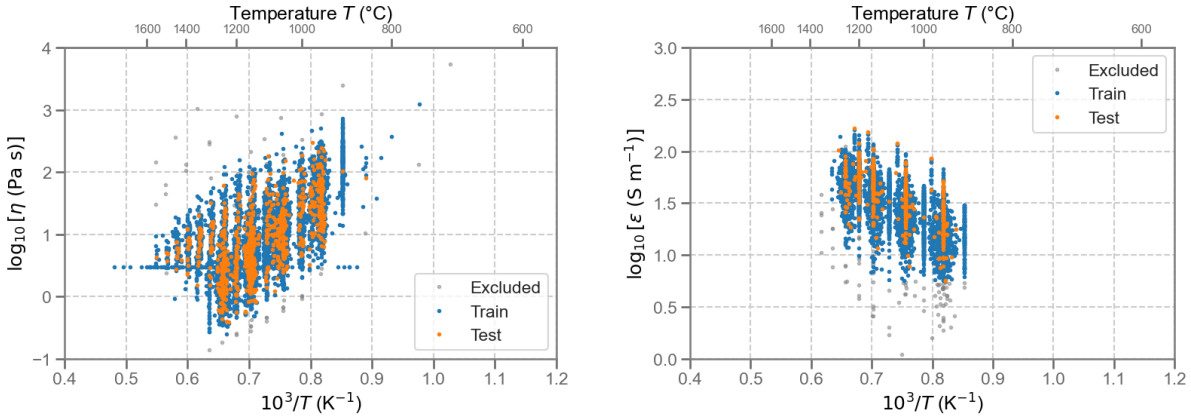

Figure 2.1. Measured (a) logarithm viscosity and (b) logarithm electrical conductivity vs. inverse temperature.

Table 2.2. Number of glasses and points in viscosity dataset.

	QA	Glasses	Points
DFHLW	TRUE	131	770
HLW	FALSE	542	2623
	TRUE	537	3265
LAW	FALSE	551	4546
	TRUE	191	1153

Table 2.3. Number of glasses and points in EC dataset.

	QA	Glasses	Points
DFHLW	TRUE	131	560
HLW	FALSE	248	1097
	TRUE	194	924
LAW	FALSE	495	3822
	TRUE	181	1181

2.1.2 Model

The temperature- and composition-dependence of viscosity and EC were modeled using the Vogel-Fulcher-Tammann (VFT) equation, which can be written as:

$$\log_{10}(\eta) = A + \frac{B}{T - T_0} \tag{2.1}$$

where $\log_{10}(\eta)$ is a decadic logarithm of viscosity in Pa·s [replaced by $\log_{10}(\varepsilon)$ for EC in S m^{-1}]; T is temperature in K; and A, B, and T_0 are parameters of the VFT equation. Parameters A and T_0 were modeled as constants while a linear model was used for the temperature dependent parameter as:

$$B = \sum_{i=1}^{n} g_i B_i \tag{2.2}$$

where n is the number of components, g_i is the i^{th} component mass fraction, and B_i is the i^{th} component coefficient. Model parameters were fitted by the least squares method.

Based on preliminary modeling, the following glasses were identified and excluded from the viscosity dataset as outliers: A60A, A80A, IG2-07, HLWD2-05, LAWPC7, LAWB42S, NBS-710, HLW02-14, HLW99-15, HLWD1-19, HLWMS-08, 10-30, CVS1-9, CVS1-12, CVS2-80, CVS3-5, CVS3-20, HAL24M1-11, LAWALG-01, LAWHNK-02, LAWHNK-05, LAWHNK-17, and HFG1-19.

Similarly, the following glasses were identified and excluded from the EC dataset as outliers: HLW02-14, HLW07-28, HLW07-40, EMHQ-LBE-04, EMHQ-LBE-04B, EMHQ-LBE-05, EMHQ-LBE-06, LAWM30, LAWM53, ORPLA6, LP4-14, LAWML1-09, LAWML1-11, LAWML1-13, HLW-APPS-10, HAIG1-13, HS24-02, HS24-04, HS24-06, HS24-32, HS24-48, HS24-49, HFG1-03, HFG1-06, HFG1-11, HFG1-14.

The criteria for exclusion were based on squared residual. Glasses with any point with a squared residual higher than 0.45 $\log_{10}^2$(Pa s) or 0.15 $\log_{10}^2$(S m^{-1}) were excluded from the final model. The distribution of model features and measured property is visualized in Figure 2.2 and Figure 2.3 for viscosity and EC, respectively. In both models, the number of components was chosen to yield high R^2 for training, testing, and DFHLW subsets.

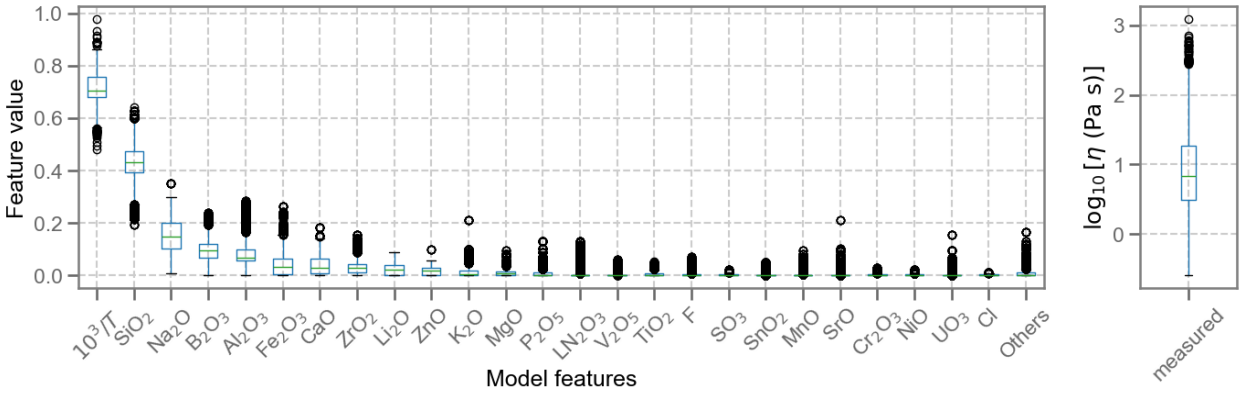

Figure 2.2. Distribution of viscosity and model features.

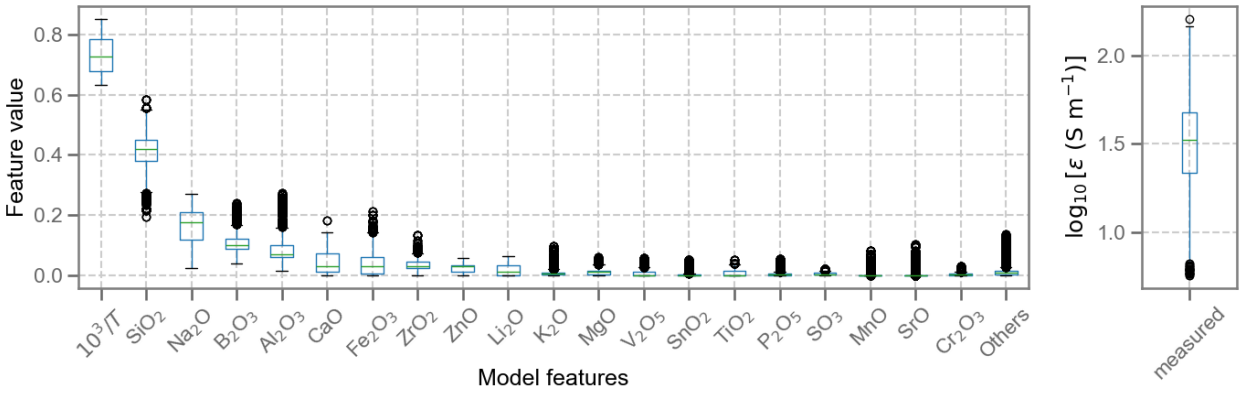

Figure 2.3. Distribution of EC and model features.

Model parameters and fitting statistics are presented in Table 2.4 and Table 2.5 and model estimates are shown in Figure 2.4 and Figure 2.5. Both models achieve relatively good metrics, with the EC model having slightly higher average error compared to the viscosity model, which is typical for all previous model iterations [e.g., Ferkl et al. (2024)]. Model precision can be increased by including non-linear terms, which is explored in Appendix D, or by employing machine learning methods, which should be investigated in the future. However, minimizing non-linear composition terms has previously been observed to improve prediction in composition spaces not well covered by data.

Table 2.4. Viscosity model coefficients and summary statistics.

Term	Coefficient	Unit	Statistic	Value
A	-2.7227	$\log_{10}$(Pa·s)	# glass components	25
B_Al_2O_3	7309.6	K	# model parameters	27
B_B_2O_3	-715.53	K	# model features	26
B_CaO	-494.92	K	R^2, all	0.948
B_Cl	7698.4	K	R^2, train	0.958
B_Cr_2O_3	4622	K	R^2, test	0.948
B_F	-2759.4	K	R^2, excluded	0.847
B_Fe_2O_3	2241.9	K	RMSE, all, $\log_{10}$(Pa·s)	0.132
B_K_2O	701.62	K	RMSE, train, $\log_{10}$(Pa·s)	0.114
B_Li_2O	-11569	K	RMSE, test, $\log_{10}$(Pa·s)	0.115
B_LN_2O_3	2371.5	K	RMSE, excluded, $\log_{10}$(Pa·s)	0.668
B_MgO	1122.4	K	# points, all	13013
B_MnO	-205.04	K	# points, train	11783
B_Na_2O	-1692.5	K	# points, test	1097
B_NiO	2033.8	K	# points, excluded	133
B_P_2O_5	4894.2	K		
B_SiO_2	6042.4	K	Pooled SD (Vienna et al. 2022b), $\log_{10}$(Pa·s)	0.0719[(a)]
B_SnO_2	4658.3	K		
B_SO_3	4849	K		
B_SrO	430.85	K		
B_TiO_2	1093.6	K		
B_UO_3	3611.6	K		
B_V_2O_5	1295.5	K		
B_ZnO	1197.9	K		
B_ZrO_2	5310.9	K		
B_Others	1699.9	K		
T_0	533.45	K		

(a) Pooled SD from Vienna et al. (2022b) is 0.1655 ln(Pa·s) or ln(Poise). Because this is a standard deviation, applying a constant unit-conversion factor does not affect its value.

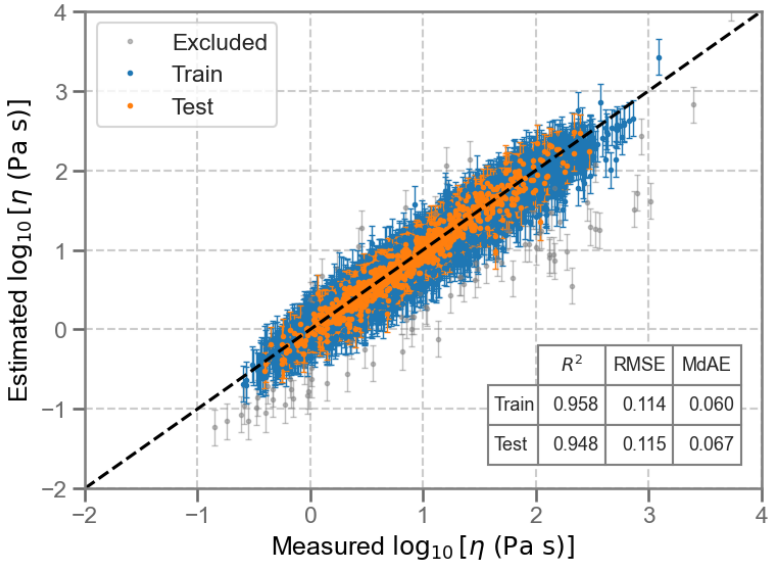

Figure 2.4. Measured vs. estimated/predicted viscosity.

Table 2.5. EC model coefficients and summary statistics.

Term	Coefficient	Unit	Statistic	Value
A	2.9337	$\log_{10}$(S m^{-1})	# glass components	20
B_Al_2O_3	-2256.4	K	# model parameters	22
B_B_2O_3	-1690.5	K	# model features	21
B_CaO	-2307.1	K	R^2, all	0.857
B_Cr_2O_3	-1121.8	K	R^2, train	0.900
B_Fe_2O_3	-1607.5	K	R^2, test	0.838
B_K_2O	-1088.9	K	R^2, excluded	0.441
B_Li_2O	4904.9	K	RMSE, all, $\log_{10}$(S m^{-1})	0.100
B_MgO	-1313.1	K	RMSE, train, $\log_{10}$(S m^{-1})	0.079
B_MnO	-1754.4	K	RMSE, test, $\log_{10}$(S m^{-1})	0.098
B_Na_2O	2031.9	K	RMSE, excluded, $\log_{10}$(S m^{-1})	0.357
B_P_2O_5	-1467.2	K	MdAE, all, $\log_{10}$(S m^{-1})	0.047
B_SiO_2	-2227.3	K	MdAE, train, $\log_{10}$(S m^{-1})	0.045
B_SnO_2	-3018.6	K	MdAE, test, $\log_{10}$(S m^{-1})	0.051
B_SO_3	-2022	K	MdAE, excluded, $\log_{10}$(S m^{-1})	0.301
B_SrO	-2056.1	K	# points, all	7584
B_TiO_2	-1410.4	K	# points, train	6867
B_V_2O_5	-1120.6	K	# points, test	492
B_ZnO	-1078.8	K	# points, excluded	225
B_ZrO_2	-2120.7	K		
B_Others	-1334.2	K	Pooled SD (Vienna et al. 2022b), $\log_{10}$(S m^{-1})	0.0897
T_0	491.73	K		

MdAE = median average error
Pooled SD from Vienna et al (2022b) is 0.2066 ln(S/cm) or ln(S/m).

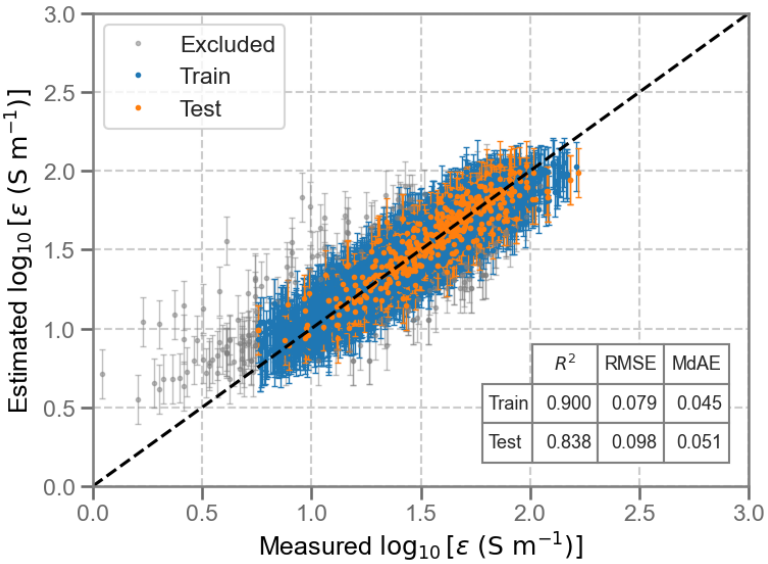

Figure 2.5. Measured vs. estimated/predicted electrical conductivity.

Composition effects on a centroid reference glass are shown in Figure 2.6 (η) and Figure 2.7 (ε). According to the viscosity model, the components can be ranked as SiO_2 > Al_2O_3 > ZrO_2 > P_2O_5 according to their ability to increase viscosity. Similarly, additional components can be

ranked as Li_2O > F > Na_2O > B_2O_3 > CaO > MnO > SrO > K_2O according to their ability to decrease viscosity. Note that the component effect does not necessarily correspond to the positive or negative sign of the model coefficients. The component effect figures are intended as an interpretive visualization of the model response under controlled compositional variations. Because some models include nonlinear terms and model terms can be correlated (e.g., higher Al_2O_3 often appears together with higher B_2O_3), including in linear models, individual coefficients might not have a direct physical interpretation, and their impacts on property can vary depending on the local composition space. In these component effect figures (also referred as spider plots), each line is generated by varying one component from its minimum to maximum value while holding the relative ratios of all other components fixed at the reference (mean) composition of the data used during model development. Consequently, the slope observed in a spider plot represents a local sensitivity and depends on the chosen center point; changing the reference composition can alter both the magnitude and sign of the apparent trend. This behavior reflects the structure of the model rather than a discrepancy between the model coefficients and the spider plots. For this reason, the spider plots are used as a composition-specific sensitivity and interpretation tool.

The rest of the components show either a minor effect on viscosity or are generally present in such small quantities that their effect on viscosity is relatively minor. According to the EC model, the EC is mostly increased by addition of Li_2O and Na_2O and decreased by addition of SnO_2, SiO_2, CaO, and Al_2O_3. These effects are consistent with previously determined component effects (e.g., Vienna et al. 2022b; Heredia-Langner et al. 2022).

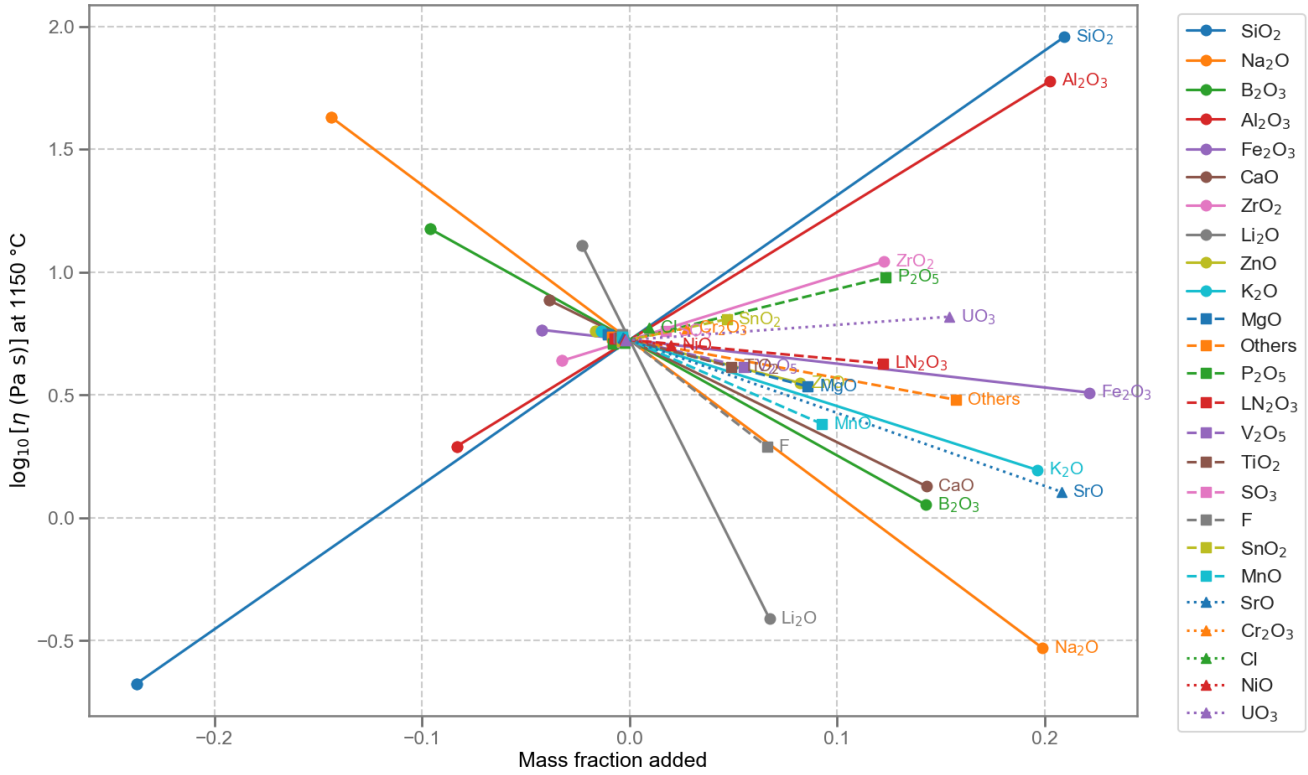

Figure 2.6. Component effects on $\log_{10}(\eta_{1150}$, Pa·s).

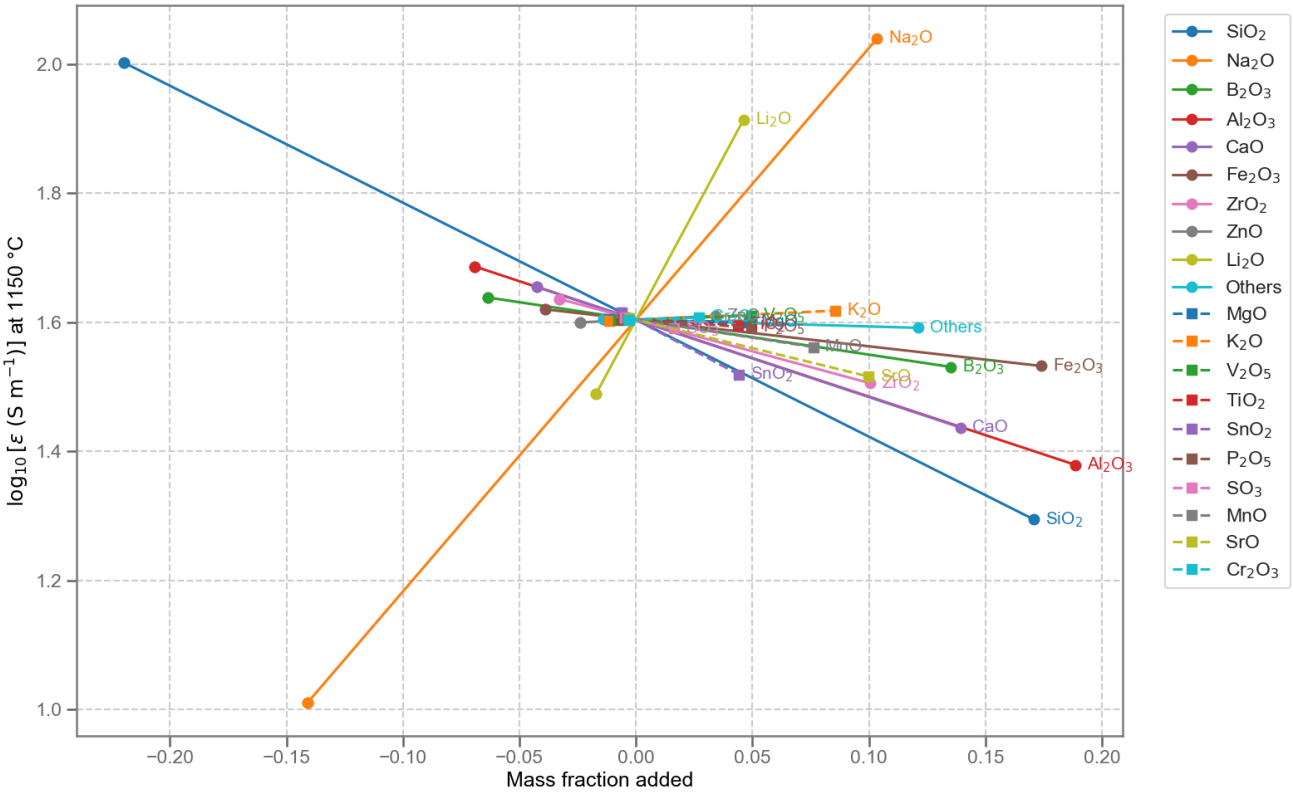

Figure 2.7. Component effects on $\log_{10}(\varepsilon_{1150}, S\ m^{-1})$.

2.2 SO_3 Solubility

Salt accumulation constraints are used to avoid excessive corrosion of melter construction materials and reduce radionuclide volatility (Vienna et al. 2014). Vienna et al. (2014) first established the correlation between the sulfur melter tolerance and the solubility of sulfur in glasses, and developed an empirical model by correlating glass composition to sulfur solubility and then to the sulfur melter tolerance. Data generated by a crucible salt saturation, three-times saturation method ($w_{SO3\text{-}3TS}$) developed by Jin et al. (2018) were used in the following model development.

2.2.1 Database

The SO_3 solubility measured by $w_{SO3\text{-}3TS}$ data were compiled from the data used in the EWG2.6 development with two additional matrices data (Table 2.6). Three glasses were excluded as outliers (listed in Table 2.7) during model development because the studentized residual exceeded the Bonferroni 95% limit. The ranges of measured $w_{SO3\text{-}3TS}$ values and component concentrations are listed in Table 2.8. The glass composition used in $w_{SO3\text{-}3TS}$ modeling was the target glass composition in mass fractions renormalized after removing the target g_{SO3}.

Table 2.6. Summary of $w_{SO3\text{-}3TS}$ model data.

Study	# of $w_{SO3\text{-}3TS}$ Points	Reference
EWG2.6	308	Vienna et al. (2024)
LAWHNK	20	Unpublished [EWG-CCP-357]
HS24	50	Unpublished [EWG-CCP-358]
Total	378	--

CCP = Calculation Control Package

Table 2.7. List of glasses excluded from $w_{SO3\text{-}3TS}$ model development

Glass	Study	Reason
LP4-17	LAW Phase 4	Studentized residual > Bonferroni 95% limit
LP5-01	LAW Phase 5	Studentized residual > Bonferroni 95% limit
LP5-13	LAW Phase 5	Studentized residual > Bonferroni 95% limit
Total	3	

Table 2.8. Range of $w_{SO3\text{-}3TS}$ and composition data used in model development, normalized mass fraction.

Component	Min	Mean	Median	Max
Al_2O_3	0.0305	0.0949	0.0832	0.2726
B_2O_3	0.0402	0.1108	0.1035	0.2414
CaO	0.0000	0.0543	0.0509	0.1297
Cl	0.0004	0.0033	0.0020	0.0241
Cr_2O_3	0.0001	0.0044	0.0031	0.0250
F	0.0000	0.0066	0.0029	0.0457
Fe_2O_3	0.0000	0.0159	0.0074	0.1254
K_2O	0.0000	0.0119	0.0030	0.0584
Li_2O	0.0000	0.0116	0.0043	0.0512
MgO	0.0000	0.0088	0.0021	0.0829
MnO	0.0000	0.0007	0.0000	0.0077
Na_2O	0.0923	0.1909	0.1994	0.2704
P_2O_5	0.0000	0.0106	0.0059	0.0403
SiO_2	0.2412	0.3857	0.3881	0.5936
SnO_2	0.0000	0.0139	0.0035	0.0508
V_2O_5	0.0000	0.0199	0.0183	0.0573
ZnO	0.0000	0.0189	0.0194	0.0575
ZrO_2	0.0000	0.0308	0.0295	0.0932
Others	0.0000	0.0061	0.0031	0.0427
$w_{SO3\text{-}3TS}$, wt%	0.602	1.472	1.401	3.060

2.2.2 Model

A model was developed to predict the $w_{SO3\text{-}3TS}$ data described in Section 2.2.1. The distribution of each composition term was evaluated in one dimension using histogram plots and two dimensions using scatterplot matrices to determine which terms had sufficient range and variation to be used in modeling.

A first-order composition model of the following form was used:

$$w_{SO_3-3TS} = \sum_{i=1}^{n} w_i r_i \tag{2.3}$$

where w_i and r_i are the i^{th} component coefficient and renormalized mass fraction, respectively, and $r_i = g_i/(1\text{-}g_{SO3})$.

It was found that Al_2O_3, B_2O_3, CaO, Cl, Cr_2O_3, F, Fe_2O_3, K_2O, Li_2O, MgO, MnO, Na_2O, P_2O_5, SiO_2, SnO_2, V_2O_5, ZnO, and ZrO_2 were statistically significant. The addition of cross-product or quadratic terms was then investigated to determine if a few higher order terms would significantly improve the model performance using:

$$w_{SO_3-3TS} = \sum_{i=1}^{n} w_i r_i + Selected\left\{\sum_{i=1}^{n} w_{ii} r_i^2 + \sum_{i=1}^{n}\sum_{j\neq i}^{n-1} w_{ij} r_i r_j\right\} \tag{2.4}$$

where w_{ii} is the i^{th} component quadratic coefficient and w_{ij} is the i^{th}-j^{th} cross product coefficient. It was found that the addition CaO×MgO, Al_2O_3×Na_2O, Al_2O_3×SiO_2, and CaO×ZnO significantly improved the model fit. The partial quadratic mixture (PQM) model has an R^2 = 0.8373 and an RMSE = 0.1812 wt%. Three glasses (LP4-17, LP5-01, and LP5-13) were removed as outliers due to high studentized residuals.

Coefficients for the model are given in Table 2.9. The predicted vs. measured plot is shown in Figure 2.8. These coefficients do not account for the -0.33 wt% offset between melter tolerance ($w_{SO3\text{-}MT}$) and 3TS. Therefore, users must adjust predicted $w_{SO3\text{-}3TS}$ values to estimate melter tolerance: $w_{SO_3-MT} = w_{SO_3-3TS} - 0.33$ (Skidmore et al. 2019). The model underpredicts $w_{SO3\text{-}3TS}$ ≥ 2.25 wt%$w_{SO3\text{-}3TS}$. As this underprediction will result in conservative formulations, no attempt was made to correct the bias.

Table 2.9. 3TS SO_3 solubility model coefficients and summary statistics, composition in normalized mass fractions (before applying retention factors) and w_{SO3} in wt%.

Term	Coefficient		Statistic	Value
Al_2O_3	4.40824		# of points, n	375
B_2O_3	2.60639		# of terms, p	23
CaO	8.17167		Mean	1.472
Cl	-5.88470		R^2_{fit}	0.8373
Cr_2O_3	-3.56445		R^2_{press}	0.8137
F	-5.12522		R^2_{adjust}	0.8271
Fe_2O_3	-1.84251		$RMSE_{fit}$, wt%	0.1812
K_2O	1.43171		$RMSE_{press}$, wt%	0.1881
Li_2O	12.48281		Pooled SD $w_{SO3\text{-}3TS}$, wt%	0.134
MgO	-0.34444			
MnO	-20.76545			
Na_2O	6.57840			
P_2O_5	1.66598			
SiO_2	0.44667			
SnO_2	-4.62115			
V_2O_5	5.50834			
ZnO	1.97556			
ZrO_2	-5.26380			
Others	-1.48448			
CaO×MgO	-102.16450			
Al_2O_3×Na_2O	-24.67890			
Al_2O_3×SiO_2	-15.32906			
CaO×ZnO	-95.43156			

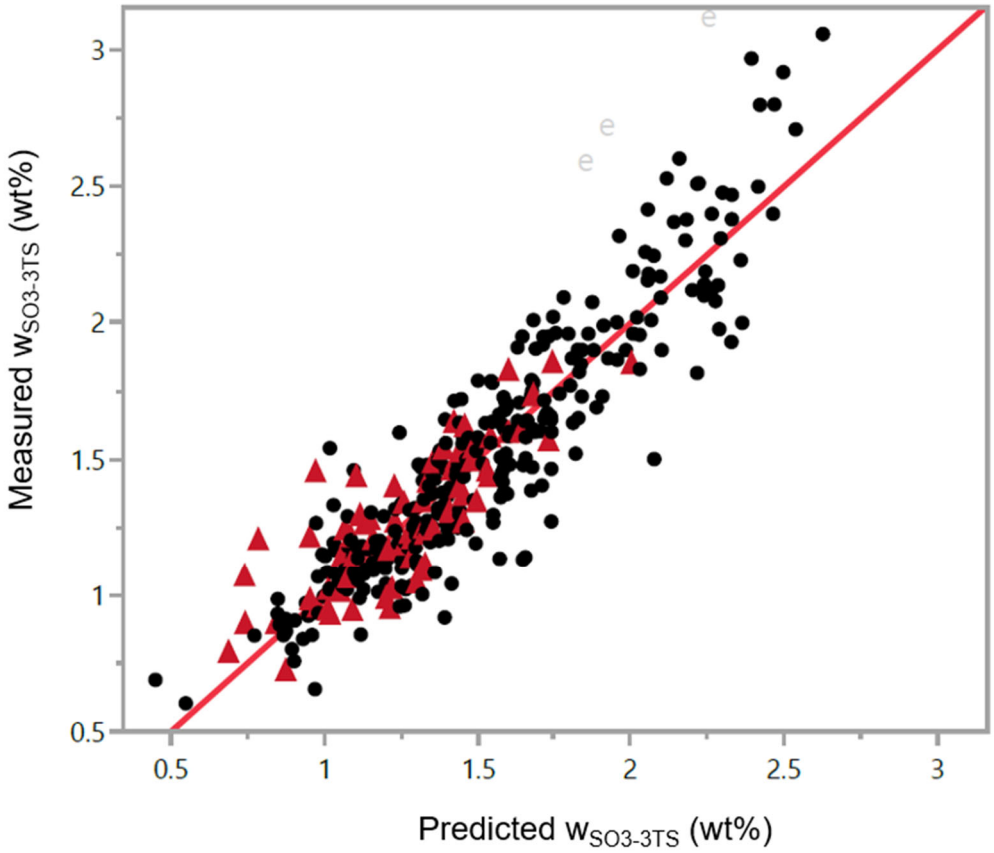

Figure 2.8. Predicted vs. measured $w_{SO3-3TS}$ in wt%. Black dots represent the data from EWG2.6, red triangles represent the data added in EWG3.0, and letter e represents the outliers. Red line is the 1:1 line to guide the eye.

Composition effects on $w_{SO3-3TS}$ are shown in Figure 2.9. As previously reported, Li_2O, CaO, V_2O_5, and Na_2O strongly increase w_{SO3} while Al_2O_3, SiO_2, and ZrO_2 decrease w_{SO3}. One unexpected impact is that of B_2O_3, which was found to increase w_{SO3} while previous studies suggested minimal impact. Further investigation is needed to determine if this is a real effect and, if so, what chemical phenomena cause this impact.

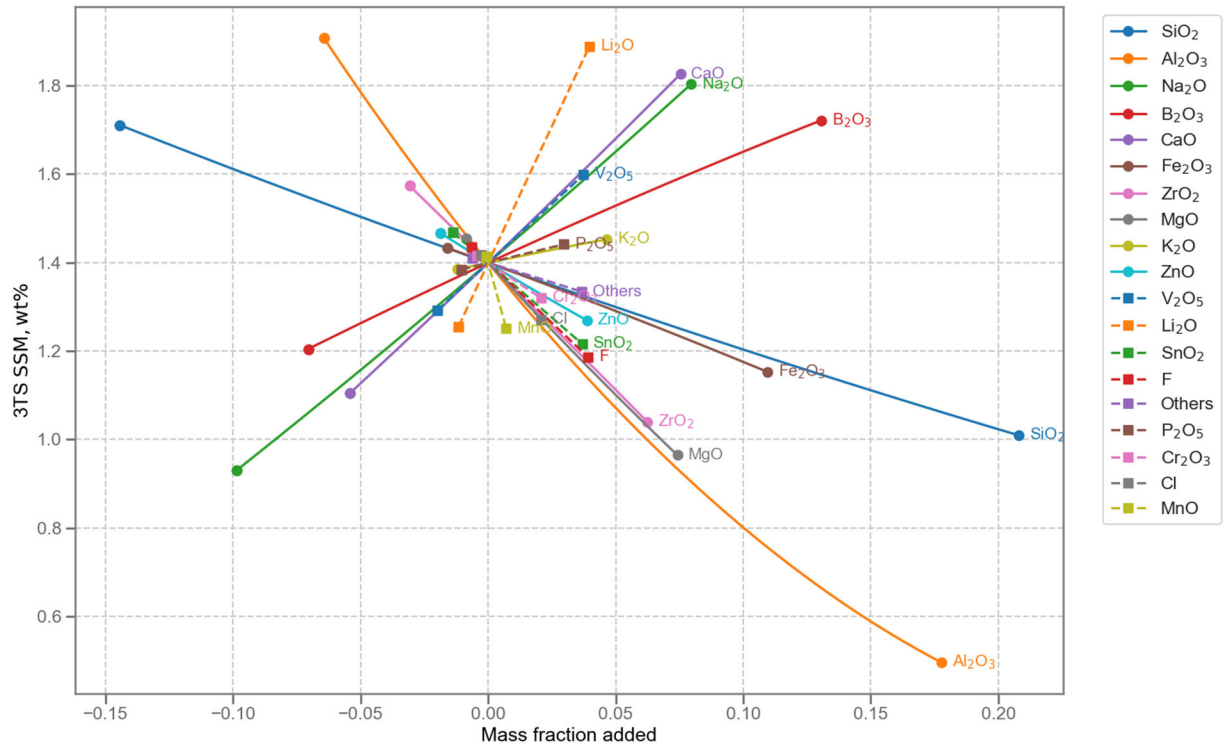

Figure 2.9. Component effects on $w_{SO3\text{-}3TS}$.

2.3 K-3 Refractory Corrosion Neck Loss

K-3 corrosion data is relatively limited in both number of glasses in the composition region of DFHLW glasses (Vienna et al. 2025). Roughly half (333 of 677) of the existing data were measured for 6 days at 1208 °C under bubbled conditions, with the remainder measured using static conditions at 1150 to 1200 °C for 3, 6, or 7 days. In all cases, the refractory-air-melt triple point resulted in the highest corrosion. This “neck” region of corrosion is the highest risk area within the HLW melter and so is it is used to model the impact of melt composition on K-3 neck corrosion (k_{neck}). Bubbled tests result in broader but shallower corrosion at the neck compared to the static tests, likely because of the changing melt-line height as air is injected and released. The lack of sufficient data coverage by any test condition necessitates the combination of data from multiple test conditions to develop the broadest possible composition-k_{neck} corrosion model.

2.3.1 Database

The k_{neck} data were drawn from several sources applying a range of test conditions. The model contained data summarized in Table 2.10. It was previously identified (Vienna et al. 2025) that data from tests performed at 1200 °C for 6 and 7 days were not statistically different. This was again confirmed during this modeling effort. With so many test conditions represented in the dataset, two models were developed: (1) a model combining all 1200-1208 °C tests performed at 6-7 days in either bubbled or static conditions (Section 2.3.2) and (2) a separate model containing data from all test conditions (Appendix E). The first model had 508 data points to model and is fit with the purpose of informing DFHLW glass formulations. The second model had 648 data to model and is fit with the purpose of better understanding the impacts of test condition on refractory corrosion.

Table 2.10. K-3 neck corrosion data summary.

Description	#	Lab	Conditions	Ref
LAW data	334	VSL	1208°C, 6d, bubbled	Muller et al. (2018)
HLW data	9	VSL	1208°C, 6d, bubbled	Muller et al. (2018)
LAW data check	4	SRNL	1200°C, 6d, static	Amoroso et al. (2024)
APPS1 glasses	15	SRNL	1200°C, 6d, static	Amoroso et al. (2024)
APPS1 glasses	16	SRNL	1200°C, 7d, static	Amoroso et al. (2024)
APPS2 glasses	16	PNNL	1150°C, 3d, static	Russell et al. (2025a)
APPS2 glasses	16	PNNL	1150°C, 7d, static	Russell et al. (2025a)
APPS2 glasses	16	PNNL	1200°C, 3d, static	Russell et al. (2025a)
APPS2 glasses	16	PNNL	1200°C, 7d, static	Russell et al. (2025a)
Touch point glasses	7	PNNL	1150°C, 3d, static	Unpublished [EWG-CCP-330]
Touch point glasses	7	PNNL	1150°C, 7d, static	Unpublished [EWG-CCP-330]
Touch point glasses	7	PNNL	1200°C, 3d, static	Unpublished [EWG-CCP-330]
Touch point glasses	7	PNNL	1200°C, 7d, static	Unpublished [EWG-CCP-330]
Touch point glasses	7	SRNL	1150°C, 3d, static	Unpublished [EWG-CCP-330]
Touch point glasses	7	SRNL	1150°C, 7d, static	Unpublished [EWG-CCP-330]
Touch point glasses	7	SRNL	1200°C, 3d, static	Unpublished [EWG-CCP-330]
Touch point glasses	7	SRNL	1200°C, 7d, static	Unpublished [EWG-CCP-330]
HAL24M1	30	SRNL	1150°C, 7d, static	Page et al. (2025)
HAL24M1	30	SRNL	1200°C, 7d, static	Page et al. (2025)
HAL24M2	20	PNNL	1150°C, 7d, static	Jin et al. (2025)
HAL24M2	20	PNNL	1200°C, 7d, static	Jin et al. (2025)
HS24	50	PNNL	1200°C, 7d, static	Unpublished [EWG-CCP-353]
Total = 677 (508 of which range from 1200-120 8°C and 6-7 days)				

PNNL = Pacific Northwest National Laboratory; SRNL = Savannah River National Laboratory; VSL = Vitreous State Laboratory

Several datapoints (21) with measured neck corrosion ≤ 0.002 in. were excluded from modeling. Russell et al. (2025a) reported that measurements below 0.004 in. (0.12 mm) were not reliable. Furthermore, Vienna et al. (2022b, 2024, 2025) reported that k_{neck} values below 0.002 in. were model fit outliers. Additional data were excluded from model fitting as summarized in Table 2.11. The range of glass component concentrations and logarithm of k_{neck} values are listed in Table 2.12.

Table 2.11. List of glasses excluded from K-3 model development

Glass	Reason
LAWC34S2	Erroneous SO_3 content in reported composition
LAWC36S2	Erroneous SO_3 content in reported composition
APPS2-01, 12/7	Studentized residual > Bonferroni 95% limit
HAL24M2-17	Studentized residual > Bonferroni 95% limit
HAL24M1-3	Studentized residual > Bonferroni 95% limit
HAL24M1-7	Studentized residual > Bonferroni 95% limit
HAL24M1-22	Studentized residual > Bonferroni 95% limit
Total	7

Table 2.12. Major component concentration ranges in ln[k_{neck}] 1200 °C only dataset, molar fractions.

Component	Min	Mean	Median	Max
Al_2O_3	0.0172	0.0626	0.0542	0.1840
B_2O_3	0.0335	0.1037	0.0941	0.2370
CaO	0.0000	0.0534	0.0438	0.1396
Cr_2O_3	0.0000	0.0013	0.0004	0.0109
Fe_2O_3	0.0000	0.0111	0.0043	0.0633
K_2O	0.0000	0.0080	0.0035	0.0589
Li_2O	0.0000	0.0238	0.0000	0.1199
Na_2O	0.0248	0.1987	0.2181	0.2877
P_2O_5	0.0000	0.0024	0.0006	0.0206
SiO_2	0.2726	0.4471	0.4570	0.6009
V_2O_5	0.0000	0.0037	0.0004	0.0210
ZnO	0.0000	0.0216	0.0244	0.0411
ZrO_2	0.0000	0.0190	0.0180	0.0532
Others	0.0013	0.0461	0.0396	0.1530
ln[k_{neck}]	-7.840	-3.757	-3.576	-1.666

2.3.2 Model

Two model forms were fit to experimental data:

$$ln[k] = k_{s1200}S_{1200} + \sum_{i=1}^{n} k_i q_i + Selected\left\{\sum_{i=1}^{n} k_{ii} q_i^2 + \sum_{i=1}^{n}\sum_{j\neq i}^{n-1} k_{ij} q_i q_j\right\} \quad (2.5)$$

where: k_{s1200} = an offset coefficient for data measured under static conditions at 1200 °C for 6 or 7 days

S_{1200} = a static method counter = 1 for static at 1200 °C and 6 or 7 days and = 0 for other conditions

k_i = the ith component coefficient for ln[k_{neck}]

k_{ii} = the ith component quadratic coefficient for ln[k_{neck}]

k_{ij} = the ith and jth components cross product coefficient for ln[k_{neck}]

q_i = the ith component normalized mole fraction in glass after excluding Cl (q_i = $x_i/(1-x_{Cl})$)

n = the number of components in the model

Initially, separate static test counters were used for 6-day and 7-day test data. No significant differences between the offsets were obtained, so for simplicity they were combined into a single counter S_{1200} and offset k_{s1200}.

A first-order model was fitted to the data to determine which components had significant effects on ln[k_{neck}]. Al_2O_3, B_2O_3, Cr_2O_3, Fe_2O_3, K_2O, Li_2O, Na_2O, P_2O_5, SiO_2, V_2O_5, ZnO, and ZrO_2 were found to have significant effects. A PQM was developed using stepwise regression, where these second-order terms were found to improve the model statistics: Al_2O_3×P_2O_5, B_2O_3×CaO,

Cr_2O_3×Li_2O, Fe_2O_3×SiO_2. This model was found to have the best fit statistics without overfitting with an R^2 = 0.8106. The model coefficients are reported in Table 2.13. The predicted values are compared to measured values in Figure 2.10.

Table 2.13. Coefficients and summary statistics for ln[k_{neck}, inch] 1200 °C only model with composition in normalized mole fractions.

Term	Coefficient		Statistic	Value
k_{S1200}	0.3653599		# of data points	483
Al_2O_3	-24.61027		# of terms	19
B_2O_3	0.16605		Mean ln[k_{neck}, in]	-3.7570
CaO	11.07139		R^2_{fit}	0.8106
Cr_2O_3	-137.8960		R^2_{Adj}	0.8032
Fe_2O_3	-68.68653		R^2_{press}	0.7846
K_2O	13.41772		R^2_{kfold}	0.7837
Li_2O	15.11487		$RMSE_{fit}$, ln[in]	0.4497
Na_2O	16.11636		$RMSE_{press}$, ln[in]	0.4705
P_2O_5	-107.31320		Pooled SD, static only[(a)], ln[in]	0.3976
SiO_2	-10.93691		Pooled SD, bubbled only, ln[in]	0.3311
V_2O_5	-38.01927		Pooled SD, static + bubbled, ln[in]	0.3401
ZnO	-21.20798			
ZrO_2	-15.43288			
Others	-2.66029			
B_2O_3×CaO	-66.68789			
Cr_2O_3×Li_2O	-2498.1200			
Al_2O_3×P_2O_5	917.07597			
Fe_2O_3×SiO_2	145.07897			

(a) The pooled SD for static conditions only contains 4 degrees of freedom compared to the 28 for bubbled conditions and spans 6- and 7-day durations.

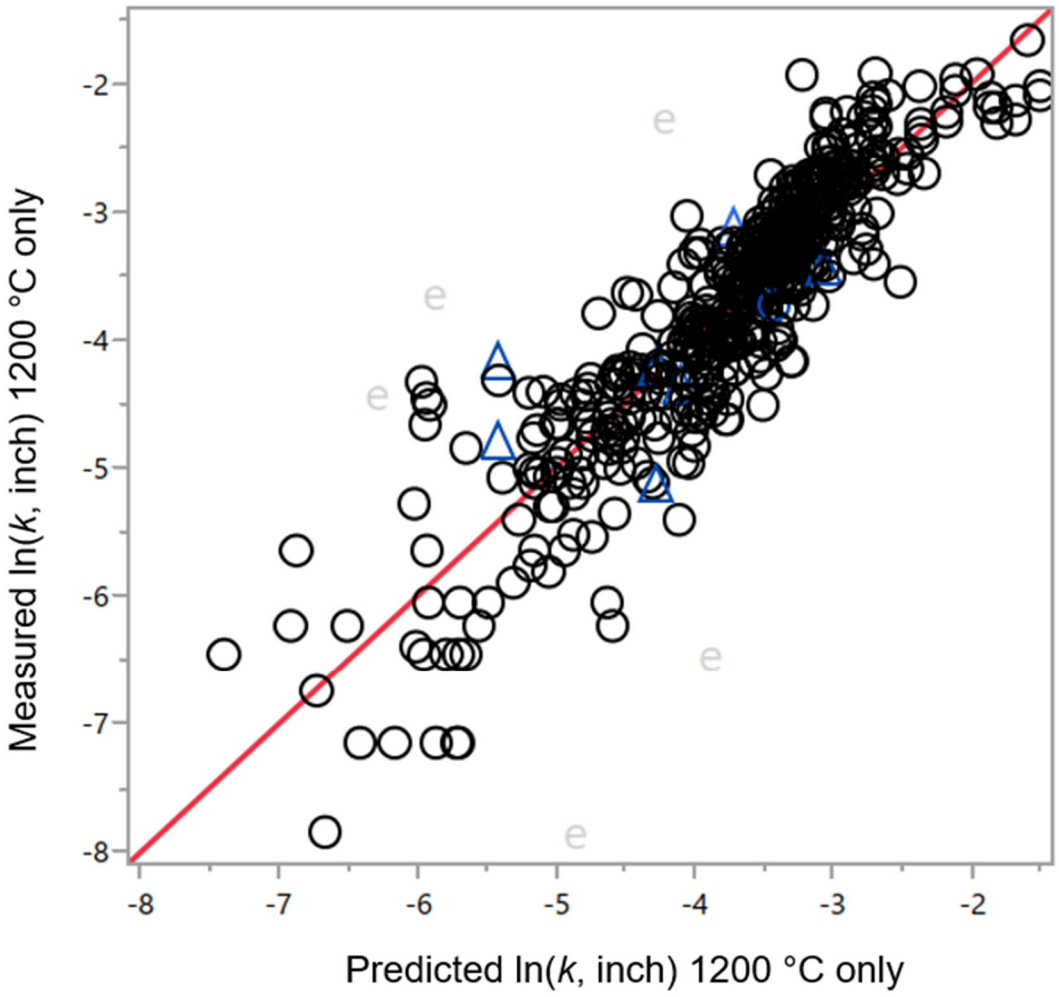

Figure 2.10. Predicted vs. measured ln[k_{neck}, in.] of the 1200 °C only model. Blue triangles represent composition extreme included in the modeling dataset, letter e represent outliers listed in Table 2.11, and gray circles represent the remainder of the data.

Composition effects on ln[k_{neck}] are shown in Figure 2.11. As previously reported, Na_2O, K_2O, and Li_2O most strongly increase ln[k_{neck}] while Cr_2O_3, P_2O_5, V_2O_5, Al_2O_3, ZnO, ZrO_2, and SiO_2 most strongly decrease ln[k_{neck}]. The effect of V_2O_5 on strongly reducing ln[k_{neck}] is not yet understood and requires further investigation.

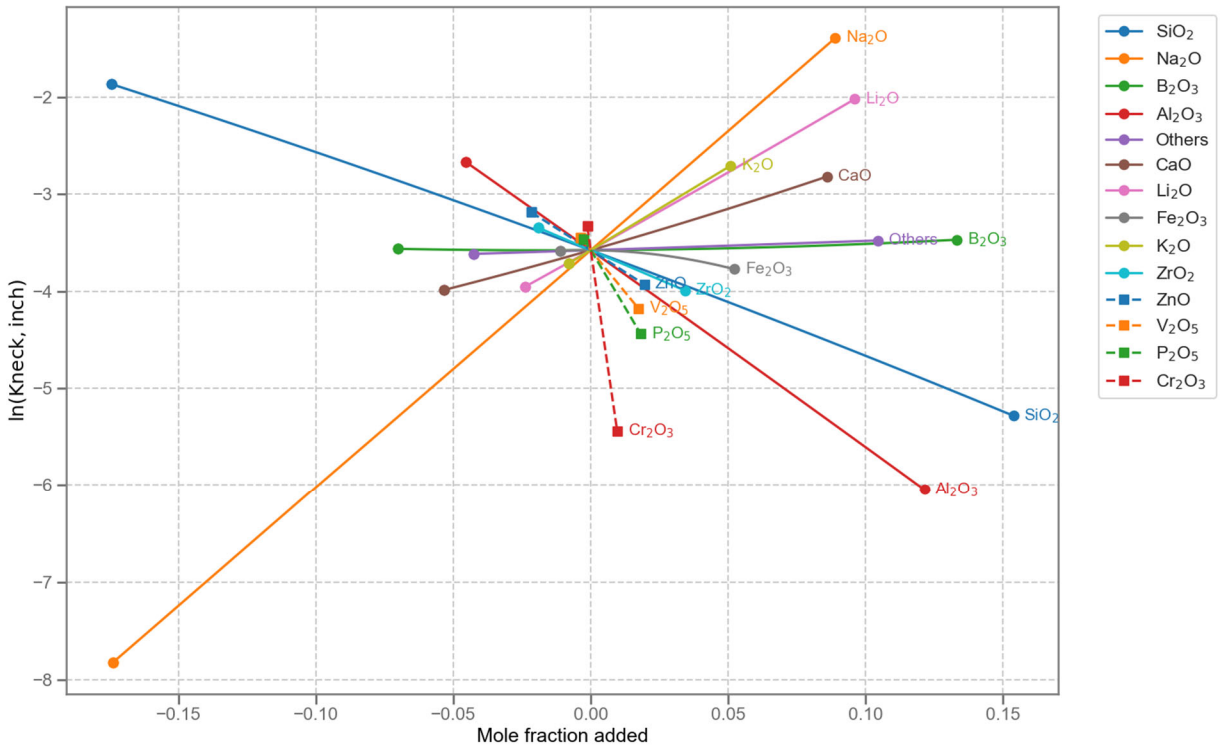

Figure 2.11. Component effects on ln[k_{neck}, inch] at 1200 °C.

2.4 P_2O_5-Bearing Phases Liquidus Temperature

Phosphate in the waste can result in the formation of a range of P-containing crystalline phases during melting process. A cold cap constituted by P-containing crystalline phases (e.g., apatites) may be detrimental to melter performance by slowing the conversion of glass forming chemicals into molten glass (Bunnell 1988). To address melter processing concerns, a T_L model was developed that will enable formulations of glasses that avoid the formation of P-containing crystalline phases during the melting process.

2.4.1 Database

Available liquidus temperature data for P-containing crystalline phases (T_L-P) were compiled into a database, as summarized in Table 2.14. The database primarily includes glasses that formed apatites [$Ca_5(PO_4)_3(F,Cl)$]. Other phosphate-containing crystals in the database include lithium phosphate [Li_3PO_4], sodium calcium phosphate [$NaCaPO_4$], zirconium phosphate [$Zr_2P_2O_7$], and rare-earth phosphates [e.g., $NdPO_4$]. Four glasses were excluded as outliers (listed in Table 2.15) during model development because studentized residual exceeded the Bonferroni 95% limit. A total of 175 glasses were compiled. Table 2.16 presents the ranges of measured T_L-P values and the range of each component concentration.

Table 2.14. Phosphate T_L data summary.

Lab/Study	# of Data	Reference
PNNL/P-Sol	9	Bai et al. (2025)
PNNL/EWG-OL	3	Russell et al. (2018)
PNNL/HLW-APPS	1	Gervasio et al. (2024)
PNNL/HLW-APPS2	2	Russell et al. (2025a)
PNNL/HAL24M1	10	Russell et al. (2025b)
PNNL/HAL24M2	5	Russell et al. (2025b)
PNNL/HS24	18	Unpublished [EWG-DP-339]
INEEL/IG1	12	Staples et al. (1999)
INEEL/IG2	11	Staples et al. (2000)
INEEL/IG3	1	Scholes et al. (2000)
INEEL/SBW1	15	Scholes et al. (2002)
VSL/HLW-E-Al; HLW-ANa	4	Matlack et al. (2007)
VSL/HLW-BP	8	Kot et al. (2007)
VSL/HLW07	1	Kot et al. (2007)
VSL/HLW-E-Bi	4	Muller et al. (2012)
VSL/HLWS	13	Matlack et al. (2012)
VSL/HWBi	15	Gan et al. (2012)
VSL/HWI-Al	3	Muller et al. (2012)
VSL/HLWS	11	Matlack et al. (2013)
VSL/HLW13	5	Kot et al. (2014)
VSL/HLW13A	6	Kot et al. (2014)
VSL/HLW14	10	Kot et al. (2015)
VSL/HLW-CP	8	Gan et al. (2015)
Total	175	

INEEL = Idaho National Engineering and Environmental Laboratory

Table 2.15. List of glasses excluded from phosphate T_L model development.

Glass	Study	Reason
HAL24M1-27	EWG-CCP-291 Rev1	Studentized residual outside the 95% simultaneous Bonferroni limits
HS24-27	EWG-DP-339	Studentized residual outside the 95% simultaneous Bonferroni limits
HS24-39	EWG-DP-339	Studentized residual outside the 95% simultaneous Bonferroni limits
HS24-50	EWG-DP-339	Studentized residual outside the 95% simultaneous Bonferroni limits
Total	4	

Table 2.16. Component range in glass (mass fraction) and T_L-P (°C) range for data used in model development.

Oxide	Min	Mean	Median	Max
Al_2O_3	0.0101	0.1296	0.1210	0.2721
B_2O_3	0.0405	0.1276	0.1209	0.2266
CaO	0.0004	0.0397	0.0379	0.1421
Cr_2O_3	0.0000	0.0051	0.0036	0.0248
Li_2O	0.0000	0.0264	0.0259	0.0676
Na_2O	0.0159	0.1167	0.1154	0.2055
P_2O_5	0.0064	0.0303	0.0298	0.1017
SiO_2	0.2146	0.3744	0.3785	0.5483
ZrO_2	0.0000	0.0201	0.0120	0.1051
Others[(a)]	0.0025	0.1301	0.1206	0.3789
T_L-P (C°)	783	993	979	1373

(a) Others = Sum of remaining components: Ag_2O, CdO, Ce_2O_3, Cl, Cs_2O, CuO, F, Fe_2O_3, HfO_2, I, K_2O, La_2O_3, MgO, MnO, MoO_3, Nd_2O_3, NiO, PbO, RuO_2, SO_3, SnO_2, Tl_2O_3, ThO_2, TiO_2, UO_3, V_2O_5, WO_3, Y_2O_3, ZnO.

2.4.2 Model

The model terms were first selected based on the evaluation of range and distribution of the major glass components. Then, a linear stepwise regression model with k-fold optimization was used to further screen the significant model terms: $T_L = \sum_{i=1}^{n} c_i g_i$, where c_i is the coefficient of the i^{th} first-order component term, n is the total number of components fitted in the model, and g_i is the target mass fraction of the corresponding component.

The major glass components of Al_2O_3, B_2O_3, Na_2O, and SiO_2 were locked in as model terms and the following components were found to have a high significance: CaO, Li_2O, Cr_2O_3, P_2O_5, and ZrO_2. This first-order model resulted in an $R^2 = 0.6781$ and an RMSE = 63.5581 °C. A PQM model was developed with all the selected first-order terms along with second-order terms (CaO×CaO, Li_2O×Li_2O, CaO×Na_2O, and CaO×SiO_2):

$$T_L = \sum_{i=1}^{n} c_i g_i + \sum_{i=1}^{n-1} \sum_{j \geq i}^{n} c_{ij} g_i g_j \quad (2.6)$$

where c_{ij} is the quadratic (for i=j) or the cross-product (for i≠j) coefficient for the $g_i g_j$ term. This model provides the best fit statistics without overfitting. Four datapoints (HAL24M1-27, HS24-27, HS24-39, and HS24-50) were found to be outliers with a studentized residual outside the 95% simultaneous Bonferroni limits and were removed from the fit. The PQM model has the fitted $R^2 = 0.7897$, a k-fold validation (k=5) $R^2 = 0.7293$, and the press $R^2 = 0.7461$. Coefficients for the PQM model are given in Table 2.17. The predicted values are compared to measured values in Figure 2.12.

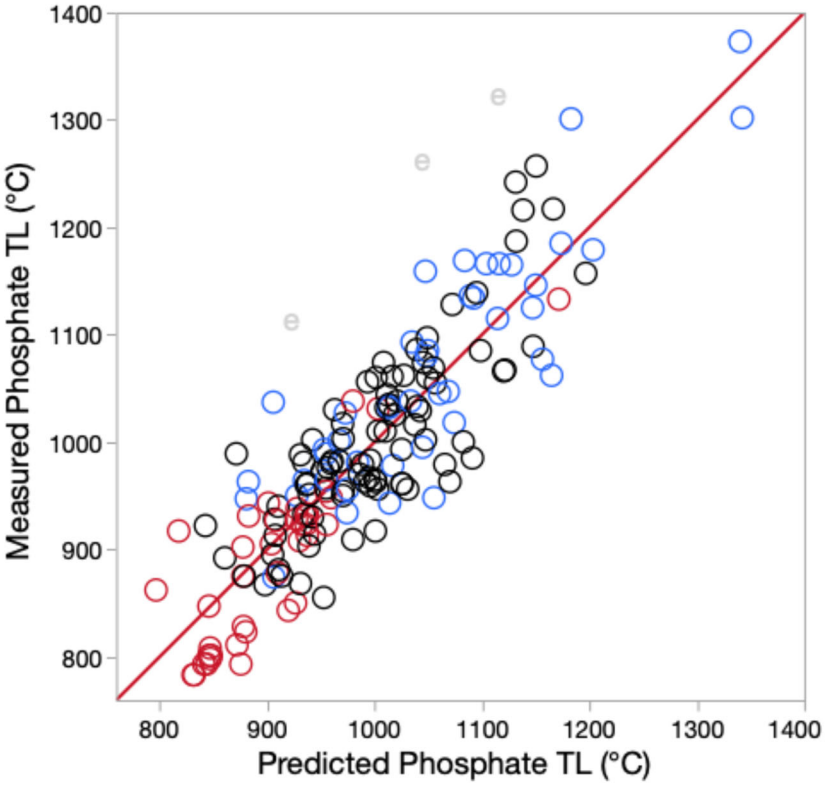

Figure 2.12. Predicted vs. measured T_L-P. Blue circles represent the PNNL glass data, black circles represent VSL glass data, and red circles represent INEEL glass data. The letter e represents excluded glasses.

Table 2.17. Model coefficient for the T_L-P model.

Term	Coefficient		Statistic	Value
Al_2O_3	1605.654		n	171
B_2O_3	791.3178		p	14
CaO	4912.843		Mean T_L-P	992.7427
Cr_2O_3	4858.988		R^2_{fit}	0.7897
Li_2O	-6899.74		R^2_{Adj}	0.7723
Na_2O	-855.214		R^2_{press}	0.7461
P_2O_5	3053.068		$RMSE_{fit}$, °C	52.0225
SiO_2	1366.154		$RMSE_{press}$, °C	54.9390
ZrO_2	1709.101		Pooled SD	(a)
Others	722.1695			
CaO×CaO	-16153.9			
Li_2O×Li_2O	69727.25			
CaO×Na_2O	23311.02			
CaO×SiO_2	-8226.47			

(a) Not enough replicate data to calculate pooled SD.

Figure 2.13 shows the component impact on the T_L-P model. T_L-P is highly increased by Cr_2O_3, P_2O_5, CaO, Al_2O_3, and ZrO_2, while Li_2O strongly decreased the T_L-P. This is consistent with the difference between magnitude and sign of the coefficient values in Table 2.17. Impacts from SiO_2, CaO, Na_2O and Li_2O were found to be non-linear, potentially due to changes in primary phases between Li-phosphates, NaCa-phosphates, and fluorapatites.

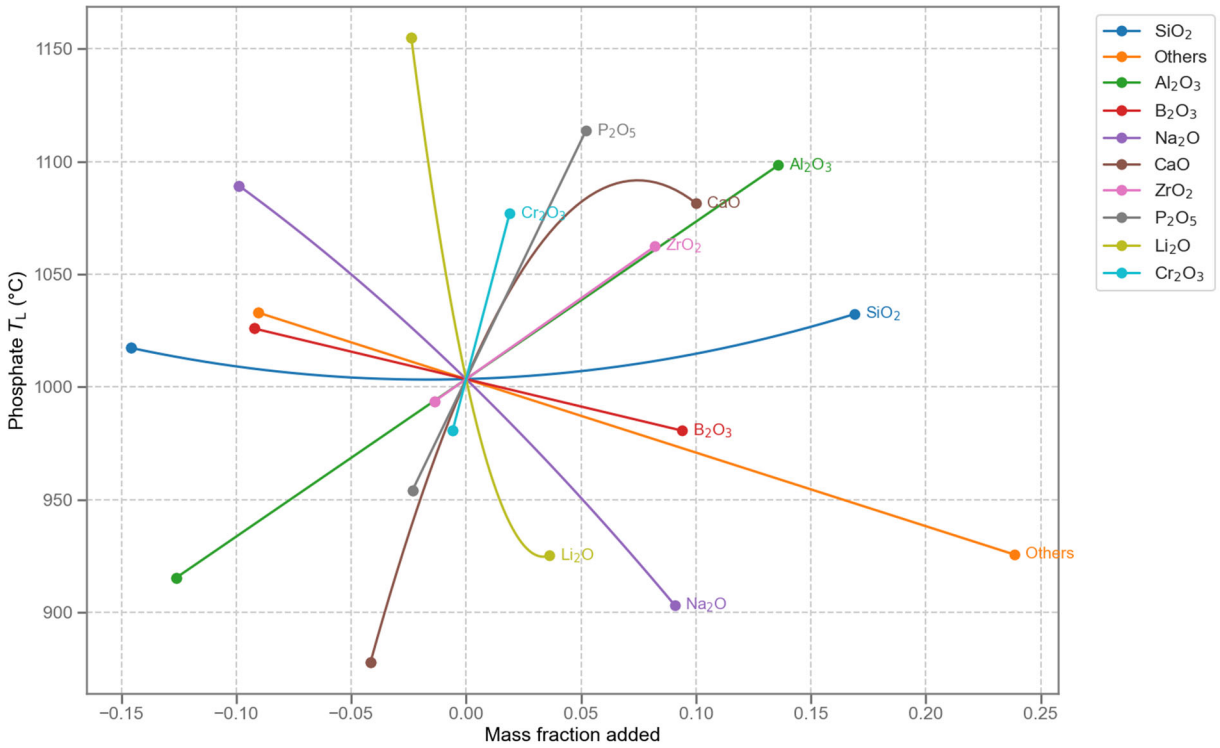

Figure 2.13. Component effects on T_L-P model.

2.5 ZrO_2-Bearing Phases Liquidus Temperature

Zirconium-bearing crystalline phases can settle in the melter, leading to processing upsets. To address melter processing concerns, a T_L-Zr model was developed that will enable formulations of glasses to avoid the formation of Zr-containing crystalline phases during the melting process.

2.5.1 Database

Available T_L data for Zr-containing crystalline phases were compiled into the database, as summarized in Table 2.18. The database includes glasses that formed primarily zircon ($ZrSiO_4$), baddeleyite (ZrO_2), wadeite ($K_2ZrSi_3O_9$), zektzerite ($NaLiZrSi_6O_{15}$), vlasovite ($Na_2ZrSi_4O_{11}$), or parakeldyshite ($Na_2ZrSi_2O_7$) measured by X-ray diffraction or scanning electron microscopy of glasses tested through various methods, including gradient furnace measurements and isothermal heat treatment. Table 2.19 lists the range of each component concentration.

Table 2.18. T_L-Zr data summary.

Study	Lab	# of Data	Reference
Hanford CVS	PNNL	13	Hrma et al. (1994); Vienna et al. (1996)
INEEL CVS phase 1	INL	5	Staples et al. (1999)
INEEL CVS phase 2	INL	5	Staples et al. (2000)
INEEL CVS phase 3	PNNL	3	Staples et al. (2000)
SP	PNNL	2	Mika et al. (1997)
TRU	PNNL	41	Crum et al. (1996)
PNNL Zr	PNNL	28	Vienna et al. (2000)
VSL HLW03	VSL	1	Piepel et al. (2007, 2008)
VSL HLW05	VSL	3	Kot et al. (2005)
VSL ALG	VSL	1	Kot et al. (2006b)
VSL HLW06	VSL	1	Kot et al. (2005)
SBW1	INL	1	Scholes et al. (2002)
VSL HLW07	VSL	4	Piepel et al. (2008)
HFGI	PNNL	5	Russell et al. (2023)
HAIG	PNNL	4	Russell et al. (2025b)
HAL24	PNNL	7	Russell et al. (2025c)
Total		124	

INL = Idaho National Laboratory

Table 2.19. Range of glass data used in the T_L-Zr model development, mass fraction.

Oxide	Min	Mean	Median	Max
Al_2O_3	0.0000	0.0562	0.0375	0.2857
B_2O_3	0.0000	0.0932	0.0822	0.2240
Cr_2O_3	0.0000	0.0022	0.0014	0.0127
F	0.0000	0.0041	0.0031	0.0652
Fe_2O_3	0.0000	0.0296	0.0397	0.1800
K_2O	0.0000	0.0062	0.0028	0.0750
Li_2O	0.0000	0.0511	0.0492	0.0901
MgO	0.0000	0.0032	0.0021	0.0800
MnO	0.0000	0.0076	0.0014	0.0677
Na_2O	0.0362	0.1174	0.1119	0.2382
SiO_2	0.2287	0.4527	0.4660	0.5957
ThO_2	0.0000	0.0012	0.0000	0.0441
UO_3	0.0000	0.0025	0.0000	0.0650
ZrO_2	0.0269	0.1073	0.1081	0.1650
Others	0.0039	0.0654	0.0791	0.1886

2.5.2 Model

The model terms were first selected based on the evaluation of range and distribution of the major glass components. Then, a linear stepwise regression model with k-fold optimization was used to further screen the significant model terms: $T_L = \sum_{i=1}^{n} c_i g_i$, where c_i is the coefficient of the i^{th} first-order component term, n is the total number of components fitted in the model, and g_i is the target mass fraction of the corresponding component. Al_2O_3, B_2O_3, Cr_2O_3, F, Fe_2O_3, K_2O,

Li_2O, MgO, MnO, Na_2O, SiO_2, ThO_2, UO_3, and ZrO_2 were found to have significant effects. A PQM was developed using stepwise regression, where these second-order terms were found to improve the model statistics: $B_2O_3 \times K_2O$ and $Na_2O \times Na_2O$:

$$T_L = \sum_{i=1}^{n} c_i g_i + \sum_{i=1}^{n-1} \sum_{j \geq i}^{n} c_{ij} g_i g_j \quad (2.7)$$

where c_{ij} is the coefficient for quadratic (for $i=j$) and the cross-product (for $i \neq j$) term $g_i g_j$. Glasses with T_L values being higher or less than a value (e.g., for glasses that did not form crystals at lower temperatures or required impractically long heat-treatment durations to reach equilibrium, the T_L was reported as being less than a certain temperature such as T_L < 850 °C. In other cases, for glasses in which increasing the temperature did not reduce the amount of crystalline phase formed, likely due to compositional changes from volatilization at elevated temperatures, the T_L was reported as greater than a certain temperature such as T_L > 1250 °C), and ZrO_2 concentration in glass < 2.2 wt%, were identified as outliers during model development. This model was found to have the best fit statistics without overfitting with an R^2 = 0.851. The model coefficients are reported in Table 2.20. The predicted values are compared to measured values in Figure 2.14.

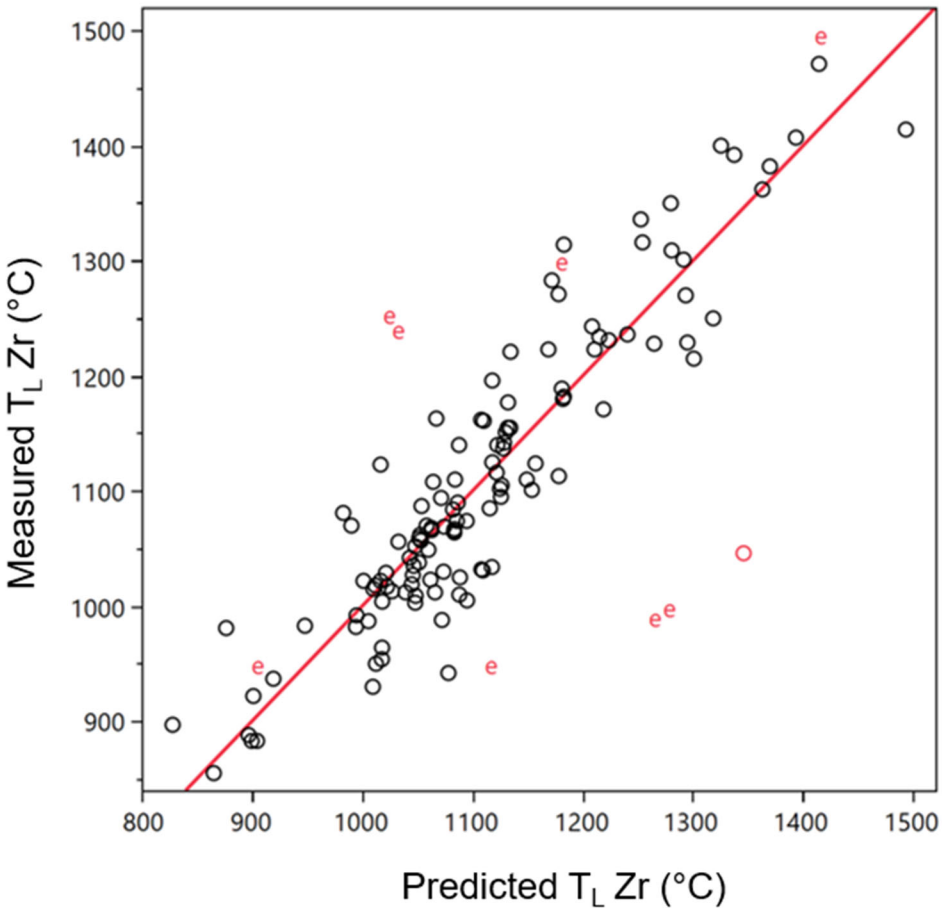

Figure 2.14. Predicted vs. measured T_L-Zr °C. Black circles represent the remainder of the data, and the red letter e represents outliers.

Table 2.20. Model coefficient for the T_L-Zr model.

Term	Coefficient		Statistic	Value
Al_2O_3	3397.7986		# of data points	124
B_2O_3	529.04867		# of terms	17
Cr_2O_3	4197.4839		Mean T_L-Zr, °C	1107.79
F	-4115.637		R^2_{fit}	0.8511
Fe_2O_3	2785.8568		R^2_{Adj}	0.8288
K_2O	11999.349		R^2_{press}	0.7848
Li_2O	-1624.633		$RMSE_{fit}$, °C	52.3799
MgO	3300.3993		$RMSE_{press}$, °C	58.7227
MnO	-828.6816		Pooled SD T_L-Zr, °C	11.9
Na_2O	-5334.063			
SiO_2	1050.8203			
ThO_2	8022.9858			
UO_3	-742.5985			
ZrO_2	5205.7163			
Others	1779.0088			
$B_2O_3 \times K_2O$	-105157.6			
$Na_2O \times Na_2O$	21008.977			

Composition effects on *T_L-Zr* are shown in Figure 2.15. As previously reported, ZrO_2, Al_2O_3, MgO, and ThO_2 strongly increase T_L-Zr while Li_2O and B_2O_3 decrease T_L-Zr. Unexpected impacts include:

- The non-linear impact of Na_2O, which presumably increases T_L-Zr of alkali-containing phases such as zektzerite, vlasovite, parakeldyshite, and potentially wadeite.
- The positive effects of Fe_2O_3 and Cr_2O_3 on T_L-Zr.
- The negative effects of F, MnO, and UO_3 on T_L-Zr.

Further investigation is needed to determine if these are real effects and, if so, what chemical phenomena is causing this impact.

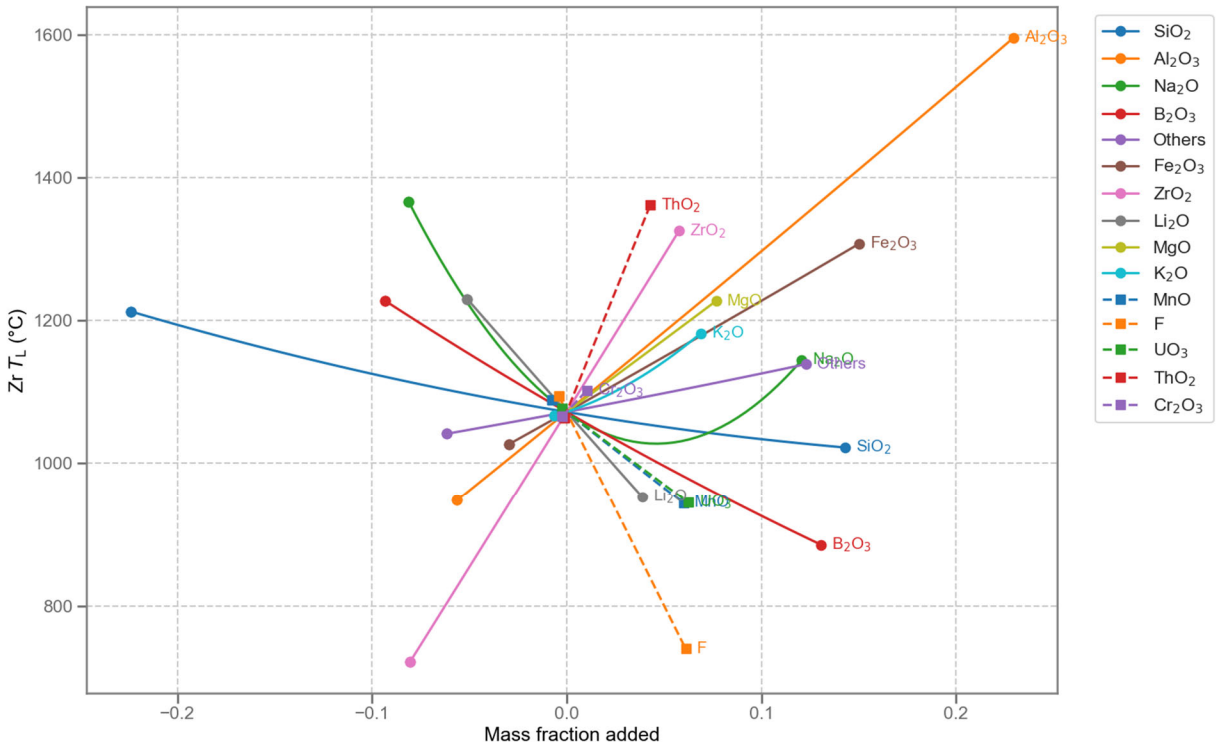

Figure 2.15. Component effects on T_L-Zr model.

2.6 Spinel C_{950} (vol%)

Spinel crystalline phases can settle in the melter leading to processing upsets. To address melter processing concerns, a model with a spinel volume percent concentration at 950 °C (C_{950}) was developed that will enable formulations of glasses that avoid the accumulation of spinel during the melting process.

2.6.1 Database

Available data for vol% spinel interpolated to 950 °C for combined transition metal spinel phases, C_{950}-Sp, were compiled into a database, as summarized in Table 2.21. The database includes glasses that formed spinels measured by X-ray diffraction or scanning electron microscopy of glasses tested through various methods, including gradient furnace measurements and isothermal heat treatment. Table 2.22 lists the 11 outliers removed during the model development. Table 2.23 lists the range of each component concentration. Glasses that did not crystallize spinel provided either negative or zero C_{950}-Sp values and were excluded from the database.

Table 2.21. C_{950}-Sp data summary.

Glass ID	Lab	# of Data	Reference
MS	PNNL	14	Hrma et al. (1999); Wilson et al. (2002)
SP	PNNL	11	Mika et al. (1997)
LSi	PNNL	28	Vienna et al. (2013)
SPA	PNNL	28	Vienna et al. (2013)
WTP-TL	PNNL	7	Vienna et al. (2003)
EM07	PNNL	38	Schweiger et al. (2011)
HAL24M1 and M2	PNNL	31	Russell et al. (2025b)
HLW-APPS2	PNNL	4	Russell et al. (2025a)
ICCM	SRNL/PNNL	3	Peeler et al. (2002)
AZ	PNNL	9	Peeler (2001), Vienna et al. (2013)
HWI	VSL	1	Matlack et al. (2008b)
HAL	PNNL	2	Schweiger et al. (2011)
HLW-E	VSL	1	Matlack et al. (2007)
Total		177	

Table 2.22. List of glasses excluded from C_{950}-Sp model development

Glass	Study	Reason
MS7-H-Ni	MS	High prediction uncertainty
SP-Mg-3	SP	Cooks D>0.1
LSi-Ni-025	LSi	Cooks D>0.1
SPA-01	SPA	Cooks D>0.09
ICCM-2	ICCM	Studentized residual outside the 95% simultaneous Bonferroni limits
WTP-TI-19	WTP-TL	Studentized residual outside the 95% simultaneous Bonferroni limits
WTP-TI-20	WTP-TL	High prediction uncertainty
WTP-TI-21	WTP-TL	Cooks D>0.1
WTP-TI-23	WTP-TL	Cooks D>0.09
WTP-TI-29	WTP-TL	Cooks D>0.1
HLW-APPS2-09	HLW-APPS2	Cooks D>0.1
Total	11	

Table 2.23. Range of glass data used in the C_{950}-Sp model development, mass fraction.

Oxide	Min	Mean	Median	Max
Al_2O_3	0.040	0.119	0.100	0.263
B_2O_3	0.030	0.106	0.097	0.238
CaO	0.000	0.012	0.001	0.099
Cr_2O_3	0.000	0.004	0.004	0.020
Fe_2O_3	0.000	0.102	0.110	0.200
K_2O	0.000	0.006	0.000	0.060
Li_2O	0.000	0.025	0.026	0.060
MgO	0.000	0.003	0.001	0.030
MnO	0.000	0.013	0.012	0.052
Na_2O	0.040	0.154	0.151	0.250
NiO	0.000	0.008	0.009	0.030
P_2O_5	0.000	0.009	0.005	0.040
SiO_2	0.218	0.373	0.371	0.502
SrO	0.000	0.008	0.002	0.086
ZnO	0.000	0.006	0.001	0.041
Other	0.011	0.052	0.045	0.145

2.6.2 Model

Literature was canvased and preliminary models were fitted to the data to determine the optimal model form. It was determined from both literature and preliminary fits that the best representation of this data set was a first order or PQM representation of C_{950}. The model terms were first selected based on the evaluation of range and distribution of the major glass components. Then, a linear stepwise regression model with k-fold optimization was used to further screen the significant model terms: $C_{950} = \sum_{i=1}^{n} c_i g_i$, where c_i is the coefficient of the i^{th} first-order component term, n is the total number of components fitted in the model, and g_i is the target mass fraction of the corresponding component, i. Al_2O_3, B_2O_3, CaO, Cr_2O_3, Fe_2O_3, K_2O, Li_2O, MgO, MnO, Na_2O, NiO, P_2O_5, SiO_2, SrO, and ZnO were found to have significant effects. A PQM was developed using stepwise regression, where the second-order terms that were found to improve the model statistics were Fe_2O_3×NiO, MnO×SiO_2, and Na_2O×SiO_2:

$$C_{950} = \sum_{i=1}^{n} c_i g_i + \sum_{i=1}^{n-1} \sum_{j \geq i}^{n} c_{ij} g_i g_j \quad (2.8)$$

where c_{ij} is the quadratic (for i = j)) or cross-product (for i ≠ j) term $g_i g_j$. This model was found to have the best fit statistics without overfitting with an R^2 = 0.845. The model coefficients are reported in Table 2.24. The predicted values are compared to measured values in Figure 2.16.

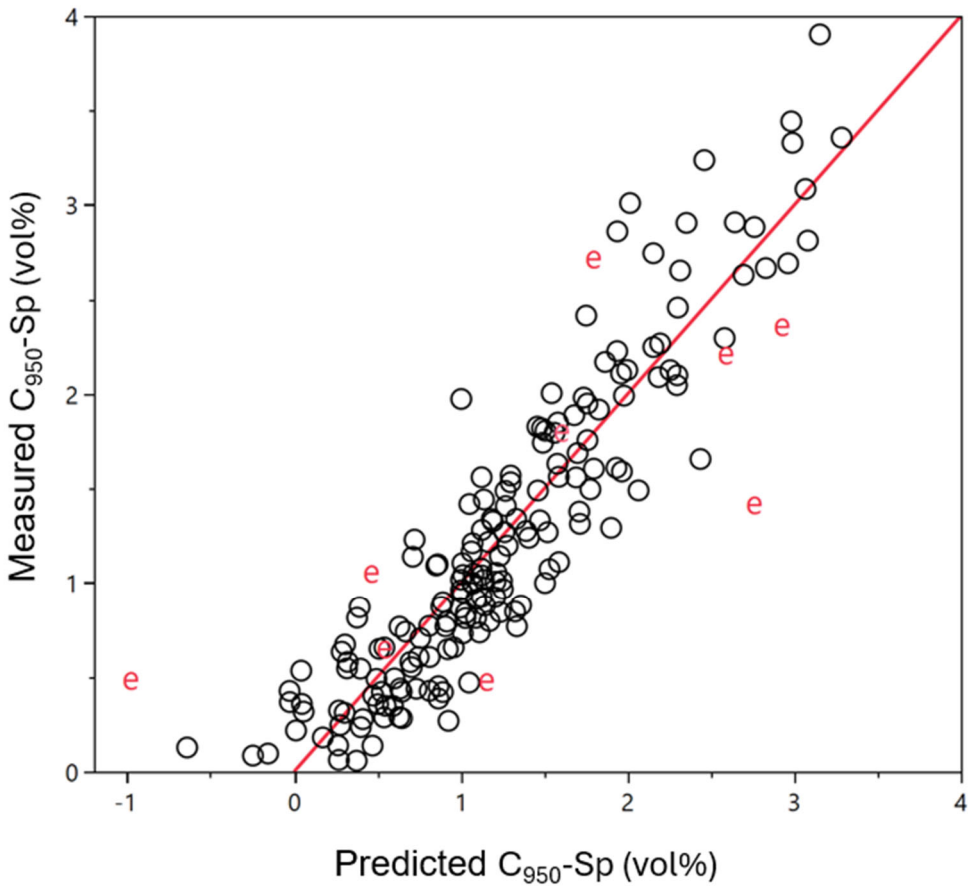

Figure 2.16. Predicted vs. measured C_{950}-Sp, vol%. Red letter e represents outliers and black circles represent the remainder of the data.

Table 2.24. Model coefficient for the C_{950}-Sp model.

Term	Coefficient		Statistic	Value
Al_2O_3	10.360389		# of data	177
B_2O_3	-11.04108		# of terms	19
CaO	-6.715472		Mean C_{950}-Sp, vol%	1.237
Cr_2O_3	23.123787		R^2_{fit}	0.845
Fe_2O_3	3.7262283		R^2_{Adj}	0.828
K_2O	-10.18084		R^2_{press}	0.793
Li_2O	-10.2127		$RMSE_{fit}$, vol%	0.341
MgO	10.621785		$RMSE_{press}$, vol%	0.374
MnO	167.76131		Pooled C_{950}-Sp SD, vol%	0.191
Na_2O	5.4137964			
NiO	-42.07507			
P_2O_5	-9.249847			
SiO_2	7.8530857			
SrO	-11.38285			
ZnO	11.757514			
Other	-2.608834			
Fe_2O_3 × NiO	1015.577			
MnO × SiO_2	-386.1018			
Na_2O × SiO_2	-56.45335			

Figure 2.17 displays the component effects on C_{950}-Sp. C_{950}-Sp is increased significantly by spinel-forming components: Cr_2O_3, NiO, ZnO, MnO, MgO, Fe_2O_3, ZnO, and Al_2O_3. C_{950}-Sp is significantly decreased by Na_2O, B_2O_3, K_2O, CaO, Li_2O, and P_2O_5. These impacts have been widely reported and were expected. More surprisingly is the strong negative effect of SrO. Removal of this term significantly reduced model predictability. Previous studies found the opposite effect of SrO on spinel formation since SrO can enter spinel structures (Vienna et al. 2025). This SrO effect warrants further evaluation.

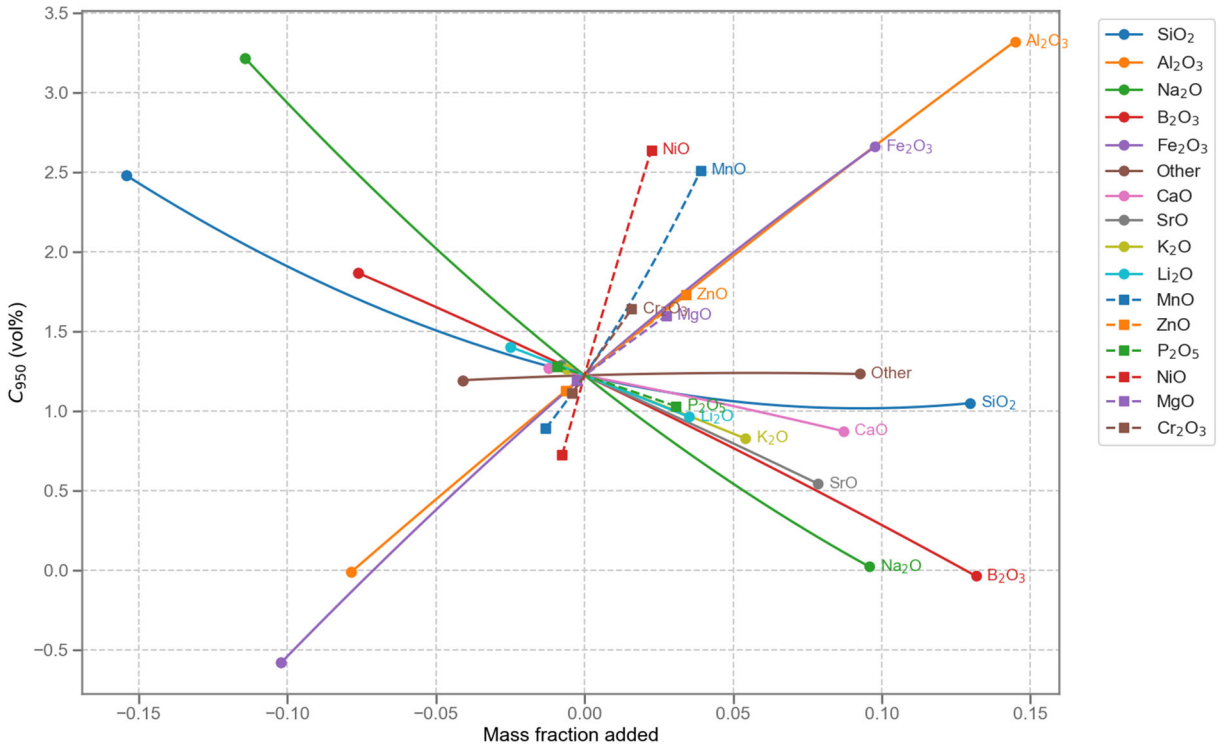

Figure 2.17. Component effects on C_{950}-Sp model.

2.7 Product Consistent Test

Acceptance of glass for repository disposal is evaluated using ASTM C1285, Method A, also known as the product consistency test (PCT). The WTP contract (DOE 2000) and the Waste Acceptance Product Specification (DOE 1996) state that PCT response in terms of normalized concentration (NC) NC_B, NC_{Na}, and NC_{Li} must be below the associated values of the Defense Waste Processing Facility (DWPF) Environmental Assessment (EA) glass determined by Jantzen et al. (1993). These values are reported in Table 2.26.

Table 2.25. WTP PCT normalized release limits for HLW glass (g/L), Jantzen et al. (1993)

Constraint Description	Value	Logarithm Value
PCT normalized B release	NC_B <16.70 (g/L)	ln(NC_B, g/L) <2.82
PCT normalized Li release	NC_{Li} <9.57 (g/L)	ln(NC_{Li}, g/L) <2.26
PCT normalized Na release	NC_{Na} <13.35 (g/L)	ln(NC_{Na}, g/L) <2.59

2.7.1 Database

The database contains glasses developed to study a wide range of potential LAW and HLW waste streams including many data from SRNL ComPro database (Johnson and Hsieh 2025; Hsieh and Johnson 2025), summarized in Table 2.26. A total of 19 glasses, shown in Table 2.27, were excluded from the final model fit because of high studentized residuals ≥ 3. Table 2.28 lists the range of each component concentration.

Table 2.26. PCT data summary.

Study Name	Lab	# of Data	Reference
APPS2	PNNL	16	Russell et al. (2025a)
HAL24M1 and HAL24M2	PNNL	50	Russell et al. (2025b)
LAWML2	PNNL	17	Unpublished [EWG-CCP-279]
WVDP Support	PNNL	20	Olson et al. (1994)
Hanford CVS1 and CVS2	PNNL	146	Hrma et al. (1994)
Hanford LLW Glass Formulation	PNNL	24	Feng et al. (1996)
Hanford CVS 3	PNNL	39	Vienna et al. (1996)
Zr Study	PNNL	28	Vienna et al. (2000)
INEEL SBW 1999	PNNL	3	Vienna et al. (1999)
INEEL DZr-CV Glasses	PNNL	24	Crum et al. (2001)
SBW Melter Glass Formulation	PNNL	25	Vienna et al. (2002)
ORP	PNNL	35	Russell et al. (2017)
Cold crucible induction melter PNNL 2010	PNNL	14	Kim et al. (2011)
ORP; EWG-LAW-PH2	PNNL	38	Russell et al. (2019a)
Pre. Frit Dev. Sludge Batch 6	SRNL	8	Fox et al. (2009)
Reduction of Constraints for Coupled Operation	SRNL	32	Raszewski and Edwards (2009)
Nepheline phase 3; DWPF	SRNL	29	Fox and Edwards (2009)
KT1, KT03 and KT04 Series for SCIX Impact on DWPF Glass Formulations	SRNL	38	Fox and Edwards (2010)
KT06 Series for SCIX Impact on DWPF Glass Formulations	SRNL	18	Fox and Edwards (2011a)
KT07 Series for SCIX Impact on DWPF Glass Formulations	SRNL	10	Fox and Edwards (2011b)
KT08 Series for SCIX Impact on DWPF Glass Formulations	SRNL	20	Fox and Edwards (2011c)
SB7a Glass Variability Study with Frit 418 and Frit 702	SRNL	28	Peeler and Edwards (2011)
SB7b Glass Variability Study	SRNL	34	Johnson and Edwards (2011)
Matrix 1 Results FY07 Enhanced DOE HLW Throughput Studies at SRNL	SRNL	37	Raszewski et al. (2008a)
Russian High Alumina - US; Rus	SRNL	45	Fox et al. (2008a)
Frit Development for Sludge Batch 5: Varying Aluminum Concentrations	SRNL	26	Fox et al. (2008b)
WTP	VSL	3	Muller et al. (2001)
WTP	VSL	2	Muller and Pegg (2003)
WTP	VSL	4	Muller et al. (2005)
ORP	VSL	1	Matlack et al. (2006)
VSL Enhanced HLW	VSL	5	Matlack et al. (2007); Muller et al. (2012)
HLWE-ANA	VSL	2	Muller et al. (2012)
Non-Durable Glasses	SRNL	29	Cozzi (2003); Cozzi et al. (2002)
Frit Selection to Support SMK Testing with SRNL Feeds	SRNL	16	Gillam et al. (2007)
Assessment of Sludge Variation on Frit 202-A11 SB3 Glasses	SRNL	30	Peeler et al. (2007)
DWPF; Refinement of the Nepheline Discriminator: Results of Phase I Study	SRNL	39	Fox et al. (2007)

Study Name	Lab	# of Data	Reference
Initial Sludge Batch 4 Tank 40 Decant Variability Study with Frit 510	SRNL	18	Raszewski et al. (2008b)
Variability Study with Frit 510 to Support a Second Tank 40 Decant	SRNL	9	Raszewski et al. (2008c)
Tank 40 Only-SB2 VS Frit 200	SRNL	60	Harbour et al. (2000)
ROC Phase 1	SRNL	24	Peeler (2001)
FY01 PHA glasses	SRNL	13	Edwards et al. (2001)
SB2 VS wt Frit 320 Glasses	SRNL	21	Herman (2002)
ROC Phase 1 Experimental	SRNL	34	Peeler (2002)
Dev. HLW	SRNL	15	Peeler et al. (2002)
SB3 VS Glasses	SRNL	42	Peeler et al. (2003)
Uranium/Thorium glasses	SRNL	13	Scholes et al. (2002)
SB3 Phase 2 VS - Redox	SRNL	12	Lorier (2004)
ADT Glasses	SRNL	8	Peeler (2004)

Table 2.27. List of glasses excluded from PCT model development.

Glass	Study	Reason
CVS1-9	Hanford CVS1	Studentized Residual ≥3
CVS2-21, CVS2-29, CVS2-30 and CVS2-82	Hanford CVS2	Studentized Residual ≥3
PEI	Hanford LLW Glass Formulation	Studentized Residual ≥3
SBW-13-18.5, SBW-23-15, SBW-23-18.5, SBW-23-20, and SBW-23-25	SBW Melter Glass Formulation	Studentized Residual ≥3
NEW-IL-42295 and NEW-OL-17130	EWG-LAW-PH1	Studentized Residual ≥3
LP2-OL-12	EWG-LAW-PH2	Studentized Residual ≥3
SB5NEPH-31 and SB5NEPH-33	Refinement of the Nepheline Discriminator: Results of Phase I Study; DWPF	Studentized Residual ≥3
RC-36	ROC Phase 1 Experimental	Studentized Residual ≥3
ND06 and ND19	Non-durable glasses	Studentized Residual ≥3
Total 19		

Table 2.28. Range of glass data used in PCT model development, molar fraction.

Oxide	Min	Median	Mean	Max
Al_2O_3	0.0000	0.0450	0.0539	0.3031
B_2O_3	0.0000	0.0758	0.0821	0.2430
BaO	0.0000	0.0001	0.0001	0.0013
CaO	0.0000	0.0127	0.0268	0.1747
CdO	0.0000	0.0000	0.0005	0.0072
Cl	0.0000	0.0000	0.0008	0.0220
F	0.0000	0.0000	0.0073	0.1853
Fe_2O_3	0.0000	0.0366	0.0347	0.0927
K_2O	0.0000	0.0005	0.0032	0.1500
Li_2O	0.0000	0.0820	0.0800	0.1893
LN_2O_3	0.0000	0.0001	0.0009	0.0237
MgO	0.0000	0.0078	0.0134	0.1324
MnO	0.0000	0.0087	0.0128	0.0767
Na_2O	0.0360	0.1427	0.1476	0.4312
NiO	0.0000	0.0040	0.0054	0.0444
P_2O_5	0.0000	0.0001	0.0018	0.0464
SiO_2	0.2004	0.5110	0.5002	0.6857
SO_3	0.0000	0.0017	0.0023	0.0201
TiO_2	0.0000	0.0001	0.0055	0.0732
V_2O_5	0.0000	0.0000	0.0011	0.0210
ZnO	0.0000	0.0002	0.0032	0.0426
ZrO_2	0.0000	0.0011	0.0093	0.0964
Others	0.0000	0.0051	0.0069	0.0784

2.7.2 Model

Based on the previous PCT model (Vienna et al. 2016) it was decided to model the average of the natural logarithms of NC_B, NC_{Li}, and NC_{Na} for each glass using mole fraction of components. The model terms were first selected based on the evaluation of range and distribution of the major glass components. Then, a linear stepwise regression model with k-fold optimization was used to further screen the significant model terms: $ln\ (NC, g \cdot L^{-1})_{ave} = \sum_{i=1}^{n} c_i x_i$, where c_i is the coefficient of the i^{th} first-order component term, n is the total number of components fitted in the model, and x_i is the target mole fraction of the corresponding component. Al_2O_3, B_2O_3, BaO, CaO, CdO, Cl, F, Fe_2O_3, K_2O, Li_2O, Ln_2O_3, MgO, MnO, Na_2O, NiO, P_2O_5, SO_3, SiO_2, TiO_2, V_2O_5, ZnO, and ZrO_2 were found to have significant effects. Stepwise regression was used to identify higher order terms that improved the model statistics (e.g., k-fold R^2), including $(Al_2O_3)^2$, $(Al_2O_3)^3$, $(Al_2O_3)^4$, $(B_2O_3)^2$, and $Al_2O_3 \times B_2O_3$:

$$ln\ (NC, g \cdot L^{-1})_{ave} = \sum_{i=1}^{n} c_i x_i + c_{Al2}\left(x_{Al_2O_3}\right)^2 + c_{B2}\left(x_{B_2O_3}\right)^2 + c_{AlB} x_{Al_2O_3} x_{B_2O_3} + c_{Al3}\left(x_{Al_2O_3}\right)^3 + c_{Al4}\left(x_{Al_2O_3}\right)^4 \quad (2.9)$$

where c_{Al2} and c_{B2} are the quadratic coefficients for Al_2O_3 and B_2O_3; c_{AlB} is the cross-product coefficient for Al_2O_3 and B_2O_3, and c_{Al3} and c_{Al4} are the cubic and quartic terms for Al_2O_3.

This model was found to have the best fit statistics without overfitting with an $R^2 = 0.7990$. Overfitting was avoided by maximizing the $R^2_{k\text{-fold}} = 0.7814$. The model coefficients are reported in Table 2.29. The predicted values are compared to measured values in Figure 2.18.

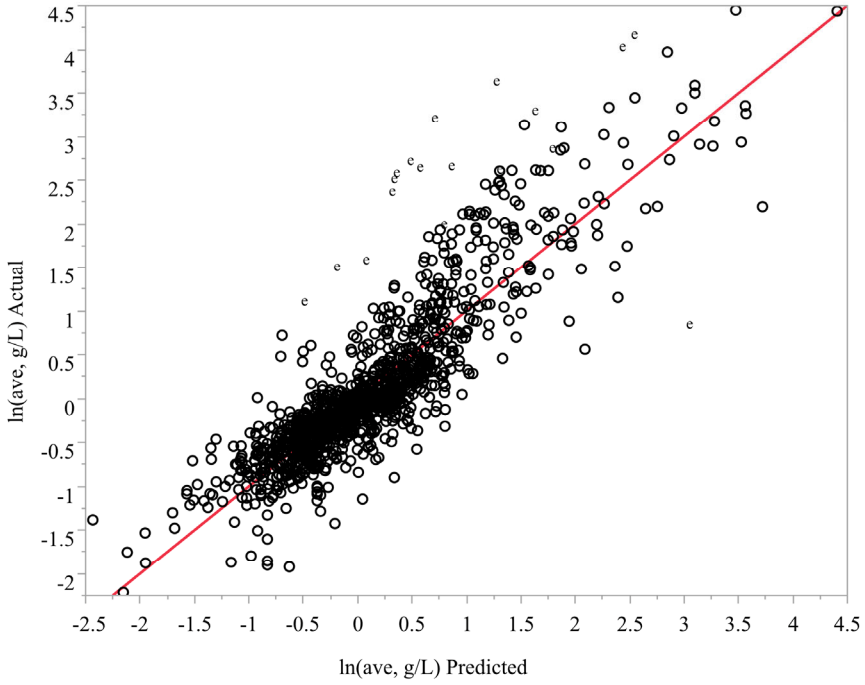

Figure 2.18. Actual vs. predicted PCT response in terms of ln(ave, g/L). Black circles are model fitting data and the letter e represents outliers (studentized residuals ≥ 3).

Table 2.29. Model coefficients for the PCT model, mole fraction basis.

Term	Coefficient		Statistic	Value
Al_2O_3	-72.36446		# of data points	1185
B_2O_3	-8.30549		# of model terms	28
CaO	-2.36054		Mean response, ln[g/L]	0.0917
Fe_2O_3	-1.57046		R^2_{fit}	0.7990
K_2O	13.04308		R^2_{Adj}	0.7943
Li_2O	9.21011		$R^2_{k\text{-}fold}$	0.7814
MgO	9.32147		$RMSE_{fit}$, ln[g/L]	0.4062
Na_2O	15.09132		$RMSE_{press}$, ln[g/L]	0.4189
NiO	5.72076		Pooled SD, ln(NC_B, g/L)	0.2494
P_2O_5	-1.70046		Pooled SD, ln(NC_{Na}, g/L)	0.2331
SiO_2	-2.26744			
ZrO_2	-10.20244			
BaO	-166.76860			
CdO	146.68384			
Cl	1.13345			
F	4.04883			
MnO	8.98148			
SO_3	6.01876			
TiO_2	-1.64115			
V_2O_5	17.68233			
ZnO	-0.01101			
LN_2O_3	10.43572			
Others	-2.92894			
$Al_2O_3 \times Al_2O_3$	746.8024			
$Al_2O_3 \times B_2O_3$	-70.0252			
$B_2O_3 \times B_2O_3$	107.3785			
$Al_2O_3 \times Al_2O_3 \times Al_2O_3$	-2874.8900			
$Al_2O_3 \times Al_2O_3 \times Al_2O_3 \times Al_2O_3$	3886.5322			

Composition effects on PCT response are shown in Figure 2.19. The components that have the largest linear effect on increasing the PCT response, listed in order of decreasing magnitude, are CdO, V_2O_5, Na_2O, K_2O, Ln_2O_3, MgO, Li_2O, and MnO. CdO has a strong effect on PCT response, which was unexpected based on past models. CdO is only a minor component, which means the overall effect was limited relative to the major glass components. The CdO term was included in the model because it improved the model R^2 by roughly 0.02 and $R^2_{k\text{-}fold}$ by 0.04. In the future, a more systematic study of CdO is needed to determine if the CdO effect is real or if it accounted for an unknown bias between datasets.

The components that decrease the PCT response, listed in order of decreasing magnitude, are Al_2O_3, ZrO_2, B_2O_3, CaO, SiO_2, and P_2O_5. In addition, non-linear effects were identified for Al_2O_3 and B_2O_3. Al_2O_3 had second-, third-, and fourth-order effects on PCT response, where additions up to roughly 4 mole% strongly decreased PCT response. Further additions of Al_2O_3 had a minimal effect on PCT response. The Al_2O_3 effects are consistent with literature reports (Vienna and Crum 2018; Reiser et al. 2021, 2022; Lu et al. 2021b). Additions of B_2O_3 showed a second-

order behavior where additions below 4 mol% decreased PCT response but further additions progressively increased the PCT response. The non-linear effect of boron is also observed previously [e.g., Vienna and Crum (2018)]. Lastly, a significant cross-product effect between Al_2O_3 and B_2O_3 was identified, where additions of Al_2O_3 and B_2O_3 together strongly decreased the PCT response.

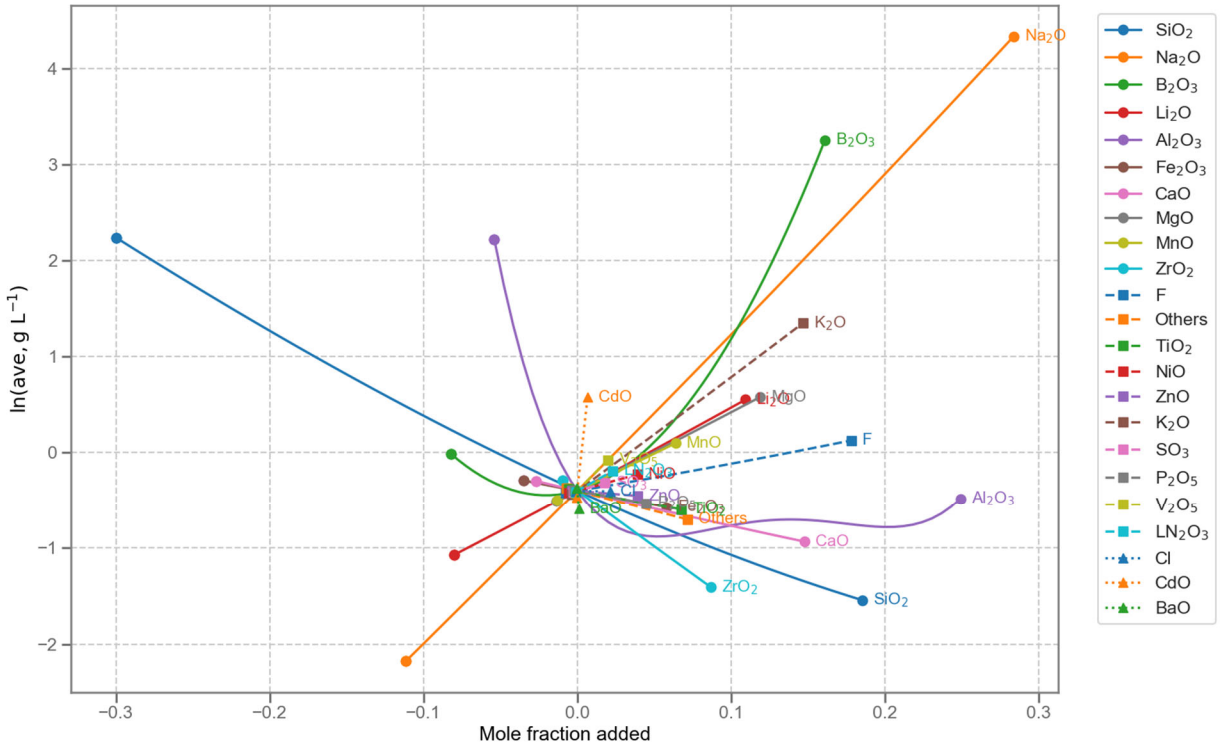

Figure 2.19. Component effects on PCT model.

2.8 Toxicity Characteristic Leaching Procedure

The U.S. Environmental Protection Agency toxicity characteristic leaching procedure (TCLP) is used to demonstrate that the underlying hazardous constituents of Hanford tank waste that are not represented in the high-level waste vitrification treatment standard are adequately protected to justify delisting of the glass (Blumenkranz 2006). The strategy for delisting is based in part on demonstrating that Hanford HLW glasses do not exceed the delisting limits described in Blumenkranz (2006). This includes developing a TCLP response vs. composition model and controlling the composition of glass such that performance-based criteria are not exceeded in production glasses.

2.8.1 Database

A database containing a total of 486 glasses with TCLP boron release data was compiled to support development of the TCLP model, as summarized in Table 2.30. Six glasses were excluded as outliers (listed in Table 2.31) during model development because the studentized residual exceeded the Bonferroni 95% limit. Table 2.32 presents the range of each component concentration.

Table 2.30. TCLP data summary.

Study	Lab	# of Data	Reference
Previous Model Dataset	PNNL	238	Kim and Vienna (2003)
WTP LAW	VSL	3	Kot et al. (2003); Muller et al. (2005)
WTP HLW Comparison	VSL	5	Kot et al. (2005b)
WTP LAW Comparison	VSL	1	Muller et al. (2003); Muller et al. (2005)
HLW02 Initial M	VSL	57	Piepel et al. (2008)
HLW03 Augmentation M	VSL	45	Piepel et al. (2008)
HLW98	VSL	21	Kot and Pegg (2001); Kot et al. (2003); Piepel et al. (2008)
WTP Regulatory Spike	VSL	12	Kot et al. (2003)
APPS	PNNL	14	Gervasio et al. (2023)
APPS2	PNNL	16	Russell et al. (2025a)
HAI24	PNNL	50	Russell et al. (2025b)
HAIG	PNNL	24	Russell et al. (2025c)
Total		486	

Table 2.31. Glasses excluded from TCLP model development.

Glass	Study	Reason
HAIG-21	HAIG	Studentized residual over 95% Bonferroni limits
LANL-8	LANL	Studentized residual over 95% Bonferroni limits
LANL-AE	LANL	Studentized residual over 95% Bonferroni limits
WETF-7	SRS LLMW	Studentized residual over 95% Bonferroni limits
HLW99-04	WTP HLW	Studentized residual over 95% Bonferroni limits
RFP-9	SRS LLMW	Studentized residual over 95% Bonferroni limits
Total	6	

Table 2.32. Range of glass data used in the TCLP model development, mole fraction.

Oxide	Min	Mean	Median	Max
Al_2O_3	0.0000	0.0436	0.0561	0.1989
B_2O_3	0.0165	0.1014	0.1077	0.2456
CaO	0.0000	0.0094	0.0326	0.3164
Fe_2O_3	0.0000	0.0255	0.0282	0.0845
K_2O	0.0000	0.0019	0.0057	0.1097
Li_2O	0.0000	0.0739	0.0716	0.2050
LN_2O_3	0.0000	0.0008	0.0022	0.0346
MgO	0.0000	0.0022	0.0165	0.1959
Na_2O	0.0000	0.1269	0.1317	0.2714
P_2O_5	0.0000	0.0023	0.0037	0.0231
SiO_2	0.2376	0.4758	0.4598	0.7524
ZnO	0.0000	0.0165	0.0121	0.0374
ZrO_2	0.0000	0.0154	0.0161	0.0908
Others	0.0004	0.0455	0.0560	0.2434

For each element *i (B*, *Ba*, *Cd*, *Ni*, *Zn*, etc.*)*, the normalized elemental release r_{ele} and its natural logarithm $ln(r_{ele})$ were calculated as:

$$\ln(r_{ele}) = \ln\left({}^{c_{ele}}/_{f_{ele}}\right) \quad (2.10)$$

where c_{ele} is the measured TCLP elemental release in the unit of mg/L and f_{ele} is the mass fraction of the element in the glass.

In many glass alteration tests, including TCLP, the response of boron can be used as an indicator of glass response. Figure 2.20 compares the $\ln(r_{ele})$ with $\ln(r_B)$. Figure 2.21 compares $\ln(r_B)$ with $\ln(r_{ele})$ for Cd, V and Cr after filtering out the glasses with low-concentration that are known to have high measurement uncertainty and instrument contamination challenges. This shows that r_B is a reliable estimator of r_{ele} for congruent components and also a conservative estimator for those components subject to solubility issues.

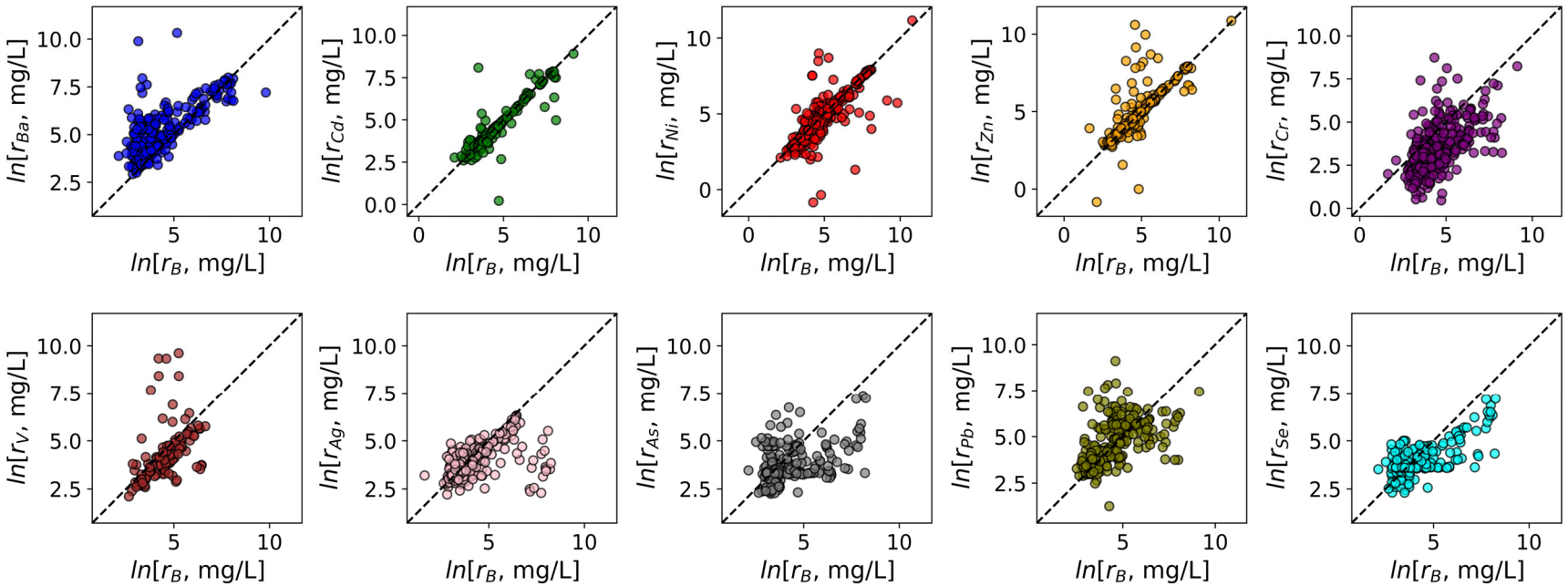

Figure 2.20. TCLP ln(r_B) response vs. ln(r_{Ba}, r_{Cd}, r_{Ni}, r_{Zn}, r_{Cr}, r_V, r_{Ag}, r_{As}, r_{Pb}, or r_{Se}) response (For Information Only).

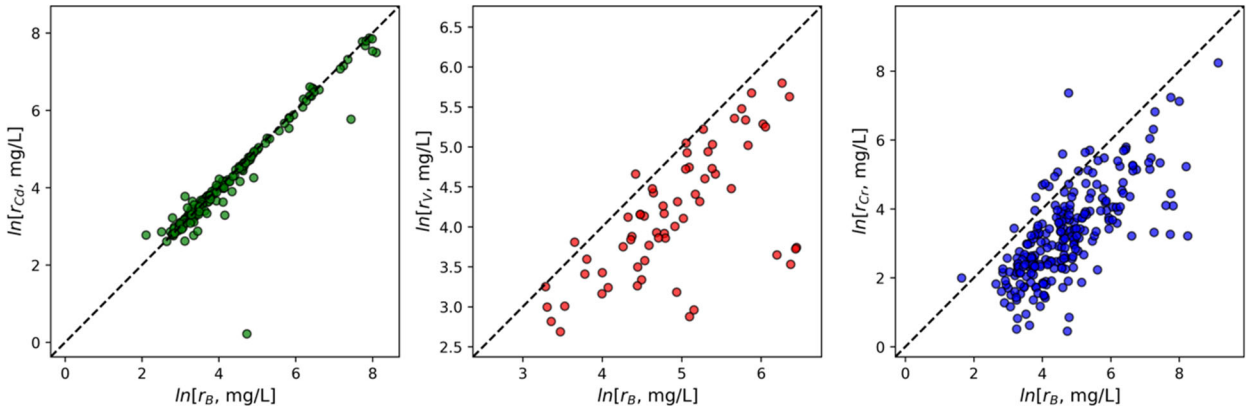

Figure 2.21. TCLP ln(r_B) response vs. ln(r_{Cd}, r_V, or r_{Cr}) response after filtering out glasses containing very small concentrations of CdO (≤ 0.05 wt%), V_2O_5 (≤ 0.05 wt%) and Cr_2O_3 (≤ 0.05 wt%) (For Information Only).

2.8.2 Model

The model terms were first selected based on the evaluation of range and distribution of the major glass components. Al_2O_3, B_2O_3, CaO, Fe_2O_3, K_2O, Li_2O, LN_2O_3, MgO, Na_2O, P_2O_5, SiO_2, ZnO, and ZrO_2 were found to have significant effects. A PQM was developed using stepwise regression, where these second-order terms were found to improve the model statistics without overfitting, $Li_2O \times SiO_2$ and $MgO \times Na_2O$:

$$\ln(r_B) = \sum_{i=1}^{n} c_i x_i + \sum_{i=1}^{n-1} \sum_{j \geq i}^{n} c_{ij} x_i x_j \quad (2.11)$$

where c_i is the coefficient of the i^{th} first-order component term, n is the total number of components fitted in the model, x_i or x_j is the target molar fraction of the corresponding component, and c_{ij} is the coefficient for the cross-product term $x_i x_j$.

This model was found to have the best fit statistics without overfitting with an $R^2 = 0.8299$. The model coefficients are reported in Table 2.33. The predicted values are compared to measured values in Figure 2.22.

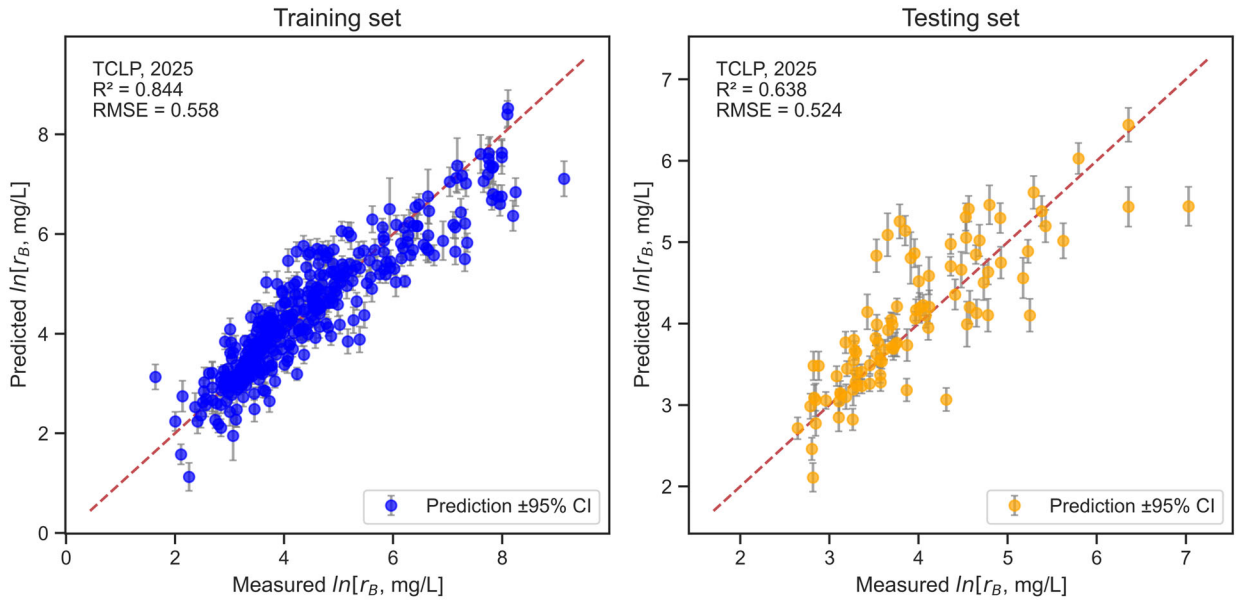

Figure 2.22. Predicted vs. measured TCLP for training and testing datasets.

Table 2.33. Model coefficients for the TCLP model.

Term	Coefficient		Statistic	Value
Al_2O_3	-10.029		# of data	480
B_2O_3	11.458		# of terms	16
CaO	14.816		Mean ln(r_B, mg/L)	4.3230
Fe_2O_3	-6.686		R^2_{fit}	0.8299
K_2O	32.905		R^2_{Adj}	0.8244
Li_2O	21.571		R^2_{press}	0.8134
LN_2O_3	-73.714		$RMSE_{fit}$, ln(r_B, mg/L)	0.5607
MgO	4.688		$RMSE_{press}$, ln(r_B, mg/L)	0.5781
Na_2O	14.294		Pooled SD, ln(r_B, mg/L)	0.2577
P_2O_5	-10.434			
SiO_2	0.245			
ZnO	6.359			
ZrO_2	-9.323			
Others	9.878			
Li_2OxSiO_2	-25.821			
$MgOxNa_2O$	89.963			

Composition effects on the TCLP response are shown in Figure 2.23. TCLP response is significantly increased by K_2O, Na_2O, CaO, and MgO, and moderately increased by B_2O_3, Li_2O, and others, while LN_2O_3, Al_2O_3, P_2O_5, ZrO_2, Fe_2O_3, and SiO_2 significantly decreased the TCLP response. During feature evaluation in model development, V_2O_5, TiO_2 and NiO were found to have a positive impact on the TCLP response. However, due to the large standard deviations of their coefficients and their relatively small contribution to overall model performance, these components were grouped into the “Others” category along with other minor components,

resulting a positive impact on TCLP model response. Future model development with additional data is needed to better resolve the effects of these components and, ideally, reduce reliance on the aggregated “Others” term.

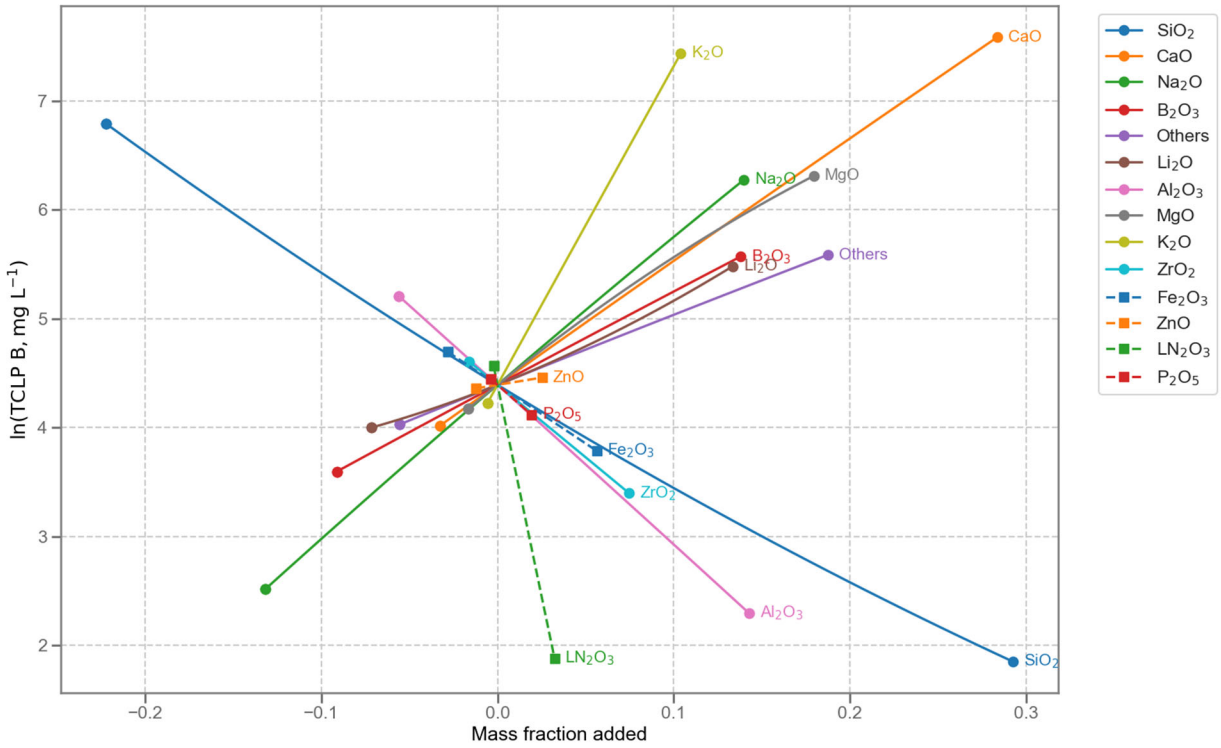

Figure 2.23. Component effects on TCLP model.

2.9 Nepheline Formation Model

A polynomial ternary (submixture) model was developed previously by Lu et al. (2021a). Distance of a point relative to the polynomial curve ($y=a + bX + cX^2$) was calculated using the Cartesian coordinates of pseudo-ternary composition shown below:

$$P = -\frac{bC + 2bB - \sqrt{3}C}{2(A + B + C)} - \frac{c(2B + C)^2}{4(A + B + C)^2} - a \qquad (2.12)$$

where: $A = x_{Na2O} + Ux_{CaO} + Vx_{MgO} + Yx_{Li2O} + Zx_{K2O}$

$B = x_{Al2O3} + Wx_{Fe2O3}$

$C = x_{SiO2} + Tx_{P2O5} + Xx_{B2O3}$

x = *molar fraction of the corresponding oxide*

The value, *P*, is calculated using the glass composition and the optimized coefficients: *a, b, c, T, U, V, W, X, Y*, and *Z*. The unit of the pseudo-ternary phase diagram is normalized mole fractions, and *P* represents distance above the polynomial curve.

Table 2.34 and Figure 2.24 show the model coefficients and pseudo-ternary phase diagram with polynomial line fit from Lu et al. (2021a). Those glass compositions with *P*>0 correspond to glasses above the curve and are predicted not to form nepheline after canister centerline cooling (CCC).

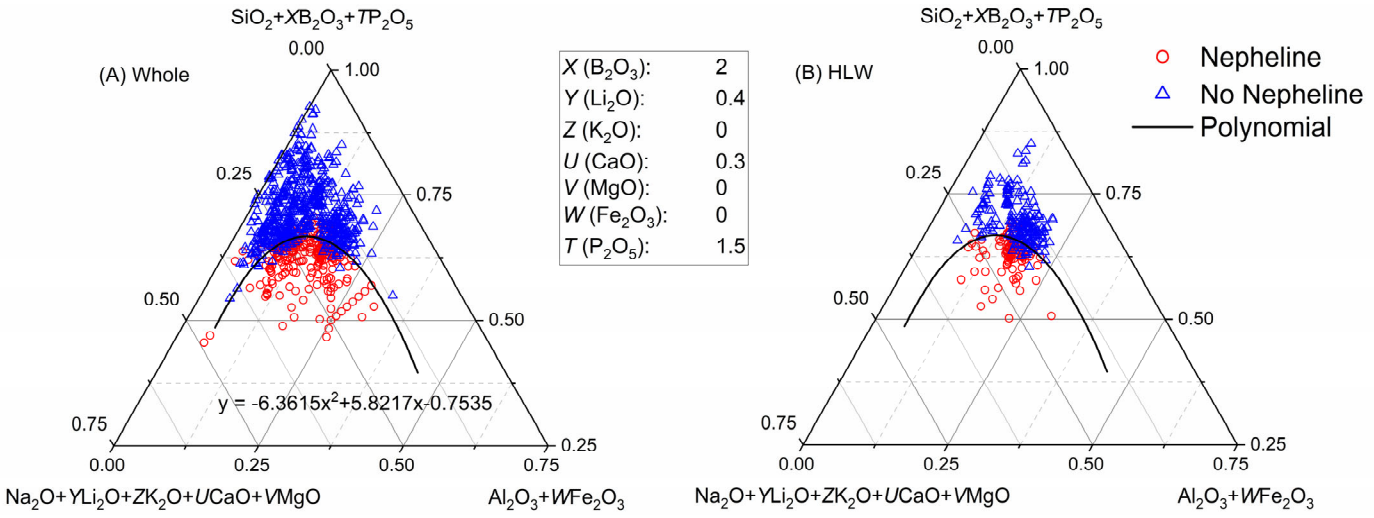

Figure 2.24. Pseudo-ternary phase diagram with polynomial line fit to the whole dataset (A) and HLW subset (B) highlighting nepheline-free glasses from Lu et al. (2021a).

Table 2.34. Model coefficients for pseudo-ternary nepheline formation model from Lu et al. (2021a).

Coefficients	Value
X (B_2O_3)	2
Y (Li_2O)	0.4
Z (K_2O)	0
U (CaO)	0.3
V (MgO)	0
W (Fe_2O_3)	0
T (P_2O_5)	1.5
Poly ***a*** (Const)	-0.7535
Poly ***b*** (X)	5.8217
Poly ***c*** (X^2)	-6.3615

Figure 2.25 shows the predicted P vs. nepheline formed after CCC for data used during model development. Less than 10% of glasses formed nepheline with *P*>0. Increasing the cutoff value would make the model more conservative, where a value of 0.031 would exclude all current glasses that formed. Figure 2.26 shows the nepheline content for the recent glass matrices, including HAL24, APPS2, LAWHNK and HS24 glasses. Figure 2.27 shows the component impact of the nepheline formation from the model by Lu et al. (2021a).

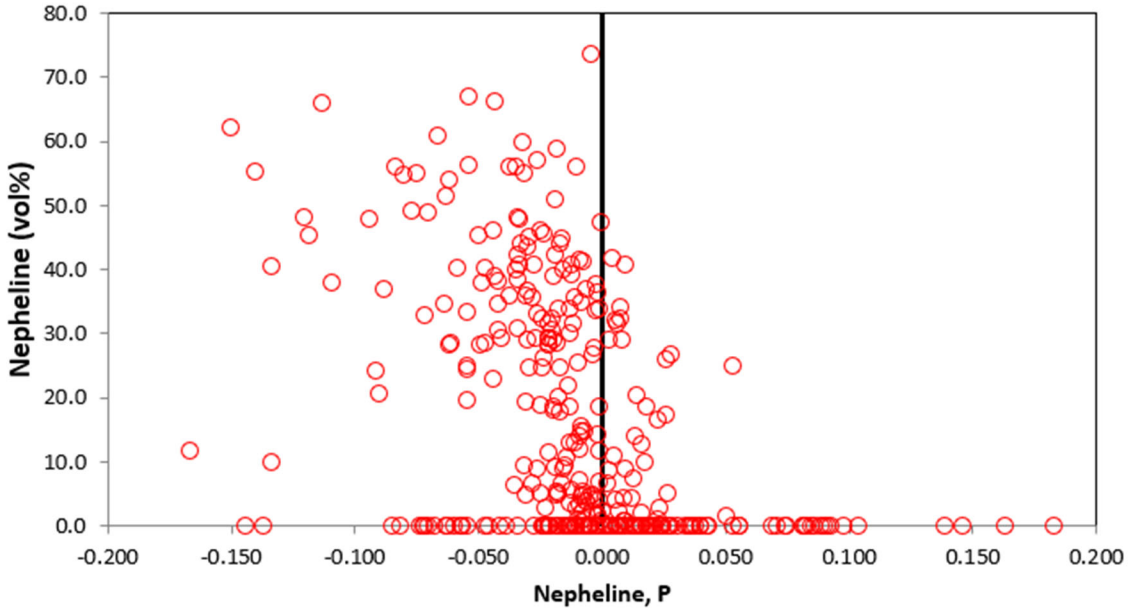

Figure 2.25. Predicted P vs. nepheline formed after CCC for data used during model development (For Information Only).

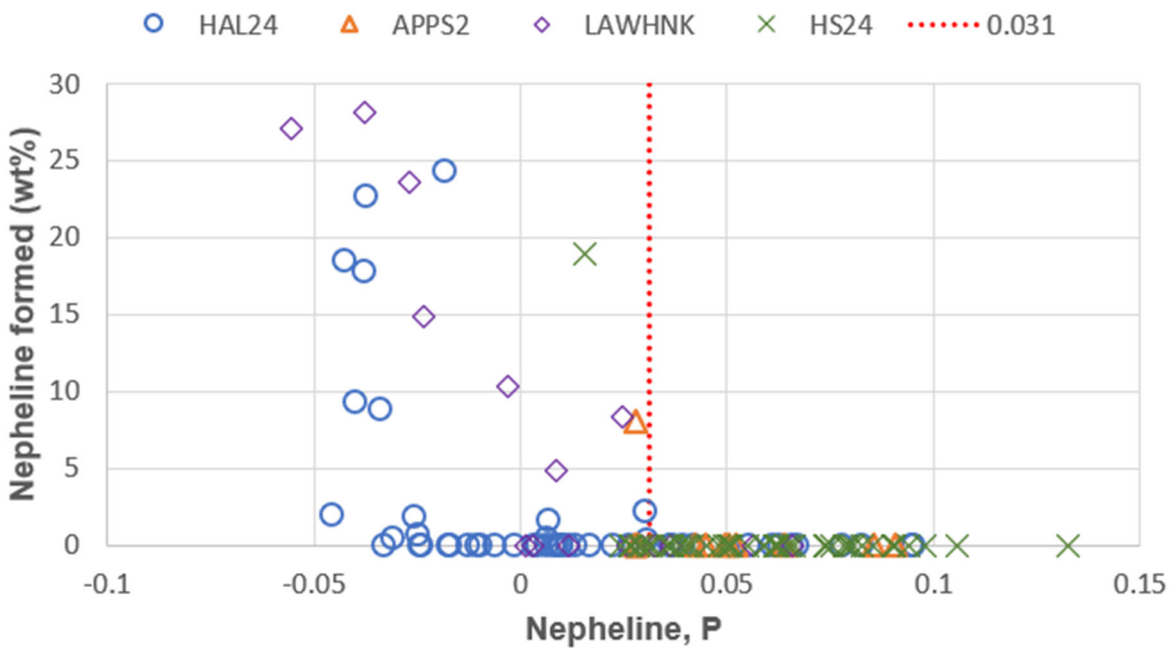

Figure 2.26. Predicted P vs. nepheline formed for HAL24, APPS2, LAWHNK and HS24 glasses (For Information Only).

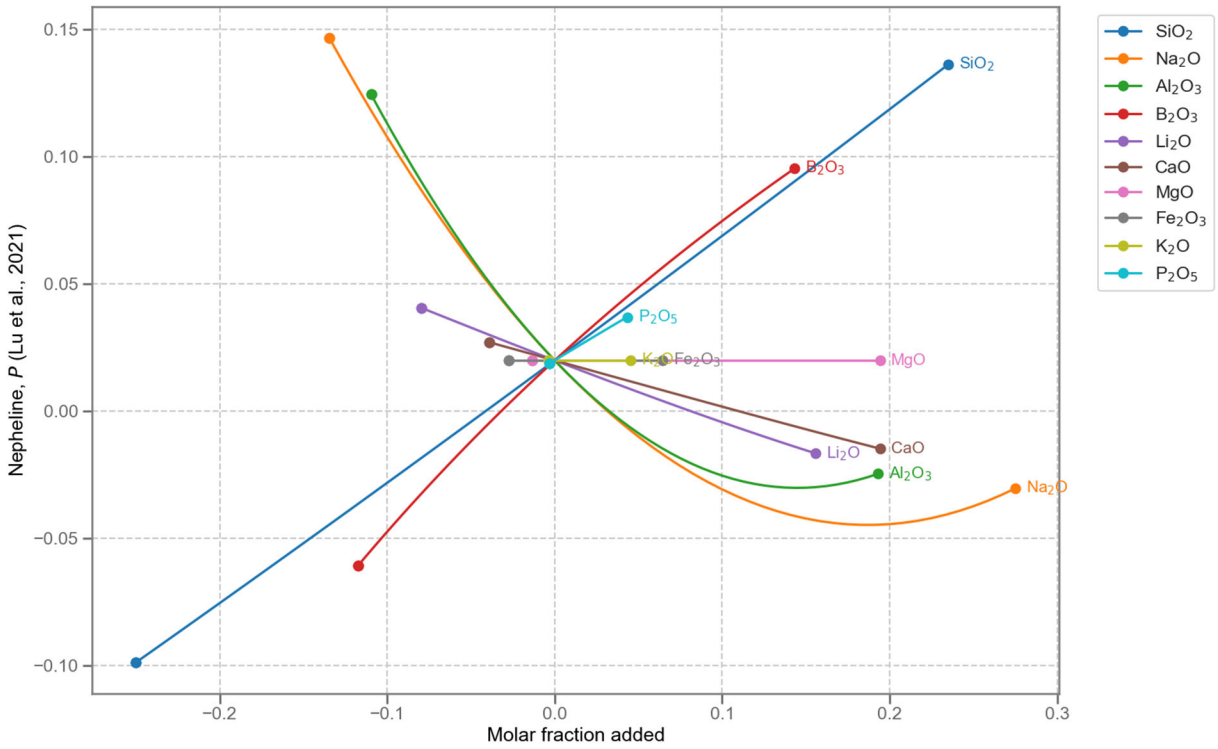

Figure 2.27. Component impact of the nepheline formation from the model by Lu et al. (2021a).

2.10 Metal Corrosion

With DFHLW, the increased alkali, halides, sulfate, and phosphate may accelerate corrosion of metallic melter components in contact with the melt or cold cap (e.g., electrodes, bubblers, thermowells, and level detectors). There is insufficient data to model the composition effects on metal corrosion, so as a temporary placeholder, component concentrations and models for other properties are recommended to reduce the risk of excessive corrosion. These rules are summarized below.

The sulfur solubility constraint limits the concentration of SO_3 to the range of compositions developed and tested for LAW glasses (Section 2.2). The concentration of P_2O_5 is limited by the T_L-P constraint (Section 2.4). The concentrations of alkali are limited by virtually all of the constraints, e.g., the NC_{Ave} (Section 2.7), EC (Section 2.1), and k_{neck} (Section 2.3). The EWG1 models formulated glasses with relatively high F content that were successfully demonstrated at melter scale and limited F concentration to 2.5 wt% in the melter feed.

Combined, these constraints will lower the risk of excessive metal corrosion until a dedicated melter corrosion model becomes available.

3.0 Formulation Methods and Constraints

This section summarizes the property constraints (Section 3.1), MV ranges (Section 3.2), composition uncertainties (Section 3.3), and optimization criteria (Section 3.4) for the EWG3.0 formulation algorithm. Example calculations can be found in Section 3.5.

3.1 Property Constraints

A combination of models from the literature and those developed in this report are recommended to predict the properties of example DFHLW glasses while glass property data gaps are being filled. These models are summarized in Table 3.1. The property constraints are preliminary and are not intended to be used for plant operation. Future sensitivity studies are needed to optimize these constraints, especially for K-3 refractory corrosion, metal corrosion, and spinel limits.

Conservative limits were selected during the design of the HLW melter due in part to a lack of data and short time-frames required. The same limits are carried forward in this effort due to lack of consensus on more relaxed limits. Three of these limits are subject to further sensitivity analyses and data collection – allowable spinel fraction in the melter (C_{950}-SP ≤ 1 vol%), metal corrosion limit (g_F ≤ 2.5 wt% BR), and refractory corrosion (k_{neck} ≤ 0.025 inch at 1208°C). Further investigation of these limits will proceed and will be delivered upon completion for use in mission planning assessments. By this strategy it is envisioned that modeling of the waste feed delivery effort by the Integrated Tank Disposition Contractor can benefit from a parallel maturity that could report increased cost-effectiveness in HLW Facility mission.

Table 3.1. List of property constraints for DFHLW glass composition estimation.

Property	Section	Constraint	Comp.[a]	U_{pred}[b]	U_{comp} (Section 3.3)	Note
PCT	Section 2.7	NC_{Ave} ≤ 12.88 g/L (or NL_{Ave} ≤ 6.44 g/m^2)	AR, Mole	Applied	95% CI	(c)
TCLP	Section 2.8	C_{Cd} ≤ 0.48, C_{Cr} ≤ 4.95, C_V ≤ 16.9 mg/L	AR, Mole	Applied	90% CI	-
Nepheline formation	Section 2.9	P ≥ 0.031 (distance to the line)	AR, Mole	None	90% CI	-
Viscosity	Section 2.1	2 ≤ η_{1150} ≤ 8 Pa·s η_{1100} < 15 Pa·s	AR, Mass	Applied	90% CI	-
EC	Section 2.1	ε_{1100} ≥ 10 S/m ε_{1200} ≤ 70 S/m	AR, Mass	Applied	90% CI	-
Melter SO_3 tolerance	Section 2.2	g_{SO3} ≤ $w_{SO3\text{-}3TS}$ - offset, wt%	BR, Mass (SO_3 removed)	Applied	90% CI	(d)
Immiscibility	Peeler and Hrma (1994)	N_{NaLi} ≥ 20 wt%	AR, Mass	None	90% CI	(e)
K-3 corrosion	Section 2.3	K_{neck} ≤ 0.025 inch (referenced to 1208°C bubbled)	AR, Mole (Cl removed)	Applied	90% CI	(f)
Phosphate T_L	Section 2.4	T_L-P ≤ 1050 °C (for g_{P2O5} ≥ 0.01)	AR, Mass	Applied	90% CI	(g)
Zirconia T_L	Section 2.5	T_L-Zr ≤ 1050°C (for g_{ZrO2} ≥ 0.027)	AR, Mass	Applied	90% CI	(h)

Property	Section	Constraint	Comp.[a]	U_{pred}[b]	U_{comp} (Section 3.3)	Note
Spinel	Section 2.6	C_{950}-Sp ≤ 1 vol%	AR, Mass	Applied	90% CI	(i)
Metal corrosion	Section 2.10	F ≤ 2.5 wt%	BR, Mass	None	90% CI	-
Non-spinel phase constraint	Vienna and Kim (2014)	g_{ThO2} + g_{ZrO2} < 13 wt%	AR, Mass	None	90% CI	-

(a) Compositions to be used for model predictions: AR (after applying retention factors), BR (before applying retention factors), Mass (mass fractions), and Mole (molar fractions).

(b) Prediction uncertainties (U_{pred}) are applied to the limits associated with all models generated in this report. They are calculated based on confidence intervals (CIs) for processing related properties: $U_{pred} = t_{1-\alpha,n-p}\sqrt{\mathbf{g}^{\mathrm{T}}[s^2(\mathbf{G}^{\mathrm{T}}\mathbf{G})^{-1}]\,\mathbf{g}}$, where n is the total number of points used to fit a model (i.e., total observations), p is the total number of model terms/coefficients. n and p values of each model can be found in the coefficient table. α is the statistical significance level (e.g., α = 0.10 for 90% confidence), and $t_{1-\alpha,n-p}$ represents 100(1−α)-percentile of the Student's t-distribution with $n - p$ degrees of freedom. For PCT and TCLP response, a simultaneous upper confidence interval (SUCI): $U_{pred} = \sqrt{pF_{1-2\alpha,(p,n-p)}}\sqrt{\mathbf{g}^{\mathrm{T}}s^2(\mathbf{G}^{\mathrm{T}}\mathbf{G})^{-1}\mathbf{g}}$, where $F_{1-2\alpha,(p,n-p)}$ represents 100(1−2α)-percentile of the F-distribution with p and $n - p$ degrees of freedom. The variance covariance matrices ($s^2[\mathbf{G}^{\mathrm{T}}\mathbf{G}]^{-1}$) are reported in Appendix A. More details on the statistical methods to develop, evaluate and validate property-composition models can be found in Appendix B by Vienna et al. (2022b).

(c) The Ave ln[NL] of the Defense Waste Processing Facility (DWPF) EA glass = (ln[8.350] + ln[6.675] + ln[4.785])/3 = 1.862. Applying an exponential function to Ave ln[NL] yields a NL_{Ave} = 6.44 g/m^2 (NC_{Ave} ≤ 12.88 g/L), which will be used to limit PCT response for the model in this report.

(d) The w_{SO3} model in this report was based on 3TS solubility data, which have been shown to be 0.33 wt% SO_3 higher than the melter tolerance data as reported by Skidmore et al. (2019). Therefore, the predicted g_{SO3} ≤ $w_{SO3\text{-}3TS}$ – 0.33 is the bounding limit. Here, g_{SO3} is BR (e.g. before accounting for any volatile loss of SO_3).

(e) Immiscibility limit is given by $N_{NaLi} = (g_{Na_2O} + 2.07g_{Li_2O})/(g_{Na_2O} + 2.07g_{Li_2O} + g_{B_2O_3} + g_{SiO_2})$ ≥ 0.2 mass fraction.

(f) k_{neck} limit was ≤ 0.04 inch in EWG2.5 (Vienna et al. 2024), but after review of all glass processing related limits, WTP revised the limit to k_{1208} ≤ 0.025 inch in future glass designs (Peters 2025).

(g) A sigmoid function is used with the T_L-P model predictions to avoid a singularity in the first derivative of composition vs. predicted response with 0 for g_{P2O5} < 0.01 and much greater than zero predicted T_L-P for g_{P2O5} ≥ 0.01. The equation used is: $T_L\ P = \frac{\sum T_i g_i}{1+e^{-2000(g_{P_2O_5}-0.009)}}$.

(h) A sigmoid function is used with the T_L-Zr model predictions with 0 for g_{ZrO2} < 0.027 and much greater than zero predicted T_L-Zr for g_{ZrO2} ≥ 0.027. The equation used is: $T_L\ Zr = \frac{\sum T_i g_i}{1+e^{-2000(g_{ZrO_2}-0.026)}}$.

(i) In EWG2.5, spinel fraction in glass was limited to 2 vol% at 950°C ($T_{2\%}$ ≤ 950°C). WTP revised the limit to $T_{1\%}$-Sp ≤ 950°C for EWG2.6 (Peters 2025). C_{950} < 1% is used in EWG3.0 and variable C_{950} values will be used in a planned sensitivity study.

3.2 Model Validity Constraints

The empirical models used to predict DFHLW glass properties are only valid within the range of data used to develop and validate the models. These MV ranges are summarized in Table 3.2. The "overall" limits in the last two columns are recommended to be used in EWG3.0. The minimum limits were generally developed by taking the maximum of the minimum values for each property and likewise the minimum of the maximums for individual properties. Some exceptions were made when the overall MV range of a component became too narrow due to certain properties. If that component has a minor impact on the property, then the property was excluded from determining the overall validity range. Since the "Others" term has a significant effect in the $w_{SO3\text{-}3TS}$, PCT, and TCLP models (while its impact on the other models is small), minor components that are not explicit model terms in these models were considered when selecting the minimum and maximum values.

In addition to the single-component limits, some of the models have multi-component limits. These include:

- K-3 corrosion model: $N_{Alk} = g_{Na_2O} + 2.07 g_{Li_2O} + 0.66 g_{K_2O}$ is between 0.1226 and 0.2821
- K-3 corrosion model: $N_{SiAl} = g_{SiO_2} + 1.6970 g_{Al_2O_3}$ is between 0.4497 and 0.7207
- K-3 corrosion model: $N_{SiB} = g_{SiO_2} + 2.0 g_{B_2O_3}$ is between 0.4590 and 0.9124

In these cases, the ratios (e.g., 2.07, 0.66) are based on ratios of molecular weights. Based on these data limits, it is recommended that the following multi-component limits be added:

- $0.1226 \leq N_{Alk} \leq 0.2821$
- $0.4497 \leq N_{SiAl} \leq 0.7207$
- $0.4590 \leq N_{SiBi} \leq 0.9124$

Table 3.2. Model validity constraints in mass fractions.

	w_{SO3}		k_{neck}		Viscosity		EC		PCT		TCLP		Nepheline		C_{950}-Sp		T_L-Zr		T_L-P_2O_5		Overall	
Comp	Min	Max	Min	Max	Min	Max	Min	Max	Min	Max	Min	Max	Min	Max	Min	Max	Min	Max	Min	Max	**Min**	**Max**
Al_2O_3	***0.0305***[a,d]	***0.2726***	***0.0300***	***0.2721***	***0***	***0.2857***	***0.0143***	***0.2721***	***0***	***0.3903***	***0***	***0.2857***	***0***	***0.4392***	***0.0400***	***0.2633***	***0***	***0.2857***	***0.0101***	***0.2721***	**0.0400**	**0.2721**
B_2O_3	***0.0402***	***0.2414***	***0.0400***	***0.2378***	***0***	***0.2389***	***0.0400***	***0.2389***	***0***	***0.2385***	***0.0002***	***0.2619***	***0***	***0.2660***	***0.0300***	***0.2378***	***0***	***0.2240***	***0.0405***	***0.2266***	**0.0405**	**0.2240**
Bi_2O_3	0	0.0155	0	0.0155	0	0.1639	0	0.0738	0	0.1638	0	0.0641	0	0.1641	0	0.0500	0	0.1000	0	0.1042		**0.0155**
CaO	***0***	***0.1297***	***0***	***0.1225***	***0***	***0.1820***	***0***	***0.1820***	***0***	***0.1500***	***0***	***0.2835***	***0***	***0.1820***	***0***	***0.0994***	0	0.0934	***0.0004***	***0.1421***		**0.0994**
CdO	-	-	0	0.0001	0	0.0400	0	0.0165	***0***	***0.0134***	0	0.0300	0	0.0134	0	0.0200	0	0.0165	0	0.0100		**0.0134**
Cl	***0.0004***	***0.0241***	0	0.0120	***0***	***0.0117***	0	0.0117	***0***	***0.0117***	0	0.0056	0	0.0080	0	0.0020	0	0.0034	0	0.0069		**0.0117**
Cr_2O_3	***0.0001***	***0.0250***	***0***	***0.0242***	***0***	***0.0300***	***0***	***0.0300***	0	0.0297	0	0.0200	0	0.0297	***0***	***0.0200***	***0***	***0.0127***	***0***	***0.0248***		**0.0127**
F	***0***	***0.0457***	0	0.0452	***0***	***0.0697***	0	0.0676	***0***	***0.0650***	0	0.0452	0	0.0251	0	0.0200	***0***	***0.0652***	0	0.0403		**0.0452**[e]
Fe_2O_3	***0***	***0.1254***	***0***	***0.1360***	***0***	***0.2640***	***0***	***0.2130***	***0***	***0.2053***	***0***	***0.1981***	0	0.2000	***0.0002***	***0.2001***	***0***	***0.1800***	0	0.1247		**0.1254**
K_2O	***0***	***0.0584***	***0***	***0.0810***	***0***	***0.2099***	***0***	***0.0972***	***0***	***0.1874***	***0***	***0.1500***	0	0.0614	***0***	***0.0600***	***0***	***0.0750***	0	0.0895		**0.0584**
Li_2O	***0***	***0.0512***	***0***	***0.0586***	***0***	***0.0901***	***0***	***0.0633***	***0***	***0.0900***	***0***	***0.0999***	***0***	***0.1255***	***0***	***0.0600***	***0***	***0.0901***	***0***	***0.0602***		**0.0512**
LN_2O_3	0	0.0289	0	0.0288	***0***	***0.1293***	0	0.0440	***0***	***0.1126***	***0***	***0.1615***	0	0.1126	0	0.0288	0	0.0728	0	0.0288		**0.0289**
MgO	***0***	***0.0829***	0	0.0492	***0***	***0.0963***	***0***	***0.0602***	***0***	***0.0801***	***0***	***0.1198***	0	0.1210	***0***	***0.0300***	***0***	***0.0800***	0	0.0432		**0.0300**
MnO	***0***	***0.0077***	0	0.0203	***0***	***0.0960***	***0***	***0.0800***	***0***	***0.0800***	0	0.0696	0	0.0613	***0***	***0.0522***	***0***	***0.0677***	0	0.0808		**0.0522**
Na_2O	***0.0923***[b]	***0.2704***	***0.0247***	***0.2601***	***0.0081***	***0.3504***	***0.0247***	***0.2692***	***0.0362***	***0.3903***	***0***	***0.2544***	***0.0200***	***0.3900***	***0.0400***	***0.2500***	***0.0362***	***0.2382***	***0.0159***	***0.2055***	**0.0400**	**0.2500**
NiO	0	0.0096	0	0.0096	***0***	***0.0218***	0	0.0212	***0***	***0.0500***	0	0.0300	0	0.0291	***0***	***0.0300***	0	0.0129	0	0.0267		**0.0218**
P_2O_5	***0***	***0.0403***	***0***	***0.0400***	***0***	***0.1312***	***0***	***0.0549***	***0***	***0.0900***	***0***	***0.0448***	0	***0.0902***	***0***	***0.0399***	0	0.0500	***0.0064***	***0.0819***		**0.0399**
SiO_2	***0.2412***[c]	***0.5936***	***0.2404***	***0.5851***	***0.1945***	***0.6413***	***0.1945***	***0.5850***	***0.1744***	***0.6092***	***0.2158***	***0.7125***	***0.1744***	***0.6015***	***0.2185***	***0.5024***	***0.2287***	***0.5957***	***0.2146***	***0.5295***	**0.2412**	**0.5024**
SO_3	-	-	0	0.0197	***0***	***0.0210***	***0***	***0.0210***	***0***	***0.0245***	0	0.0146	0	0.0175	0	0.0092	0	0.0098	0	0.0173		**0.0210**
SnO_2	***0***	***0.0508***	0	0.0500	***0***	***0.0503***	***0***	***0.0503***	0	0.0503	0	0.0479	0	0.0503	0	0.0030	0	0.0023	0	0.0073		**0.0503**
SrO	0	0.0002	0	0.0788	***0***	***0.2110***	***0***	***0.1029***	0	0.1014	0	0.1445	0	0.1014	***0***	***0.0864***	0	0.1029	0	0.1001		**0.0864**
ThO_2	-	-	-	-	0	0.0781	0	0.0601	0	0.0534	0	0.0597	0	0.0003	0	0	***0***	***0.0441***	0	0.0183		**0.0441**
TiO_2	0	0.0386	0	0.0501	***0***	***0.0535***	***0***	***0.0500***	***0***	***0.0800***	0	0.0200	0	0.0300	0	0.0209	0	0.0100	0	0.0059		**0.0500**
UO_3	-	-	-	-	***0***	***0.1558***	0	0.0650	0	0.2598	0	0.0892	0	0.1558	-	-	***0***	***0.0650***	0	0.0410		**0.0650**
V_2O_5	***0***	***0.0573***	***0***	***0.0515***	***0***	***0.0599***	***0***	***0.0571***	***0***	***0.0514***	0	0.0515	0	0.0400	0	0.0495	0	0.0332	0	0.0506		**0.0514**
ZnO	***0***	***0.0575***	***0***	***0.0536***	***0***	***0.0986***	***0***	***0.0582***	***0***	***0.0503***	***0***	***0.0488***	0	0.0503	***0***	***0.0405***	0	0.0390	0	0.0400		**0.0405**
ZrO_2	***0***	***0.0932***	***0***	***0.0932***	***0***	***0.1548***	***0***	***0.1336***	***0***	***0.1650***	***0***	***0.1600***	0	0.1604	0	0.0909	***0.0269***	***0.1650***	***0***	***0.0961***		**0.0932**
Others[f]	***0***	***0.0205***	0	0.0083	0	0.1312	0	0.0347	***0***	***0.0341***	***0***	***0.0730***	0	0.0188	0	0.0390	0	0.0298	0	0.0480		**0.0205**

(a) Green entries represent values that exceed the overall MV limits (i.e., the overall limits do not exceed these component concentrations).
(b) Red entries represent values that are within the overall MV limits (i.e., the overall limits exceed these component concentrations, where the models are extrapolating).
(c) Blue entries represent values selected as the overall ranges.
(d) Bold italic entries indicate those components are model terms.
(e) Due to metal corrosion, in the EWG3.0 formulation, an additional F limit is applied, which is 2.5 wt% in feed (e.g., before applying retention factors).
(f) The "Others" term has a significant effect in w_{SO3}, PCT, and TCLP models (highlighted as bold italic), while the impact for the other models is small (not highlighted in this case). Note that the "Others" values in this table were calculated for each property model as 1 – sum of the component explicitly listed in this table, which is different (e.g., fewer minor components included) from the "others" term defined within each model.

3.3 Composition and Process Uncertainties

Figure 3.1 shows a schematic diagram of the DFHLW glass formulation method based on the baseline HLW (e.g., pretreated HLW) glass formulation algorithm (Vienna and Kim 2014). The ternary diagram on the left represents the multidimensional glass composition region predicted for a particular waste steam at the top of the diagram; the concentrations of the potential GFCs are expressed across the bottom. The property constraints (calculated using glass property models) limit the portion of the composition region where glass can be formulated, as shown by the solid blue lines for different properties. Model prediction uncertainties further narrow the composition space in which glass can be formulated, as shown by the dashed yellow lines.

A glass can be formulated anywhere within the region defined by the property limits with associated prediction uncertainties. The composition of the glass is not precisely known due to various uncertainties/errors induced by compositions of waste and GFCs, mixing/sampling, composition analysis, and mass or volume measurements, among others. Therefore, various sources of composition uncertainties must be accounted for, as shown by the yellow disk. The final glass formulation region is the region surrounded by the dotted lines (representing property limits with prediction uncertainty) within which a plausible composition (represented by the yellow circle) can fit.

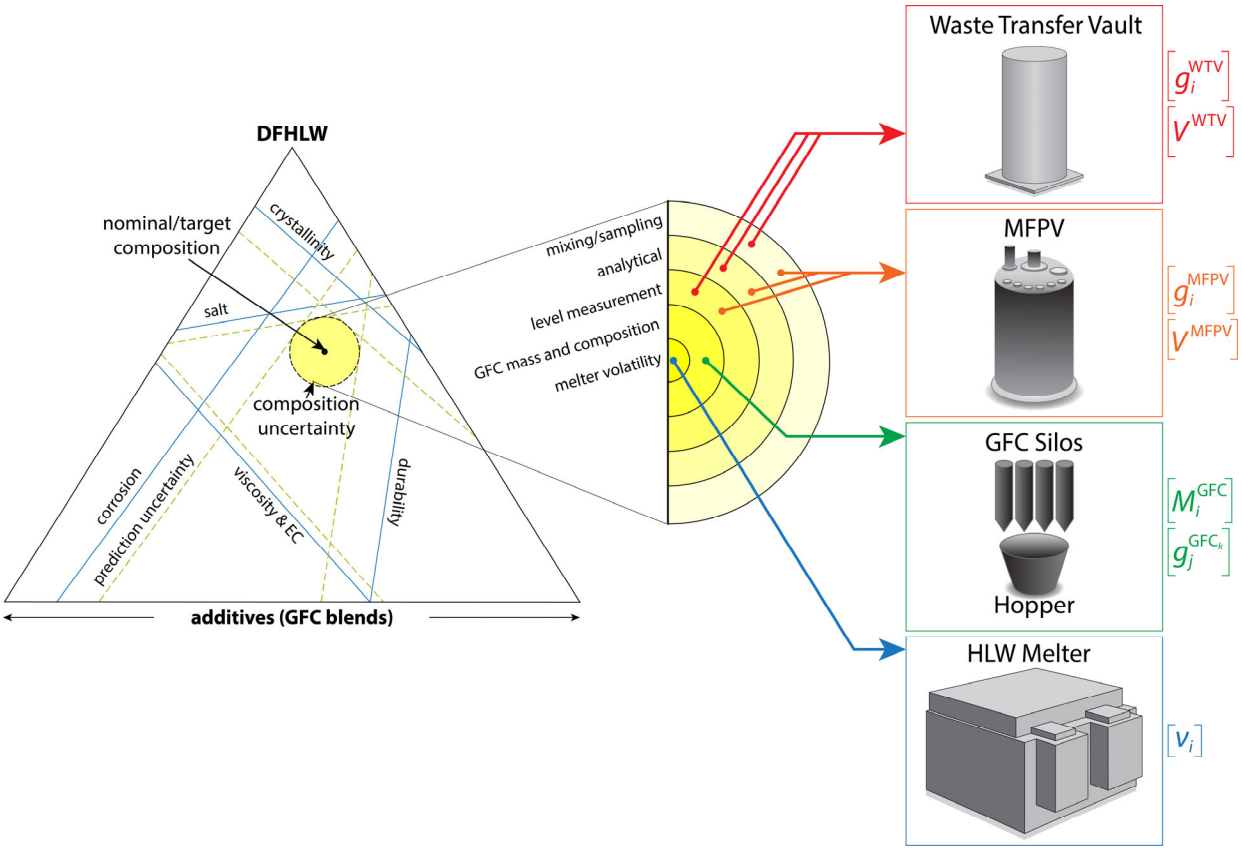

Figure 3.1. Schematic representation of the DFHLW glass processing envelope.

The final waste glass composition can be calculated using the mass balance Eq. (3.1):

$$g_i = \frac{\left[\sum_{j=1}^{n^{wastes}} c_{ij}^{oxide\ in\ waste} M_j^{waste} + \sum_{k=1}^{n^{GFCs}} g_{ik}^{oxide\ in\ GFC} M_k^{GFC}\right] \nu_i}{\sum_{i=1}^{n^{oxides}} \left[\sum_{j=1}^{n^{wastes}} c_{ij}^{oxide\ in\ waste} M_j^{waste} + \sum_{k=1}^{n^{GFCs}} g_{ik}^{oxide\ in\ GFC} M_k^{GFC}\right] \nu_i} \quad (3.1)$$

where:
- g_i = mass fraction of i[th] oxide in final waste glass (g/g)
- $c_{ij}^{oxide\ in\ waste}$ = concentration of the i[th] component measured in the j[th] waste (g/g)
- M_j^{waste} = mass of the j[th] waste (kg)
- n^{wastes} = number of wastes mixed
- $g_{ik}^{oxide\ in\ GFC}$ = mass fraction of the i[th] oxide in the k[th] GFC (g/g)
- M_k^{GFC} = mass of the k[th] GFC (kg)
- n^{GFCs} = number of GFCs added
- ν_i = fraction of i[th] oxide retained in the glass (g/g)

However, each of the variables have uncertainty values. Due to the form of the mass balance equation, there is no closed form analytical solution to propagate uncertainties. A Monte Carlo (MC) approach was taken to estimate the composition/process uncertainties.

MC simulations are a class of computational methods that rely on repeated random sampling to model the probability of different outcomes in processes that cannot easily be predicted due to the presence of uncertain variables. MC methods use probability distribution for modeling random variables. Different types of probability distributions are used to describe the uncertain variable, such as normal, triangular, and Program Evaluation and Review Techniques (PERT) (also called the beta-PERT or three-point estimation technique, which was proposed for estimating the effect of uncertainty using the PERT). Then, many iterations, or simulations, are conducted using numerical computations that generate different outcomes (compositions and predicted properties in this case) and their probability of occurrence. In other words, the MC method provides an estimate of the uncertainty in glass composition and associated predicted properties.

The calculation of uncertainties of $c_i^{oxide\ in\ waste}$, M_j^{waste}, $g_{ik}^{oxide\ in\ GFC}$, M_k^{GFC} and ν_i were reported in Vienna and Kim (2014) (Appendices A and B), with a few modifications reported in the following paragraphs.

GFC particle and powder densities used in this report are listed in Table 3.3. Particle density is used to estimate the impact of GFCs on solution volume to (1) ensure accurate total volume calculations and avoid overfilling, and (2) convert compositions to concentrations for comparison with analytical results. Powder density is used to determine the fill capacity of the blend and mix hoppers and to assess whether multiple batches are required. More details can be found in Vienna and Kim (2014). GFC min, max, and most likely compositions can be found in Appendix C of this report. Retention factors and decontamination factors can be found in Appendix F of this report.

Table 3.3. Particle and powder densities of GFCs.

GFC	Formula	Particle Density (g/L)	Powder Density (lb/ft^3)	Powder Density (g/L)	Hopper Volume (ft^3)
Kyanite	Al_2SiO_5	3395.9	76.2	1220.6	10
Boric acid	H_3BO_3	1505.7	54.8	877.8	10
Wollastonite	$CaSiO_3$	2899.3	58.5	937.1	10
Na_2CO_3	Na_2CO_3	2530.9	66.3	1062.0	10
Li_2CO_3	Li_2CO_3	2114.4	61.8	989.9	10
Cr_2O_3	Cr_2O_3	5231.9	65.0	1041.2	3
Silica	SiO_2	2643.0	69.1	1106.9	10
Zincite	ZnO	5606.5	42.5	680.8	10
Zircon	$ZrSiO_4$	4709.4	121.9	1952.7	3
V_2O_5	V_2O_5	3388.0	46.0	736.9	10
Sucrose	$C_{12}H_{22}O_{11}$	1553.8	54.2	868.2	-

The glass formulation results include the mass of each GFC ($M_{GFC,\alpha}$) per batch volume (V_{Batch}) in g/L. The volume contribution of GFCs per batch is estimated using Eq. (3.2) and particle densities of each GFC ($\rho_{P,\alpha}$) listed in Table 3.3.

$$V_{GFC} = \sum \frac{M_{GFC,\alpha}}{\rho_{P,\alpha}} \tag{3.2}$$

The waste transfer volume (V_{Wtrf} in L/batch) is calculated for each waste campaign according to:

$$V_{Batch} = V_{Working} - V_{Heel} = V_{Wtrf} + V_{Flush} + V_{GFC} + V_{DCW} + V_{Dil} \tag{3.3}$$

where
- $V_{Working}$ = a melter feed preparation vessel (MFPV) working volume, nominally 18,290 L (~5,100-gal batch minus 300-gal margin for trim chemicals and other unplanned events)
- V_{Batch} = target MFPV batch volume in L
- V_{Heel} = heel volume, 6405 L was assumed for example calculations; composition impact from heel was not accessed
- V_{Flush} = the sum of flush water volume from Vienna et al. (2022a), nominally 770.5 L
- V_{GFC} = glass-forming chemical volume from Eq. (3.2)
- V_{DCW} = dust control water; GFC dust control water assumed to be 4% of GFC mass
- V_{Dil} = dilution water (described below)

The glass yield (Y) is given by:

$$Y = \frac{M_{WOx} \times V_{Wtrf}}{WL \times V_{Batch}} \quad (3.4)$$

where Y = glass yield in grams of glass per liter of melter feed
M_{WOx} = ratio of mass of waste oxides (g) per volume of waste (L) in a campaign determined by $M_{WOx} = \Sigma M_{T,i} f_i$, where f_i is the ratio of component mass to glass oxide mass from Vienna and Kim (2014)
V_{Wtrf} = the waste transfer volume in L/batch from Eq. (3.3)
WL = the waste oxide loading $WL = M_{WOx}/M_G$, where M_G is the glass mass derived from glass formulations

A constraint of $Y \leq 550$ g L^{-1} was applied when calculating waste transfer volume and dilution water, based on Reynolds (2006).

A Python programing code was developed and used to perform the calculations. The Microsoft Excel add-in RiskAmp was used to check and confirm the results obtained from the programing code. The mass balance equation with parameter probability distributions was used in an MC routine to generate 10,000 realizations of the target glass composition. For each glass composition realization, each of the properties and composition constraints were calculated. The half-width of each property distribution (an example is shown in Figure 3.2) for the associated confidence level (CL) listed in Table 3.1 was used:

$$U_{comp}^{prop} = Q_{CL\%}^{prop} - Q_{50\%}^{prop} \text{ (for upper limit) or } Q_{50\%}^{prop} - Q_{100-CL\%}^{prop} \text{ (for lower limit)} \quad (3.5)$$

where $Q_{CL\%}^{prop}$ is CL% percentile of the distribution of property value realizations and $Q_{50\%}^{prop}$ is median predicted property value or CL% = 50% percentile of the distribution of 10,000 property value realizations. 95% confidence level for PCT (as dictated by DOE 2012) and 90% confidence level for TCLP (as described in 24590-WTP-RPT-ENV-06-001, Rev. 0[1]). For processing related properties (spinel, viscosity, and electrical conductivity) no written requirements dictate the confidence level, so, a preliminary value of 90% was selected.

Figure 3.2 shows an example of the probability distribution calculated by this method.

[1] 24590-WTP-RPT-ENV-06-001, Rev. 0. *Petition to Delist Immobilized High-Level Waste Generated at the Hanford Tank Waste Treatment and Immobilization Plant*. Bechtel National, Inc. Richland, WA.

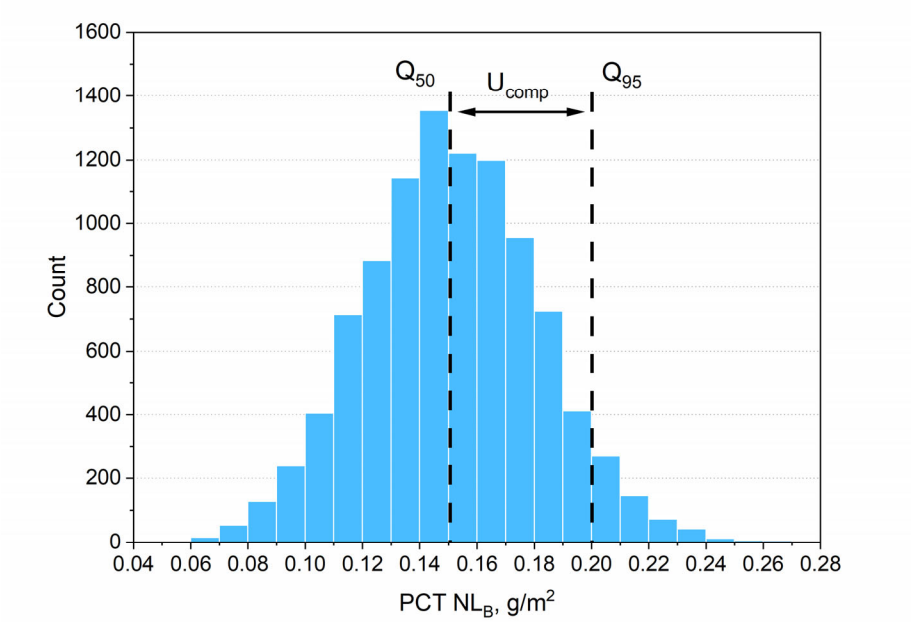

Figure 3.2. Example histogram of predicted PCT NL_B values from a 10,000-run Monte Carlo simulation (For Information Only).

The constraints are thus expressed as lower- and upper-combined CIs:

$$L_\alpha^L \le t(P_\alpha) - U_\alpha^{pred} - U_\alpha^{comp} \text{ and } L_\alpha^U \ge t(P_\alpha) + U_\alpha^{pred} + U_\alpha^{comp} \quad (3.6)$$

where L_α^L and L_α^U are the lower and upper limits on transformed property α [$t(P_\alpha)$], U_α^{pred} is the uncertainty in prediction of $t(P_\alpha)$, and U_α^{comp} is the expression of composition uncertainty expressed in units of $t(P_\alpha)$.

The values of uncertainty scale with the level of confidence obtained; Table 3.1 presents the level of confidence for each property.

3.4 Optimization Criteria

The glass compositions are optimized by varying the concentrations of GFCs and waste to maximize the waste loading while simultaneously satisfying the property and composition constraints. Unguided optimization often results in selection of GFCs that are not ideal – for example, Cr_2O_3 addition in cases of low K-3 corrosion glasses or V_2O_5 addition in cases of low SO_3 glasses. To address these concerns, the following logic statements are used in the optimization: (1) a Cr_2O_3 upper limit of 0.6 wt% in the final glass is imposed if Cr_2O_3 is selected as a GFC, and (2) V_2O_5 is only added as a GFC when SO_3 concentration in glass before applying retention factor is ≥ 0.7 wt%.

The V_2O_5 addition rule is based on the EWG2.6 formulation results using the 1,305 campaigns by Lu et al. (2025). From the results, 774 of the 1,305 campaigns had pre-retention $g_{SO3} \le 0.7$ wt%. Among these 774 batches, 80% were not limited by SO_3 solubility. Therefore, 0.7 wt% was selected as the cutoff for allowing V_2O_5 addition. Coincidentally, the limit for pre-retention g_{SO3} in baseline LAW glass is 0.7 wt%, for which no V_2O_5 is added.

After applying these formulation rules and the constraints in Sections 3.1 and 3.2, the waste loading of glass is maximized by adjusting the concentrations of GFCs in Table 3.3.

These optimization criteria will result in a reasonable set of glasses for design, testing, and planning purposes in the near-term. As data collection and modeling efforts continue, glass formulation approaches and compositions will evolve without jeopardizing the validity of the work performed.

3.5 Example Calculations

To demonstrate the glass formulation approach suggested, example calculations are described here. Six example waste compositions (high in Al_2O_3, F, Na_2O, P_2O_5, and SO_3; and requiring significant dilution water) were selected from the feed vector supplied by Britton (2023), as summarized in Table 3.4 and Appendix B. Glass was optimized for each of the six example wastes using the constraints presented in Table 3.1 and Table 3.2. Appendix C presents the nominal compositions of the current list of GFCs. Appendix F lists the minimum, most likely, and maximum ln[DF] and nominal retention factor. For PCT, 99% SUCI was used, and for the other properties, 99% CI was used for prediction uncertainty – although the confidence level should be adjusted to match the desired application of the models.[1] The formulations, resulting glass compositions, and predicted properties are summarized in Table 3.5, Table 3.6, and Table 3.7, respectively.

Table 3.4. Compositions (mass fraction of oxides and halogen) of the six wastes used in example calculations. Compositions in mg/L element can be found in Appendix B.

Example #:	1	2	3	4	5	6
	High Al_2O_3	High F	High Na_2O	High P_2O_5	High SO_3	Dilution Water
Ac_2O_3	2.005E-12	4.392E-13	9.360E-13	2.542E-13	8.536E-13	7.536E-12
Ag_2O	1.035E-04	6.046E-04	1.716E-05	0.000E+00	0.000E+00	5.341E-06
Al_2O_3	6.241E-01	4.492E-02	1.267E-01	1.962E-01	1.593E-01	1.672E-01
Am_2O_3	7.214E-09	6.811E-08	8.465E-07	3.325E-06	9.012E-06	1.360E-06
As_2O_5	5.420E-04	3.424E-05	7.257E-04	0.000E+00	0.000E+00	3.568E-04
B_2O_3	2.936E-03	4.120E-03	6.985E-04	0.000E+00	0.000E+00	3.319E-04
BaO	1.970E-04	7.422E-05	1.164E-04	1.744E-13	3.529E-13	4.382E-05
BeO	4.899E-05	1.739E-04	1.991E-05	0.000E+00	0.000E+00	5.164E-06
Bi_2O_3	9.619E-05	5.008E-04	5.008E-05	1.839E-02	4.659E-05	2.501E-05
CaO	1.113E-03	1.054E-03	1.618E-03	3.652E-03	6.674E-03	3.545E-03
CdO	7.087E-05	4.724E-05	1.709E-04	1.386E-11	5.617E-11	9.001E-05
Ce_2O_3	4.139E-04	7.537E-06	4.142E-04	0.000E+00	0.000E+00	1.907E-04
Cl	4.198E-03	3.368E-03	8.362E-03	2.759E-03	2.546E-03	3.574E-03
Cm_2O_3	1.655E-14	1.230E-13	2.817E-10	2.365E-11	1.376E-09	1.721E-10
CoO	3.871E-04	3.208E-06	4.106E-05	2.797E-12	1.537E-11	1.299E-05
Cr_2O_3	3.886E-03	1.049E-02	3.113E-03	2.503E-03	4.271E-03	3.090E-03
Cs_2O	3.923E-06	2.592E-06	1.142E-05	6.099E-06	1.237E-05	7.172E-06

[1] The baseline glass formulation algorithm applies 95% SUCI for PCT and 90% CI for other properties (Vienna and Kim 2014).

Example #:	1	2	3	4	5	6
CuO	4.427E-05	9.002E-06	9.940E-05	0.000E+00	0.000E+00	5.059E-05
Eu_2O_3	6.944E-11	1.998E-11	7.093E-10	5.414E-10	4.451E-09	5.402E-10
F	3.559E-03	1.449E-01	3.490E-03	1.495E-02	6.399E-02	5.092E-02
Fe_2O_3	4.191E-04	2.282E-03	3.028E-02	2.392E-01	1.658E-01	4.134E-02
Gd_2O_3	0.000E+00	0.000E+00	0.000E+00	0.000E+00	0.000E+00	0.000E+00
HgO	2.719E-06	5.375E-07	1.197E-06	1.104E-04	9.815E-05	3.799E-05
I	4.293E-07	4.563E-07	6.609E-07	6.229E-06	1.183E-06	2.690E-06
K_2O	8.083E-03	1.624E-02	3.747E-03	1.389E-03	4.056E-03	3.116E-03
La_2O_3	2.405E-09	4.856E-04	1.178E-04	5.143E-04	7.750E-03	1.031E-04
Li_2O	2.640E-04	1.540E-05	1.392E-04	0.000E+00	0.000E+00	7.072E-05
MgO	5.867E-04	1.779E-03	9.938E-04	0.000E+00	0.000E+00	4.990E-04
MnO	4.554E-05	1.331E-04	3.017E-03	1.055E-02	1.172E-02	7.173E-03
MoO_3	3.482E-04	1.946E-05	1.890E-04	0.000E+00	0.000E+00	7.307E-05
Na_2O	3.350E-01	5.151E-01	7.807E-01	3.558E-01	4.910E-01	5.630E-01
Nb_2O_5	4.807E-10	1.126E-10	2.415E-10	1.016E-10	3.750E-09	1.194E-10
Nd_2O_3	4.127E-04	1.592E-04	8.332E-04	0.000E+00	0.000E+00	4.290E-04
NiO	8.925E-05	1.576E-04	6.714E-04	6.427E-03	7.177E-03	2.419E-03
NpO_2	1.547E-06	6.851E-07	6.365E-06	3.370E-07	1.248E-05	7.102E-06
P_2O_5	2.869E-03	1.222E-02	1.352E-02	9.039E-02	1.310E-02	1.075E-02
Pa_2O_5	3.574E-09	8.895E-10	2.377E-09	5.197E-10	1.812E-09	3.732E-09
PbO	3.804E-04	9.625E-05	1.247E-03	1.775E-02	3.255E-03	1.259E-03
PdO	0.000E+00	0.000E+00	0.000E+00	0.000E+00	0.000E+00	0.000E+00
Pr_2O_3	0.000E+00	0.000E+00	0.000E+00	0.000E+00	0.000E+00	0.000E+00
PuO_2	1.716E-07	7.311E-06	7.450E-06	6.758E-05	4.386E-05	4.198E-05
RaO	1.459E-13	3.948E-14	9.104E-14	4.923E-13	7.696E-13	9.502E-12
Rb_2O	0.000E+00	0.000E+00	0.000E+00	0.000E+00	0.000E+00	0.000E+00
Rh_2O_3	0.000E+00	0.000E+00	0.000E+00	0.000E+00	0.000E+00	0.000E+00
RuO_2	1.330E-24	2.934E-24	1.343E-04	6.809E-25	5.551E-24	7.809E-05
SO_3	3.366E-03	3.850E-02	1.405E-02	1.145E-02	4.727E-02	2.645E-02
Sb_2O_3	2.539E-04	3.552E-06	5.894E-05	2.972E-14	1.302E-13	7.309E-15
SeO_2	4.972E-04	1.207E-05	3.583E-04	2.629E-08	8.426E-08	3.588E-07
SiO_2	4.595E-03	5.274E-03	9.071E-04	8.060E-03	1.687E-03	1.366E-02
Sm_2O_3	1.576E-06	2.827E-07	1.417E-05	1.130E-05	2.989E-05	9.195E-06
SnO_2	7.630E-07	1.777E-07	3.273E-07	1.240E-07	7.362E-06	1.584E-07
SrO	2.834E-07	2.119E-06	3.536E-05	4.882E-04	4.588E-04	8.322E-05
Ta_2O_5	0.000E+00	0.000E+00	0.000E+00	0.000E+00	0.000E+00	0.000E+00
Tc_2O_7	5.837E-05	7.725E-06	2.690E-06	8.374E-06	1.095E-05	5.040E-06
TeO_2	0.000E+00	0.000E+00	0.000E+00	0.000E+00	0.000E+00	0.000E+00
ThO_2	2.667E-06	9.522E-06	1.549E-04	1.210E-03	1.916E-03	2.474E-02
TiO_2	5.903E-05	1.453E-05	1.368E-05	0.000E+00	0.000E+00	0.000E+00
Tl_2O	0.000E+00	4.252E-06	1.698E-04	0.000E+00	0.000E+00	0.000E+00
UO_3	3.226E-04	1.627E-02	7.860E-04	1.790E-02	3.288E-03	2.154E-02
V_2O_5	3.154E-04	6.327E-05	7.317E-05	0.000E+00	0.000E+00	0.000E+00

Example #:	1	2	3	4	5	6
WO_3	0.000E+00	0.000E+00	9.424E-04	0.000E+00	0.000E+00	5.482E-04
Y_2O_3	1.234E-12	3.861E-05	2.881E-04	3.351E-09	7.580E-09	1.615E-04
ZnO	2.640E-04	1.897E-05	1.961E-04	0.000E+00	0.000E+00	1.075E-04
ZrO_2	4.396E-05	1.808E-01	7.642E-04	1.877E-04	4.540E-03	5.290E-02
SUM	1	1	1	1	1	1

Table 3.5. Formulation of example glasses (mass% of component oxide in glass).

Component	1	2	3	4	5	6
Kyanite	0.000	14.336	11.064	0.000	0.000	0.000
Boric acid	21.948	15.567	12.731	6.028	12.096	7.546
Wollastonite	10.790	9.199	3.756	11.845	18.373	7.239
Na_2CO_3	0.000	6.241	0.000	0.000	0.000	0.000
Li_2CO_3	1.879	2.446	0.000	2.239	0.222	0.000
Cr_2O_3	0.000	0.225	0.505	0.000	0.453	0.473
Silica	23.755	31.598	34.940	33.411	32.701	38.867
Zincite	0.577	2.003	3.954	1.176	0.000	2.572
Zircon	4.010	2.321	3.987	4.089	0.000	0.000
V_2O_5	0.000	0.000	0.000	0.000	5.081	5.068
Waste	37.041	16.065	29.064	41.213	31.074	38.234
SUM	100.00	100.00	100.00	100.00	100.00	100.00

Table 3.6. Target glass composition (after applying retention factors) in mass fraction of oxides and halogen.

Example #	1	2	3	4	5	6
Ac_2O_3	7.449E-13	7.117E-14	2.730E-13	1.051E-13	2.679E-13	2.909E-12
Ag_2O	3.772E-05	9.608E-05	4.907E-06	0.000E+00	0.000E+00	2.022E-06
Al_2O_3	2.329E-01	9.094E-02	1.014E-01	8.219E-02	5.101E-02	6.545E-02
Am_2O_3	2.628E-09	1.083E-08	2.421E-07	1.349E-06	2.774E-06	5.150E-07
As_2O_5	1.557E-04	4.290E-06	1.637E-04	0.000E+00	0.000E+00	1.065E-04
B_2O_3	2.195E-01	1.565E-01	1.270E-01	6.003E-02	1.212E-01	7.573E-02
BaO	7.319E-05	1.203E-05	3.394E-05	7.215E-14	1.108E-13	1.692E-05
BeO	1.820E-05	2.818E-05	5.806E-06	0.000E+00	0.000E+00	1.993E-06
Bi_2O_3	3.504E-05	7.959E-05	1.433E-05	7.458E-03	1.434E-05	9.467E-06
CaO	5.255E-02	4.501E-02	1.863E-02	5.881E-02	9.125E-02	3.650E-02
CdO	2.690E-05	9.681E-06	5.384E-05	1.183E-06	1.763E-11	3.735E-05
Ce_2O_3	1.537E-04	1.221E-06	1.208E-04	0.000E+00	0.000E+00	7.361E-05
Cl	8.530E-04	3.107E-04	1.331E-03	6.251E-04	4.363E-04	7.526E-04
Cm_2O_3	6.149E-15	1.993E-14	8.217E-11	9.781E-12	4.320E-10	6.643E-11
CoO	1.438E-04	5.198E-07	1.198E-05	1.157E-12	4.823E-12	5.016E-06
Cr_2O_3	1.383E-03	3.803E-03	5.709E-03	9.943E-04	5.653E-03	5.705E-03
Cs_2O	1.284E-06	3.703E-07	2.936E-06	2.224E-06	3.423E-06	2.440E-06

Example #	1	2	3	4	5	6
CuO	1.644E-05	1.459E-06	2.899E-05	0.000E+00	0.000E+00	1.953E-05
Eu_2O_3	2.579E-11	3.238E-12	2.069E-10	2.239E-10	1.397E-09	2.085E-10
F	9.677E-04	1.719E-02	7.451E-04	4.526E-03	1.470E-02	1.438E-02
Fe_2O_3	6.779E-04	1.935E-03	9.947E-03	9.966E-02	5.292E-02	1.636E-02
Gd_2O_3	0.000E+00	0.000E+00	0.000E+00	0.000E+00	0.000E+00	0.000E+00
HgO	0.000E+00	0.000E+00	0.000E+00	0.000E+00	0.000E+00	0.000E+00
I	8.150E-08	3.779E-08	9.851E-08	1.317E-06	1.898E-07	5.306E-07
K_2O	2.912E-03	2.572E-03	1.081E-03	5.674E-04	1.243E-03	1.177E-03
La_2O_3	8.933E-10	7.869E-05	3.437E-05	2.127E-04	2.433E-03	3.979E-05
Li_2O	1.869E-02	2.434E-02	4.056E-05	2.216E-02	2.207E-03	2.726E-05
MgO	3.344E-04	4.209E-04	3.667E-04	1.339E-04	1.848E-04	2.876E-04
MnO	1.262E-04	1.155E-04	9.186E-04	4.482E-03	3.866E-03	2.843E-03
MoO_3	1.268E-04	3.092E-06	5.406E-05	0.000E+00	0.000E+00	2.766E-05
Na_2O	1.238E-01	1.461E-01	2.268E-01	1.464E-01	1.533E-01	2.161E-01
Nb_2O_5	1.786E-10	1.825E-11	7.044E-11	4.203E-11	1.177E-09	4.608E-11
Nd_2O_3	1.533E-04	2.580E-05	2.430E-04	0.000E+00	0.000E+00	1.656E-04
NiO	3.298E-05	2.540E-05	1.948E-04	2.644E-03	2.241E-03	9.289E-04
NpO_2	5.748E-07	1.110E-07	1.856E-06	1.394E-07	3.916E-06	2.741E-06
P_2O_5	1.060E-03	1.969E-03	3.920E-03	3.718E-02	4.090E-03	4.127E-03
Pa_2O_5	1.328E-09	1.441E-10	6.933E-10	2.150E-10	5.688E-10	1.440E-09
PbO	1.401E-04	1.578E-05	3.609E-04	7.274E-03	1.012E-03	4.817E-04
PdO	0.000E+00	0.000E+00	0.000E+00	0.000E+00	0.000E+00	0.000E+00
Pr_2O_3	0.000E+00	0.000E+00	0.000E+00	0.000E+00	0.000E+00	0.000E+00
PuO_2	6.375E-08	1.185E-06	2.173E-06	2.795E-05	1.377E-05	1.620E-05
RaO	4.192E-14	4.948E-15	2.054E-14	1.574E-13	1.868E-13	2.837E-12
Rb_2O	0.000E+00	0.000E+00	0.000E+00	0.000E+00	0.000E+00	0.000E+00
Rh_2O_3	0.000E+00	0.000E+00	0.000E+00	0.000E+00	0.000E+00	0.000E+00
RuO_2	4.846E-25	4.663E-25	3.841E-05	2.762E-25	1.709E-24	2.956E-05
SO_3	1.080E-03	5.292E-03	3.463E-03	4.007E-03	1.251E-02	8.609E-03
Sb_2O_3	7.293E-05	4.451E-07	1.330E-05	9.505E-15	3.161E-14	2.182E-15
SeO_2	1.428E-04	1.512E-06	8.081E-05	8.410E-09	2.045E-08	1.071E-07
SiO_2	3.086E-01	4.338E-01	4.286E-01	4.130E-01	4.261E-01	4.351E-01
Sm_2O_3	5.855E-07	4.580E-08	4.133E-06	4.676E-06	9.382E-06	3.549E-06
SnO_2	2.834E-07	2.880E-08	9.548E-08	5.128E-08	2.311E-06	6.113E-08
SrO	1.053E-07	3.434E-07	1.031E-05	2.019E-04	1.440E-04	3.212E-05
Ta_2O_5	0.000E+00	0.000E+00	0.000E+00	0.000E+00	0.000E+00	0.000E+00
Tc_2O_7	9.360E-06	5.404E-07	3.387E-07	1.495E-06	1.484E-06	8.398E-07
TeO_2	0.000E+00	0.000E+00	0.000E+00	0.000E+00	0.000E+00	0.000E+00
ThO_2	9.908E-07	1.543E-06	4.519E-05	5.006E-04	6.013E-04	9.548E-03
TiO_2	1.210E-04	1.366E-03	1.083E-03	1.166E-04	8.704E-05	7.368E-05
Tl_2O	0.000E+00	5.329E-07	3.831E-05	0.000E+00	0.000E+00	0.000E+00
UO_3	1.382E-04	2.646E-03	2.475E-04	7.422E-03	1.032E-03	8.313E-03
V_2O_5	1.149E-04	1.005E-05	2.093E-05	0.000E+00	5.033E-02	5.018E-02

Example #	1	2	3	4	5	6
WO_3	0.000E+00	0.000E+00	2.749E-04	0.000E+00	0.000E+00	2.116E-04
Y_2O_3	4.582E-13	6.257E-06	8.404E-05	1.386E-09	2.379E-09	6.235E-05
ZnO	5.883E-03	2.021E-02	3.976E-02	1.180E-02	0.000E+00	2.602E-02
ZrO_2	2.697E-02	4.506E-02	2.704E-02	2.758E-02	1.429E-03	2.047E-02
SUM	1	1	1	1	1	1

Table 3.7. Predicted glass properties; limiting values are bold.

Example #:	1	2	3	4	5	6
Melt temperature, °C:	1150	1150	1150	1150	1150	1150
Property (no uncertainties)						
ln(PCT NC_{Ave}, g/L)	0.5372	-0.1878	0.1841	-0.9552	0.3033	0.5785
ln(TCLP r_B, mg/L)	4.4701	5.0789	4.8619	3.9210	5.7383	5.3341
NP P[(a)]	0.0391	0.0784	0.0369	0.0428	0.0867	0.0452
w_{SO3}, wt%	1.2270	1.2817	1.1806	1.1298	1.9644	1.5173
ln(k_{neck}, inch)	-5.5049	-4.3356	-4.1941	-4.2991	-4.2298	-4.2465
$\log_{10}(\eta_{1150}$, Pa·s)	0.8027	0.5511	0.8034	0.8301	0.4344	0.6675
$\log_{10}(\eta_{1100}$, Pa·s)	1.0126	0.7460	1.0133	1.0417	0.6224	0.8693
$\log_{10}(\varepsilon_{1100}$, S/m)	1.2995	1.4648	1.6565	1.4795	1.3700	1.6546
$\log_{10}(\varepsilon_{1200}$, S/m)	1.4660	1.6145	1.7866	1.6277	1.5294	1.7850
T_L-P, °C	1057.2	931.4	903.2	1008.8	1080.2	962.4
T_L-Zr, °C	1087.9	783.0	1046.2	1015.5	769.0	967.3
SP C_{950}, vol%	0.3732	-0.6134	-0.8752	0.4107	-0.8604	-0.9939
Prediction uncertainty (U_{pred})						
ln(PCT NC_{Ave}, g/L)	0.5196	0.3337	0.3995	0.4614	0.5598	0.5291
ln(TCLP r_B, mg/L)	0.5384	0.3446	0.6291	0.5800	0.5163	0.4969
w_{SO3}, wt%	0.1182	0.0993	0.0803	0.1540	0.1107	0.1004
ln(k_{neck}, inch)	0.3566	0.1663	0.1606	0.4060	0.3092	0.2238
$\log_{10}(\eta_{1150}$, Pa·s)	0.0125	0.0088	0.0090	0.0095	0.0142	0.0137
$\log_{10}(\eta_{1100}$, Pa·s)	0.0132	0.0093	0.0095	0.0102	0.0151	0.0145
$\log_{10}(\varepsilon_{1100}$, S/m)	0.0131	0.0078	0.0078	0.0126	0.0126	0.0113
$\log_{10}(\varepsilon_{1200}$, S/m)	0.0119	0.0073	0.0077	0.0115	0.0115	0.0106
T_L-P, °C	36.5	30.1	42.7	30.4	53.0	37.6
T_L-Zr, °C	62.2	59.2	82.2	56.5	67.0	73.3
SP C_{950}, vol%	0.4170	0.5321	0.5472	0.4075	0.4861	0.5576
Composition uncertainty (U_{comp})						
ln(PCT NC_{Ave}, g/L)	0.2039	0.1146	0.2672	0.2215	0.2241	0.3000
ln(TCLP r_B, mg/L)	0.1830	0.0975	0.1661	0.1414	0.1414	0.1795
NP P	0.0081	0.0036	0.0059	0.0066	0.0056	0.0059
w_{SO3}, wt%	0.0507	0.0309	0.0698	0.0566	0.0537	0.0750
ln(k_{neck}, inch)	0.2858	0.1426	0.3446	0.2042	0.2317	0.3338
$\log_{10}(\eta_{1150}$, Pa·s) up	0.0879	0.0494	0.0907	0.0634	0.0662	0.0893
$\log_{10}(\eta_{1150}$, Pa·s) low	0.0905	0.0449	0.0867	0.0623	0.0627	0.0863
$\log_{10}(\eta_{1100}$, Pa·s)	0.0932	0.0523	0.0961	0.0672	0.0701	0.0946
$\log_{10}(\varepsilon_{1100}$, S/m)	0.0367	0.0231	0.0585	0.0388	0.0419	0.0547
$\log_{10}(\varepsilon_{1200}$, S/m)	0.0335	0.0215	0.0508	0.0342	0.0378	0.0495
T_L-P, °C	11.2	7.6	21.4	10.8	8.3	15.1

Example #:	1	2	3	4	5	6
Melt temperature, °C:	1150	1150	1150	1150	1150	1150
T_L-Zr, °C	36.4	32.0	38.0	19.0	27.7	45.1
SP C_{950}, vol%	0.2098	0.0966	0.2128	0.1818	0.1607	0.2082
Property (with uncertainties)						
PCT NC_{Ave}, g/L	3.5276	1.2975	2.3414	0.7616	2.9661	4.0862
TCLP r_B, mg/L	179.74	249.90	286.31	103.79	599.42	407.70
TCLP C_{Cd}, mg/L	0.0042	0.0021	0.0135	0.0001	0.0000	0.0133
TCLP C_V, mg/L	0.0116	0.0014	0.0034	0.0000	**16.9000**	11.4593
TCLP C_{Cr}, mg/L	0.1701	0.6502	1.1183	0.0706	2.3183	1.5914
NP P	**0.0310**	0.0748	**0.0310**	0.0362	0.0811	0.0393
w_{SO3}, wt%	1.0580	1.1516	1.0306	0.9192	1.7999	1.3419
w_{SO3}-offset, wt%	0.7280	0.8216	0.7006	0.5892	**1.4699**	**1.0119**
g_{SO3} in br glass, wt%	0.1278	0.6226	0.4094	0.4738	**1.4699**	**1.0119**
k_{neck}, inch	0.0077	0.0178	**0.0250**	**0.0250**	**0.0250**	**0.0250**
η_{1150} up, Pa·s	**8.00**	4.07	**8.00**	**8.00**	3.27	5.89
η_{1150} low, Pa·s	5.01	3.14	5.10	5.73	2.28	3.69
η_{1100}, Pa·s	13.15	6.42	13.15	13.16	5.10	9.52
ε_{1100}, S/m	17.77	27.16	38.92	26.80	20.68	38.78
ε_{1200}, S/m	32.47	43.98	**70.00**	47.14	37.91	**70.00**
T_L-P + Sigmoid, °C	47.7	37.7	64.1	**1050.0**	61.4	52.8
T_L-Zr + Sigmoid, °C	**1050.0**	874.1	**1050.0**	**1050.0**	94.6	118.4
SP C_{950}, vol%	**1.00**	0.02	-0.12	**1.00**	-0.21	-0.23
g_F in br glass, wt%	0.14	**2.50**	0.11	0.66	2.13	2.10

(a) Unit for NP P is described in the text.

Table 3.8 lists the results from waste transfer volume calculations. NO_2, NO_3 and TOC values for each waste can be found in Appendix B.

Table 3.8. Waste transfer volume calculation results.

Example #:	1	2	3	4	5	6
Waste transfer volume, L	9721.27	5398.41	8742.09	9905.78	9266.91	7564.36
Total GFC volume, L	1218.20	2984.55	2148.08	1016.95	1646.74	1840.87
Dust control water volume, L	101.31	274.77	203.21	104.19	151.97	177.05
Sucrose volume, L	73.73	41.07	21.12	87.58	48.88	0.00
Water addition, L/MFPV	770.50	770.50	770.50	770.50	770.50	770.50
Feed concentration, g glass/L feed	245.87	550.00	524.97	310.60	397.65	550.00
Dilution water volume, L	0.00	2415.69	0.00	0.00	0.00	1532.22

3.6 Model Recommendations

Table 3.9 summarizes the recommendations from the models and constraints for immobilizing DFHLW. With the range of flowsheet options currently being considered, it may also be useful to consider how these and previous models can be applied to estimate loading of PTHLW. The current system plan (Schubick et al. 2023) uses a combination of models and constraints based on those from Vienna et al. (2016) (EWG1) and augmented with revised nepheline model (Lu et al. 2021a), increased F limit (Jin et al. 2020), and various additional tweaks in Glass Model

Calculator (GMC v1.4) for convenience; we'll call these models EWG1.4. Starting with these models, we've selected alternative models for those cases when the same property can be predicted significantly more precisely in the PTHLW glass composition region (primarily using EWG2.6 models). This revised PTHLW model and constraint set is also listed in Table 3.9 as EWG1.5.

The intended application of EWG1.5 models includes late stages of the Hanford tank cleanup mission which may include immobilization of CST. The main chemical constituents of CST are TiO_2, Nb_2O_5, SiO_2, and ZrO_2 (approximate wt%: 37, 23, 19, and 18). The EWG1.5 models contain data with sufficient fractions of TiO_2, SiO_2, and ZrO_2 to estimate their effects. However, sufficient data on Nb_2O_5 was not gathered. Literature was summarized to develop a single component limit for Nb_2O_5 until sufficient data is collected and valid models are developed. Several researchers developed successful glasses with CST combined with tank waste sludge (Russell et al. 2019b, Matlack et al. 2018, Andrews et al. 1997, Kot et al. 2016). In addition, Fox and Edwards (2010 and 2011a) evaluated the effect of systematic variations in Nb_2O_5 on Savannah River Site sludge containing glass properties. The main problem with CST and Nb_2O_5 is that they cause crystallization in the melter. Depending on the glass composition including what the sludge and how much sludge is being blended, the loading of Nb_2O_5 can range from 1.2 to 2.3 wt% in glass without crystals forming at melt temperatures. Based on these results, we recommend using the "others" component to estimate the effect of Nb_2O_5 on glass properties and instituting a separate 2 wt% Nb_2O_5 limit.

Similarly, a number of different LAW glass models and constraints are available. Table 3.9 summarizes two such model and constraint sets. The WTP baseline models based on Piepel et al. (2007) and Kim and Vienna (2012). Version 1 of the enhanced LAW glass models (ELGs) are reported by Vienna et al. (2022b). It's our recommendation that for operations under the TSCR flowsheet, the WTP baseline be used for design of LAW glasses, while for operations after the Advanced Modular Pretreatment System (AMPS) begins processing, the rate of LAW generation should match LAW Facility throughput, giving advantage to the use of ELG1 formulations. Table 3.10 lists the modal validity ranges for HLW and LAW glass formulation algorithms. Table 3.11 lists the GFCs used in DFHLW, pretreated HLW, LAW (TSCR), and LAW (AMPS) glass formulation algorithms.

Table 3.9. Models and constraints recommendations for treating DFHLW, pretreated HLW, LAW (TSCR), and LAW (AMPS).

Property	DFHLW (EWG3.0)		PTHLW (EWG1.5)		LAW (TSCR) (WTP Baseline)		LAW (AMPS) (ELG1)	
	Model	Constraint	Model	Constraint	Model	Constraint	Model	Constraint
PCT	EWG3.0	$NC_{Ave}+U_s \leq 12.87$ g/L	Vienna and Crum (2018)	$NL_{Ave} \leq 6.44$ g/m^2	Kim and Vienna (2012)	$NL+U_{pred} < 2$ g/m^2, (for B, Na and Si)	Vienna et al. (2022b)	$NL \leq 2$ g/m^2, (for B and Na)
VHT	NA	NA	NA	NA	Kim and Vienna (2012)	$r_a + U_{pred} < 50$ g/m^2/d	Vienna et al. (2022b)	$p < 0.190$
TCLP	EWG3.0	$C_{Cd} + U_S \leq 0.48$ mg/L, $C_V + U_S \leqslant 16.9$ mg/L, $C_{Cr} + U_S \leqslant 4.95$ mg/L	Kim and Vienna (2003)	$C_{Cd} \leq 0.48$ mg/L	NA	NA	NA	NA
Nepheline formation	Lu et al. (2021a)	$NP\ P + U_{Comp} \geq 0.031$	Lu et al. (2021a)	$p \geq 0.000$	NA	NA	Lu et al. (2021a)	$p \geq 0.028$
Viscosity	EWG3.0	$2 \leq \eta_{1150} \pm U_s \leq 8$ Pa·s $\eta_{1100} + U_s < 15$ Pa·s	EWG2.6	$2 \leq \eta_{1150} \leq 8$ Pa·s $\eta_{1100} < 15$ Pa·s	Kim and Vienna (2012)	$2 \leq \eta_{1150} \pm U_{pred} \leq 8$ Pa·s $\eta_{1100} + U_{pred} < 15$ Pa·s	Vienna et al. (2022b)	$2 \leq \eta_{1150} \leq 8$ Pa·s $\eta_{1100} < 15$ Pa·s
EC	EWG3.0	$\varepsilon_{1100} - U_s \geq 0.1$ S/cm $\varepsilon_{1200} + U_s \leq 0.7$ S/cm	EWG2.6	$\varepsilon_{1100} \geq 0.1$ S/cm $\varepsilon_{1200} \leq 0.7$ S/cm	Kim and Vienna (2012)	$\varepsilon_{1100} - U_{pred} \geq 0.2$ S/cm $\varepsilon_{1200} + U_{pred} \leq 0.7$ S/cm	Vienna et al. (2022b)	$\varepsilon_{1100} \geq 0.2$ S/cm $\varepsilon_{1200} \leq 0.7$ S/cm
Melter SO_3 tolerance	EWG3.0	$g_{SO3} \leq w_{SO3}$–offset-U_S, wt%	EWG2.6	$g_{SO3} \leq w_{SO3}$ - offset, wt%	NA	NA	Vienna et al. (2022b)	$g_{SO3} \leq w_{SO3}$, wt%
Immiscibility	Peeler and Hrma (1994)	$N_{NaLi} \geq 20$ wt%	Peeler and Hrma (1994)	$N_{NaLi} \geq 20$ wt%	NA	NA	NA	NA
K-3 corrosion	EWG3.0	$k_{neck} + U_s \leq 0.025$ in	NA	NA	NA	NA	Vienna et al. (2022b)	$k_{1208} \leq 0.04$ in
Phosphate T_L	EWG3.0	T_L-P + $U_s \leq 1050$°C (for $g_{P2O5} > 0.01$)	EWG2.6	T_L-P ≤ 1050°C (for $g_{P2O5} \geq 0.01$)	NA	NA	NA	NA
Zirconia T_L	EWG2.6	T_L-Zr + $U_s \leq 1050$°C (for $g_{ZrO2} \geq 0.027$)	EWG2.6	T_L-Zr ≤ 1050°C (for $g_{ZrO2} \geq 0.027$)	NA	NA	NA	NA
Spinel	EWG3.0	$C_{950} + U_s \leq 950$ °C	Vienna et al. (2016)	$T_{2\%} \leq 950$°C	NA	NA	NA	NA
Melter and canister centerline cooling crystallization constraint	NA	NA	NA	NA	NA	NA	Vienna et al. (2022b)	Section 9.9
Multi MV limits	EWG3.0	This report, Section 3.2	Vienna et al. (2016)	$SiO_2+B_2O_3 > 32$ wt%	Kim and Vienna (2012)	Table 13	Vienna et al. (2022b)	13.5 wt% ≤ Nalk ≤27.018 wt% $SiO_2 + 1.697Al_2O_3$ ≤61.6 wt%
Additional considerations	Sigmoid for T_L models				Formulation correlation in Kim and Vienna (2012)			

NC = normalized concentration by 7-day PCT; NL = normalized loss by 7-day PCT
$U_s = U_{pred} + U_{comp}$

Table 3.10. Modal validity ranges for HLW and LAW glass formulation algorithms.

Waste type:	HLW						LAW			
Algorithm:	WTP-2014		EWG1.5 (PTHLW)[a]		EWG3.0 (DFHLW)		WTP baseline (TSCR)		ELG1 (AMPS)	
Reference:	Vienna and Kim (2014)		Vienna et al. (2016) and (2025)		This report		Kim and Vienna (2012)		Vienna et al. (2022b)	
	Min	Max	Min	Max	Min	Max	Min	Max	Min	Max
Al_2O_3	0.018 [0.019]	0.13 [0.085]	0.03	0.3	0.04	0.2721	0.035	0.09	0.035	0.1475
B_2O_3	0.045	0.15	0.04	0.22	0.0405	0.224	0.06	0.131	0.06	0.1383
Bi_2O_3	0	In others	0	0.0537	0	0.0155	-	-	-	-
CaO	0	0.01	0	0.10	0	0.0994	0	0.105	0	0.1278
CdO	0	0.001 [0.016]	0	0.015	0	0.0134	-	-	-	-
Cl	-	-	0	0.0117	0	0.0117	-	-	-	-
Cr_2O_3	0	0.006 [0.005]	0	0.0158	0	0.0127	0	0.0059	0	0.0063
F	0	0.0044	0	0.025	0	0.0452	0	0.0035	0	0.013
Fe_2O_3	0.014 [0.019]	0.15 [0.14]	0	0.1206	0	0.1254	0	0.08	0	0.1198
K_2O	0	0.016	0	0.0584	0	0.0584	0	0.054	0	0.059
Li_2O	0 [0.019]	0.06	0	0.0512	0	0.0512	0	0.058	0	0.0584
MgO	0	0.012	0	0.0432	0	0.03	0	0.05	0	0.0502
MnO	0	0.08 [0.07]	0	0.0677	0	0.0522	-	-	-	-
Na_2O	0.039	0.2 [0.15]	0.041	0.2695	0.04	0.25	0.025	0.23	0.0247	0.2657
NiO	0	0.01	0	0.0266	0	0.0218	-	-	-	-
P_2O_5	0	0.045	0	0.045	0	0.0399	0	0.03	0	0.0403
SiO_2	0.35	0.53	0.2459	0.53	0.2412	0.5024	0.384	0.521	0.3352	0.5226
SO_3	-	-	0	0.028	0	0.021	-	-	-	-
SnO_2	-	-	0	0.0504	0	0.0503	-	-	-	-
SrO	0	0.1	0	0.0788	0	0.0864	-	-	-	-
ThO_2	0	0.06	0	0.0440	0	0.0441	-	-	-	-
TiO_2	0	0.01	0	0.0294	0	0.05	0	0.03	0	0.0501
UO_3	0	0.065 [0.063]	0	0.063	0	0.065	-	-	-	-
V_2O_5	-	-	0	0.0570	0	0.0514	-	-	-	-
ZnO	0	0.04	0	0.04	0	0.0405	0.01	0.054	0	0.0582
ZrO_2	0	0.096 [0.091]	0	0.0932	0	0.0932	0	0.05	0	0.0675
LN_2O_3	-	-	0	0.0152	0	0.0289	-	-	-	-
Others	0	0.0519 [0.0429]	0	0.0199	0	0.0205	0	0.0028	-	-

(a) An additional constraint on Nb_2O_5 (≤ 2 wt%) is recommended for EWG1.5, as discussed in the main text. SO_3 was maximum $w_{SO3\text{-}3TS}$ minus 0.33 wt% melter offset.

Table 3.11. GFCs used (labeled as Y) in DFHLW, pretreated HLW, LAW (TSCR), and LAW (AMPS) glass formulation algorithms.

GFCs	EWG3.0 (DFHLW)	EWG1.5 (PTHLW)	WTP Baseline (LAW TSCR)	ELG1 (LAW AMPS)
Kyanite	Y	Y	Y	Y
Boric acid	Y	Y	Y	Y
Borax	**N**	**N**	**N**	**N**
Wollastonite	Y	Y	Y	Y
Na_2CO_3	Y	Y	Y	**N**
Li_2CO_3	Y	Y	Y	Y
Cr_2O_3	Y	Y	**N**	Y
Silica	Y	Y	Y	Y
Zincite	Y	Y	Y	Y
Zircon	Y	Y	Y	Y
V_2O_5	Y	Y	**N**	Y
SnO_2	**N**	**N**	**N**	Y
Olivine	**N**	Y	Y	Y
Rutile	**N**	**N**	Y	Y
Fe_2O_3	**N**	**N**	Y	**N**
Sucrose	Y	Y	Y	Y

4.0 Conclusions

An iterative approach was adopted to develop property data, models, and formulation constraints and optimality criteria for DFHLW glasses. This report documents the current iteration results – EWG3.0. These models incorporate the data currently available for Hanford HLW and LAW glasses, including a set of DFHLW glasses.

The EWG1 formulation method was developed in 2016 for application to pretreated waste at the Hanford Site (Vienna et al. 2016). It was applied to designing preliminary DFHLW glasses for the WTP, and a subset of these glasses was tested to evaluate how well the models and constraints for pretreated wastes applied to DFHLW glasses (Gervasio et al. 2024). Measured property data for the 15 APPS glasses were only partially predicted by the original EWG1 models. The shortcomings were explained by the combination of LAW and HLW in the DFHLW feeds and therefore DFHLW glasses. A new set of models and constraints were developed for datasets that combined LAW glasses with DFHLW glasses – EWG2.5.

A second set of glasses (APPS2) were formulated using the current estimates of DFHLW feed from Britton and Andersen (2024) and the EWG2.5 properties and constraints. Some (7/16) of the APPS2 glasses failed at least one design constraint (Russell et al. 2025a). In addition, it was suggested that the crystallinity (from 2% to 1% spinel ≤ 950°C) and k_{neck} (from 0.04 to 0.025 in.) constraints be tightened to reduce risk of complications to melter testing (Peters 2025). Based on the tightening of constraints and the failure to conservatively estimate key properties, it was decided that an additional set of intermediate models (EWG2.6) would be needed before EWG3.0 models became available.

Since the EWG2.6 models became available, a significant amount of additional data has become available for model development. This additional data includes 215 glasses designed and tested to fill gaps in the DFHLW composition region. This report documents the development and proposed method of applying the EWG3.0 models to form a method to formulate DFHLW glasses for interim design support activities while additional data are collected and models developed for final plant operation (e.g., EWG5). New models were developed to predict η_T, ε_T, w_{SO3}, k_{neck}, T_L-P, C_{950}-Sp, PCT, and TCLP of DFHLW glasses. These models include data not available during the fitting of EWG2.6 models and represent an incremental improvement in the ability to design glasses. These models and associated glasses designed using them do not represent the glasses that will be used during plant operation. Rather, they are intended to supply a reasonable estimate of ultimate glass compositions and waste loading to allow design support flowsheet calculations to be confirmed for final design.

The property and composition constraints were tabulated along with the proposed use of prediction uncertainty and which GFCs should be used. Based on the EWG3.0 models and constraints, six example glass compositions were conducted to demonstrate the proper application of the method.

5.0 References

10 CFR 830, *Nuclear Safety Management*. Code of Federal Regulations, as amended.

Amoroso, J. W., M. Page, and N. Rod. 2024. *Corrosion Testing of Refractory in Contact with Molten Glasses Designed for Waste Vitrification - APPS1 Matrix Glasses*. Savannah River National Laboratory, SRNL-STI-2024-00055, Rev. 2. Aiken, SC.

Andrews, M. K. and P. J. Workman. 1997. *Glass Formulation Development and Testing for the Vitrification of DWPF HLW Sludge Coupled with Crystalline Silicotitanate (CST) (U).* Westinghouse Savannah River Company, WSRC-TR-97-00312. Aiken, SC.

Bai, J., J. V. Crum, X. Lu, J. D. Vienna, and A. A. Kruger. 2025. "Liquidus temperature of phosphate crystalline phases in borosilicate waste glasses." *Journal of the American Ceramic Society*, 109 (1): e70255. https://doi.org/10.1111/jace.70255

Bernards J. K., G. A. Hersi, T. M. Hohl, R. T. Jasper, P. D. Mahoney, N. K. Pak, S. D. Reaksecker, A. J. Schubick, E. B. West, L. M. Bergmann, et al. 2020. *River Protection Project System Plan*. U.S. Department of Energy, Office of River Protection, ORP-11242, Rev. 9. Richland, WA.

Bernards, J. K., G. A. Hersi, K. T. Pak, A. J. Schubick, L. M. Bergmann, A. N. Praga, and S. N. Tilanus. 2021. *High-Level Waste Analysis of Alternatives Model Results Report*. Washington River Protection Solutions, RPP-RPT-61957, Rev. 2. Richland, WA.

Blumenkranz, D. B. 2006. *Petition to Delist Immobilized High-Level Waste Generated at the Waste Treatment and Immobilization Plant*. U.S. Department of Energy, Office of River Protection, DOE/ORP-2006-03, Rev. 0. Richland, WA.

Britton, M. D. 2023. *Revised DFHLW Washing and Blending Study Campaign Inventory*. Washington River Protection Solutions, WRPS-2300881, Richland, WA.

Britton, M. D. and C. K. Anderson. 2024. *Direct-Feed High-Level Waste Feed Vectors Assessment*. Washington River Protection Solutions, RPP-RPT-64878, Rev. 0, Richland, WA.

Bunnell, L. 1988. *Laboratory work in support of west valley glass development*, Pacific Northwest Laboratory, PNL-6539. Richland, WA.

Chapman, C. 2007. *High Level Waste Vitrification Plant Capacity Enhancement Study*. Waste Treatment and Immobilization Plant, 24590-HLW-RPT-PE-07-001. Richland, WA.

Cozzi, A. D. 2003. *Durability Assessment of High Alkali Glasses in Support of the Accelerated Clean-Up Mission: Experimental Results of the "'ND"' Glasses*. Savannah River Site, WSRC-TR-2003-00287. Aiken, SC.

Cozzi, A. D., K. G. Brown, D. K. Peeler, and T. B. Edwards. 2002. *Selecting Compositions for the Phase 1 of the PCT Assessment Study*. Westinghouse Savannah River Company, WSRC-RP-2002-00297, Rev. 0. Aiken, SC.

Crum, J. V., J. D. Vienna, D. K. Peeler, and I. A. Reamer. 2001. *Formulation Efforts for Direct Vitrification of INEEL Blend Calcine Waste Simulate: Fiscal Year 2000*. Pacific Northwest National Laboratory, PNNL-13483. Richland, WA.

Crum, J. V., M. J. Schweiger, P. Hrma, and J. D. Vienna. 1996. "Liquidus temperature model for Hanford high-level waste glasses with high concentrations of zirconia." *MRS Online Proceedings Library* 465: 79-85. https://doi.org/10.1557/PROC-465-79

DOE Order 414.1D, *Quality Assurance*. U.S. Department of Energy, Washington, DC.

DOE. 1996. *Waste Acceptance Product Specifications for Vitrified High-Level Waste Forms (WAPS)*. U.S. Department of Energy, Office of Environmental Management, DOE/EM-0093. Washington, DC.

DOE. 2000. *Design, Construction, and Commissioning of the Hanford Tank Waste Treatment and Immobilization Plant*. U.S. Department of Energy, Office of River Protection, Contract DE-AC27-01RV14136, as amended. Richland, WA.

DOE. 2012. *Waste Acceptance Product Specifications for Vitrified High-Level Waste Forms*. U.S. Department of Energy, EM-WAPS, Rev 3. Washington, DC.

DOE. 2013. *Hanford Tank Waste Retrieval, Treatment, and Disposition Framework*. U.S. Department of Energy, Washington, DC.

Edwards, T. B., J. R. Harbour, and R. J. Workman. 2001. *Impact Of Cooling Rate On The Durability Of PHA Glasses (U)*. Savannah River Site, WSRC-TR-2001-00123, Rev 0. Aiken, SC.

Feng, X., P. R. Hrma, and J. H. Westsik Jr, 1996. *Glass Optimization for Vitrification of Hanford Site Low-Level Tank Waste*. Pacific Northwest National Laboratory, PNNL-10918. Richland, Washington.

Ferkl P., X. Lu, A. A. Kruger, and J. D. Vienna. 2024. "Temperature and composition dependence modeling of viscosity and electrical conductivity of low-activity waste glass melts." *Journal of Non-Crystalline Solids* 640. https://doi.org/10.1016/j.jnoncrysol.2024.123119

Fox, K. M., D. K. Peeler, T. B. Edwards, et al. 2008a. *International Study of Aluminum Impacts on Crystallization in U.S. High Level Waste Glass*. Savannah River National Laboratory, SRNL-STI-2008-00057. Aiken, SC.

Fox, K. M., J. D. Newell, T. B. Edwards, et al. 2007. Refinement of the Nepheline Discriminator: Results of a Phase I Study. Westinghouse Savannah River Company, WSRC-STI-2007-00659. Aiken, SC.

Fox, K. M., T. B. Edwards, D. R. Best, et al. 2008b. *Frit Development for High Level Waste Sludge Batch 5: Compositional Trends for Varying Aluminum Concentrations*. Savannah River National Laboratory, SRNL-STI-2008-00060. Aiken, SC.

Fox, K., and T. Edwards, 2011c. *Impacts of Small Column Ion Exchange Streams on DWPF Glass Formulation: KT08, KT09, and KT10-Series Glass Compositions*. Savannah River Site, SRNL-STI-2011-00178. Aiken, SC.

Fox, K., and T. Edwards. 2009. *Experimental Results of the Nepheline Phase III Study*. Savannah River National Laboratory, SRNL-STI-2009-00608, Rev. 0. Aiken, SC.

Fox, K., and T. Edwards. 2010. *Impacts of Small Column Ion Exchange Streams on DWPF Glass Formulation: KT01, KT02, KT03, and KT04-Series Glass Compositions.* Savannah River Site, SRNL-STI-2010-00566. Aiken, SC.

Fox, K., and T. Edwards. 2011a. *Impacts Of Small Column Ion Exchange Streams On DWPF Glass Formulation: KT05-AND KT06-Series Glass Compositions*. Savannah River Site, SRNL-STI-2010-00687. Aiken, SC.

Fox, K., and T. Edwards. 2011b. *Impacts Of Small Column Ion Exchange Streams On DWPF Glass Formulation KT07-Series Glass Compositions*. Savannah River Site, SRNL-STI-2010-00759. Aiken, SC.

Fox, K., D. Miller, and T. Edwards. 2009. *Preliminary Frit Development and Melt Rate Testing for Sludge Batch 6 (SB6)*. Savannah River Site, SRNL-STI-2009-00440. Aiken, SC.

Gan, H., K. Gilbo, A. E. Papathanassiu, W. K. Kot, and I. L. Pegg. 2015. *Calcium Phosphate Constraints in HLW Glasses: Phosphate Liquidus Model.* Vitreous State Laboratory, the Catholic University of America, VSL-15R3420-1. Washington, DC.

Gan, H., W. K. Kot, and I. L. Pegg. 2012. *Development of High Waste-Loading HLW Glasses for High Bismuth Phosphate Wastes.* Vitreous State Laboratory, the Catholic University of America, VSL-12R2550-1, Washington, DC.

Gervasio, V., J. J. Neeway, J. D. Vienna, J. B. Lang, B. E. Westman, J. T. Reiser, C. E. Lonergan, X. Lu, S. M. Baird, D. A. Cutforth, and M. Peterson. 2023. *Enhanced Hanford Low-Activity Waste Glass Property Data Development: Phase 5 and Phase 6.* Pacific Northwest National Laboratory, PNNL-34331. Richland, WA.

Gervasio, V., R. L. Russell, J. Marcial, X. Lu, N. A. Lumetta, L. M. Seymour, J. T. Reiser, J. Neeway, S. Chong, D. A. Cutforth, et al. 2026. *Low-Activity Waste High Sodium and Potassium Glass Testing (LAWHNK) Matrix*. Pacific Northwest National Laboratory, PNNL-38969. Richland, WA.

Gervasio, V., X. Lu, J. T. Reiser, M. Peterson, N. L. Canfield, J. B. Lang, J. C. Rigby, J. L. George, D. A. Cutforth, J. M. Westman, et al. 2024. *Direct Feed High-Level Waste APPS Model Glass Testing (DFHLW APPS) Matrix*. Pacific Northwest National Laboratory, PNNL-35503. Richland, WA.

Gillam Jr, J. H., K. M. Fox, T. B. Edwards, and D. K. Peeler. 2007. *Frit Selection to Support Steklo Metallicheskie Konstruktsii (SMK) Melter Testing with SRNL Feeds*. Savannah River Site, WSRC-STI-2007-00363. Aiken, SC.

Gunnell, L., X. Lu, J. D. Vienna, D. S., Kim, B. J. Riley, and J. Hedengren. 2025. “Uncertainty propagation and sensitivity analysis for constrained optimization of nuclear waste vitrification.” *Journal of the American Ceramic Society* 108 (7): e20446. https://doi.org/10.1111/jace.20446

Harbour, J. R., T. B. Edwards, and R. J. Workman. 2000. *Summary of Results for Macrobatch 3 Variability Study*. Savannah River Site, WSRC-TR-2000-00351. Aiken, SC.

Heredia-Langner, A., V. Gervasio, S. K. Cooley, C. E. Lonergan, D. S. Kim, A. A. Kruger, and J. D. Vienna. 2022. "Hanford low-activity waste glass composition-temperature-melt viscosity relationships." *International Journal of Applied Glass Science* 13 (4): 514-525. https://doi.org/10.1111/ijag.1658

Herman, C. C. 2002. *Summary of Results for Expanded Macrobatch 3 Variability Study*. Savannah River Site, WSRC-TR-2001-00511, Rev. 0. Aiken, SC.

Hrma, P, J. D. Vienna, M. Mika et al. 1999. *Liquidus Temperature Data for DWPF Glass*. Pacific Northwest National Laboratory, PNNL-11790. Richland, WA.

Hrma, P. R., G. F. Piepel, M. J. Schweiger et al. 1994. *Property/composition relationships for Hanford high-level waste glasses melting at 1150°C*. Pacific Northwest National Laboratory, PNL-10359, Vol. 1. Richland, WA.

Hsieh, M. C., and F. C. Johnson. 2025. *Data Qualification Report: SRNL Glass Composition-Properties (ComPro) Database*. Savannah River National Laboratory, SRNL-STI-2009-00094-x. Aiken, SC.

Jantzen, C. M., N. E. Bibler, D. C. Beam, C. L. Crawford, and M. A. Pickett. 1993. *Characterization of the Defense Waste Processing Facility (DWPF) Environmental Assessment (EA) Glass Standard Reference Material (U)*. Westinghouse Savannah River Company, WSRC-TR-92-346, Rev. 1. Aiken, SC.

Jin, T., D. Kim, J. D. Vienna, and M. S. Fountain. 2020. *Fluorine Limits and Impacts in High-Level Waste Glass Compositions.* Pacific Northwest National Laboratory, PNNL-30072. Richland, WA.

Jin, T., D. Kim, L. P. Darnell, B. L. Weese, N. L. Canfield, M. Bliss, M. J. Schweiger, J. D. Vienna, and A. A. Kruger. 2018. "A crucible salt saturation method for determining sulfur solubility in glass melt." *International Journal of Applied Glass Science* 10 (1): 92-102. https://doi.org/10.1111/ijag.12366

Jin, T., L. Q. Le, N. L. Canfield, K. C. Bryce, E. T. Nienhuis-Marcial, X. Lu, and J. D. Vienna. 2025. *K-3 Refractory Corrosion Test Results, HAL24M2*. Pacific Northwest National Laboratory, PNNL-37964. Richland, WA.

Johnson, F. C., and M. C. Hsieh. 2025. *The User Guide for the ComPro Database*. Savannah River National Laboratory, SRNL-STI-2009-00093-X. Aiken, SC.

Johnson, F., and T. Edwards. 2011. *Sludge Batch 7b Glass Variability Study*. Savannah River Site, SRNL-STI-2011-00440. Aiken, SC.

Kim, D. S., and J. D. Vienna. 2003. *Model for TCLP Releases from Waste Glasses*. Pacific Northwest National Laboratory, PNNL-14061, Rev. 1. Richland, WA.

Kim, D. S., and J. D. Vienna. 2012. *Preliminary ILAW Formulation Algorithm Description*. River Protection Project, Hanford Tank Waste Treatment and Immobilization Plant, 24590-LAW-RPT-RT-04-0003, Rev. 1. Richland, WA.

Kim, D., M. J. Schweiger, C. P. Rodriguez, et al. 2011. *Formulation and Characterization of Waste Glasses with Varying Processing Temperature*. Pacific Northwest National Laboratory, PNNL-20774. Richland, WA.

Kot, W. K., H. Gan, and I. L Pegg. 2006b. *Preparation and Testing of HLW Matrix Glasses to Support Development of WTP Phase 2 Property-Composition Models*. Vitreous State Laboratory, the Catholic University of America, VSL-06R6780-2. Washington, DC.

Kot, W. K., H. Gan, and I. L. Pegg. 2003. *Regulatory Spike Testing for RPP-WTP HLW Glasses*, Vitreous State Laboratory, the Catholic University of America, VSL-03L3780-1. Washington, DC.

Kot, W. K., H. Gan, and I. L. Pegg. 2005. *Preparation and Testing (T1% and PCT) of HLW Matrix Glasses to Support WTP Property-Composition Model Development*. Vitreous State Laboratory, the Catholic University of America, VSL-05R5780-2. Washington, DC.

Kot, W. K., H. Gan, and I. L. Pegg. 2006a. *Preparation and Testing of HLW Glasses to Support Development of WTP IHLW Formulation Algorithm*. Vitreous State Laboratory, the Catholic University of America, VSL-06R1240-1. Washington, DC.

Kot, W. K., I. Joseph, and Ian L. Pegg. 2005. *Comparison of HLW Simulant, Actual Waste, and Melter Glasses*. Vitreous State Laboratory, the Catholic University of America, VSL-05R5760-1. Richland, WA.

Kot, W. K., K. Gilbo, H. Gan, I. Joseph, and I. L. Pegg. 2014*. Enhanced HLW Glass Property-Composition Models – Phase 1*. Vitreous State Laboratory, the Catholic University of America, VSL-14R3080-1. Washington, DC.

Kot, W. K., K. Gilbo, H. Gan, I. Joseph, and I. L. Pegg. 2015. *Enhanced HLW Glass Property-Composition Models – Phase 2*. Vitreous State Laboratory, the Catholic University of America, VSL-15R3400-1. Washington, DC.

Kot, W. K., M. Penafiel, M. Brandys, and I. L. Pegg. 2016. *Vitrification of Inorganic Ion-Exchange Media,* Vitreous State Laboratory, the Catholic University of America, VSL-16R3710-1. Washington, D.C.

Kot, W. K., L. Myers, and I. L. Pegg. 2007. *Baseline HLW Glass Formulations for Bismuth Phosphate Wastes*. Vitreous State Laboratory, the Catholic University of America, VSL-07R1240-2. Washington, DC.

Kot, W., and I. Pegg. 2001. *Glass Formulation and Testing with RPP-WTP HLW Simulants*. Vitreous State Laboratory, the Catholic University of America, VSL-01R2540-2. Washington, DC.

Kot, W., K. Klatt, and I. Pegg. 2003. *Glass formulation to Support Melter Runs with HLW Simulants.* Vitreous State Laboratory, the Catholic University of America, VSL-03R3760-2. Washington, DC.

Kruger, A. A., and J. D. Vienna, 2013, *Enhanced HLW Glass Models.* Briefing for Secretary S. Chu, 18 March 2013. Richland, WA.

Lorier, T. 2004. *SB3 Phase 2 Variability Study: The Impact of REDOX on Durability for the Frit 418-SB2/3 System*. Savannah River Site, WSRC-TR-2003-00539, Aiken, SC.

Lu, X., and J. D. Vienna. 2023. "Selection of Example DFHLW Glasses for Validation Tests." Memo to RL Hanson, dtd 7/26/2023. River Protection Project, Waste Treatment and Immobilization Plant, CCN-335241. Richland, WA.

Lu, X., et al. 2024a. *DFHLW Process Control Chemical Limits Memo.* Pacific Northwest National Laboratory, PNNL-SA-199714, Richland, WA.

Lu, X., I. Sargin, and J. D. Vienna. 2021a. "Predicting nepheline precipitation in waste glasses using ternary submixture model and machine learning." *Journal of American Ceramic Society* 104: 5636-5647. https://doi.org/10.1111/jace.17983

Lu, X., J. D. Vienna, D. Wang, B. Mathew, and P. Ferkl. 2025. *Evaluation of DFHLW EWG2.6 Formulations and Processing Rates*. Pacific Northwest National Laboratory, PNNL-38134. Richland, WA.

Lu, X., J. T. Reiser, B. P. Parruzot, L. Deng, I. M. Gussev, J. C. Neuefeind, T. R. Graham, H. Liu, J. V. Ryan, S. H. Kim, et al. 2021b. "Effects of Al:Si and (Al+Na):Si ratios on the properties of the international simple glass, part II: structure." *Journal of American Ceramic Society* 104: 183-207. https://doi.org/10.1111/jace.17447

Lu, X., J. D. Vienna, and P. Ferkl. 2024b. *Evaluation of DFHLW EWG Formulations and Processing Rates*. Pacific Northwest National Laboratory, PNNL-36196. Richland, WA.

Matlack, K. S., W. K. Kot, and I. L. Pegg. 2018. *Vitrification of Inorganic Ion Exchange Media*. Vitreous State Laboratory, the Catholic University of America, VSL-18R4380-1. Washington, D.C.

Matlack, K. S., H. Gan, M. Chaudhuri, W. K. Kot, W. Gong, T. Bardakci, and I. L. Pegg. 2008b. *Melt Rate Enhancement for High Aluminum HLW Glass Formulations. Final Report*. Vitreous State Laboratory, the Catholic University of America, VSL-08R1360-1, Rev. 0. Washington, DC.

Matlack, K. S., H. Gan, W. Gong, I. L. Pegg, C. C. Chapman, and I. Joseph. 2007. *Final Report High Level Waste Vitrification System Improvements.* Vitreous State Laboratory, the Catholic University of America, VSL-07R1010-1, Rev. 0. Washington, DC.

Matlack, K. S., W. Gong, I. S. Muller, I. Joseph, and I. L. Pegg. 2006. *LAW Envelope C Glass Formulation Testing to Increase Waste Loading*. Vitreous State Laboratory, the Catholic University of America, VSL-05R5900-1. Washington, DC.

Matlack, K. S., W. Kot, H. Gan, and I. L. Pegg. 2012. *Enhanced Sulfate Management in HLW Glass Formulations*. Vitreous State Laboratory, the Catholic University of America, VSL-12R2540-1. Washington, DC.

Matlack, K. S., W. Kot, H. Gan, Z. Feng, and I. L. Pegg. 2013. *Management of High Sulfur HLW*. Vitreous State Laboratory, the Catholic University of America, VSL-13R2920-1. Washington, DC.

Matlack, K. S., W. Kot, W. Gong, and I. L. Pegg. 2008a. *Small Scale Melter Testing of HLW Algorithm Glasses: Matrix 2 Tests*. Vitreous State Laboratory, the Catholic University of America, VSL-08R1220-1. Washington, DC.

Mika, M., M. J. Schweiger, J. D. Vienna, et al. 1997. "Liquidus temperature of spinel precipitating high-level waste glasses." *MRS Online Proceedings Library* 465: 71. https://doi.org/10.1557/PROC-465-71

Muller, I. S., A. C. Buechele, and I. L. Pegg. 2001. *Final Report Glass Formulation and Testing with RPP-WTP LAW Simulants*. Vitreous State Laboratory, the Catholic University of America, VSL-01R3560-2. Washington, DC.

Muller, I. S., and I. L. Pegg. 2003. *Final Report Baseline LAW Glass Formulation Testing*. Vitreous State Laboratory, the Catholic University of America, VSL-03R3460-1. Washington, DC.

Muller, I. S., et al. 2003. *LAW Glass Formulation to Support AZ-102 Actual Waste Testing,* Vitreous State Laboratory, the Catholic University of America, VSL-03R3470-1, Rev. 0. Washington, DC.

Muller, I. S., I. Joseph, and I. L. Pegg, 2005. *Final Report Comparison of LAW Simulant, Actual Waste, and Melter Glasses*. Vitreous State Laboratory, The Catholic University of America, VSL-05R5460-1, Rev. 0. Washington, DC.

Muller, I., W. K. Kot, H. K. Pasieka, K. Gilbo, F. Perez-Cardenas, I. Joseph, and I. L. Pegg. 2012. *Compilation and Management of ORP Glass Formulation Database*. Vitreous State Laboratory, the Catholic University of America, VSL-12R2470-1. Washington, DC.

Muller I. S., K. Gilbo, M. Chaudhuri, I. L. Pegg, and I. Joseph. 2018. *K-3 Refractory Corrosion and Sulfate Solubility Model Enhancement (Final Report)*. Vitreous State Laboratory, The Catholic University of America, VSL-18R4360-1, Rev. 0. Washington, DC.

NQA-1-2012, *Quality Assurance Requirements for Nuclear Facility Application*. American Society of Mechanical Engineers, New York, NY.

Olson, K. M., S. C. Marschman, G. F. Piepel, and G. K. Whiting. 1994. *Product Consistency Testing of West Valley Compositional Variation Glasses*. Pacific Northwest National Laboratory, PNL-10191. Richland, WA.

Page, M. A., J. W. Amoroso, and N. Rod. 2025. *Corrosion Testing of Refractory inContact with Molten Glasses Designed for Waste Vitrification-HAL24 M1 Matrix Glasses*. Savannah River National Laboratory, SRNL-STI-2025-00473. Aiken, SC.

Parsons. 2023. *Waste Treatment and Immobilization Plant High Level Waste Treatment Analysis of Alternatives*. Parsons Corporation, DE-NA0002895, Boston, MA.

Peeler, D. K. 2001. *Reduction of Constraints: Applicability of the Homogeneity Constraint for Macrobatch 3*. Savannah River Site, WSRC-TR-2000-00358, Rev. 0. Aiken, SC.

Peeler, D. K. 2002. *Reduction of Constraints: Phase 1 Experimental Assessment of Centroid-Based Sludge-Only Glasses*. Savannah River Site, WSRC-TR-2002-00120. Aiken, SC.

Peeler, D. K. 2004. *The Impact of the Proposed delta Gp Limits on Glass Formulation Efforts: Part II. Experimental Results*. Savannah River Site, WSRC-TR-2004-00348. Aiken, SC.

Peeler, D. K., and P. Hrma. 1994. "Predicting liquid immiscibility in multicomponent nuclear waste glasses." *Ceramics Transactions* 45: 219-229.

Peeler, D. K., K. M. Fox, T. B. Edwards, et al. 2007. *An Experimental Assessment of the Impact of Sludge Variation on Frit 202-A11-SB3 Glass System*. Savannah River National Laboratory, WSRC-STI-2007-00616. Aiken, SC.

Peeler, D. K., T. B. Edwards, C. C. Herman, et al. 2003. *Sludge Batch 3 Phase 1 Variability Study*. Savannah River Site, WSRC-TR-2002-00549. Aiken, SC.

Peeler, D. K., T. B. Edwards, C. C. Herman, I. A. Reamer, R. J. Workman, and J. D. Vienna. 2002. *Development of High Waste Loading Glasses for Advanced Melter Technologies*. Savannah River National Laboratory, WSRC-TR-2002-00426, Rev. 0. Aiken, SC.

Peeler, D., and T. Edwards. 2011. *The Sludge Batch 7a Glass Variability Study with Frit 418 and Frit 702*. Savannah River Site, SRNL-STI-2011-00063. Aiken, SC.

Peters, R. 2025. "DFHLW Glass Constraints – Supersedes CCN 342375." Memo to D Bauer dtd 2/21/25. Bechtel National Inc., CCN 342390.Richland, WA.

Piepel, G. F., S. K. Cooley, A. Heredia-Langner, et al. 2008. *Final Report IHLW PCT, Spinel T1%, Electrical Conductivity, and Viscosity Model Development*. Vitreous State Laboratory, the Catholic University of America, VSL-07R1240-4, Rev. 0. Washington, DC.

Piepel, G. F., S. K. Cooley, I. S. Muller, H. Gan, I. Joseph, and I. L. Pegg. 2007. *ILAW PCT, VHT, Viscosity, and Electrical Conductivity Model Development.* Vitreous State Laboratory, the Catholic University of America, *VSL-07R1230-1*. Washington, DC.

Raszewski, F. C., T. B. Edwards, D. K. Peeler, D. R. Best, I. A. Reamer, and R. J. Workman. 2008b. *Initial Sludge Batch 4 Tank 40 Decant Variability Study with Frit 510*. Savannah River Site, WSRC-STI-2008-149. Aiken, SC.

Raszewski, F. C., T. B. Edwards, D. K. Peeler, D. R. Best, I. A. Reamer, and R. J. Workman. 2008c. *Variability Study with Frit 510 to Support a Second Tank 40 Decant*. Savannah River Site, WSRC-STI-2008-315. Aiken, SC.

Raszewski, F., and T. Edwards. 2009. *Reduction of Constraints for Coupled Operations*. Savannah River Site, SRNL-STI-2009-00465. Aiken, SC.

Raszewski, F., T. Edwards, and D. Peeler. 2008a. *Matrix 1 Results of the FY07 Enhanced DOE High-Level Waste Melter Throughput Studies at SRNL*. Savannah River Site, SRNL-STI-2008-00056, Aiken, SC.

Reiser, J. T., B. Parruzot, S. Gin, J. F. Bonnett, C. S. Smoljan, L. M. Seymour, J. V. Ryan, and J. D. Vienna. 2022. “Effects of Al:Si and (Al+Na):Si Ratios on the Static Corrosion of Sodium-Alumino-Borosilicate Glasses.” *International Journal of Applied Glass Science* 13 (1): 94-111. https://doi.org/10.1111/ijag.16109

Reiser, J. T., X. Lu, B. P. Parruzot, H. Liu, T. Subramani, H. Kaya, R. Kissinger, J. V. Crum, J. V. Ryan, A. Navrotsky, et al. 2021. “Effects of Al:Si and (Al+Na):Si ratios on the properties of the international simple glass, part I: physical properties.” *Journal of American Ceramic Society* 104: 167-182. https://doi.org/10.1111/jace.17449

Reynolds, J. G. 2006. “Reconciliation of High-Level Waste Rheology Data.” Memorandum, River Protection Project-Waste Treatment Plant, CCN-137198. Richland, WA.

Russell, R. L., B. P. McCarthy, S. K. Cooley, et al. 2019a. *Enhanced Hanford Low- Activity Waste Glass Property Data Development : Phase 2*. Pacific Northwest National Laboratory, PNNL-28838, Rev. 1; EWG-RPT-021, Rev. 1. Richland, WA.

Russell, R. L., D. S. Kim, J. D. Vienna, J. B. Lang, S. M. Baird, D. L. Bellofatto, et al. 2023. *Enhanced Hanford High-Fluoride Waste Glass Property Data Development: Phase 1*. Pacific Northwest National Laboratory, PNNL-35037; EWG-RPT-043. Richland, WA.

Russell, R. L., D. S. Kim, J. D. Vienna, V. Gervasio, C. H. Skidmore, B. J. Riley, and R. A. Peterson. 2019b. *Cold Crucible Vitrification of Non-Radioactive CST and Simulated Hanford Tank Waste.* Pacific Northwest National Laboratory, PNNL-28895. Richland, WA.

Russell, R. L., J. B. Lang, Y. S. Chou, S. K. Cooley, B. P. McCarthy, J. D. Vienna, L. P. Darnell, G. F. Piepel, V. Gervasio, M. J. Schweiger, et al. 2018. *Glass Compositions and Properties of Enhanced Waste Glass with High Alumina Content for High-Level Waste*. Pacific Northwest National Laboratory, PNNL-27138. Richland, WA.

Russell, R. L., T. Jin, B. P. McCarthy, et al. 2017. *Enhanced Hanford Low-Activity Waste Glass Property Data Development : Phase 1*. Pacific Northwest National Laboratory, PNNL-26630, EWG-RPT-012, Rev. 0. Richland, WA.

Russell, R. L., V. Gervasio, S. M. Baird, D. L. Bellofatto, D. A. Cutforth, J. L. George, and J. D. Vienna. 2025c. *Enhanced Hanford High-Aluminum Waste Glass Property Data Development*. Pacific Northwest National Laboratory, PNNL-38071. Richland, WA.

Russell, R. L., V. Gervasio, X. Lu, N. A. Lumetta, N. L. Canfield, L. M. Seymour, and J. T. Reiser, et al. 2025b. *Expansion of the Direct Feed High-Level Waste Glass Composition in the High Al Range*. Pacific Northwest National Laboratory, PNNL-38313. Richland, WA.

Russell, R. L., V. Gervasio, X. Lu, S. Chong, J. T. Reiser, N. L. Canfield, J. L. George, N. A. Lumetta, J. J. Neeway, L. M. Seymour, et al. 2025a. *Direct Feed High-Level Waste APPS Model Glass Testing (DFHLW APPS) Matrix, Phase 2*. Pacific Northwest National Laboratory, PNNL-37506. Richland, WA.

Scholes, B. A., D. K. Peeler, and J. D. Vienna. 2000. *The Preparation and Characterization of INTEC Phase 3 Composition Variation Study Glasses*. Idaho National Engineering and Environmental Laboratory, INEEL/EXT-2000-01566. Idaho Falls, ID.

Scholes, B. A., J. D. Vienna, D. K. Peeler, and T. B. Edwards. 2002. *The preparation and Characterization of INTEC Sodium Bearing Waste Phase 1 Composition Variation Study Glasses*. Idaho National Engineering and Environmental Laboratory, INEEL/EXT-02-00386. Idaho Falls, ID.

Schubick, A. J., L. M. Bergmann, T. M. Hohl, R. T. Jasper, J. McMullin, K. T. Pak, G. V. Smith, U. E. Zaher, S. D. Reaksecker, and S. L. Weld. 2023. *River Protection Project System Plan*. U.S. Department of Energy, Office of River Protection, ORP-11242, Rev. 10. Richland, WA.

Schweiger, M. J., B. J. Riley, J. V. Crum, P. R. Hrma, C. P. Rodriguez, B. M. Arrigoni, et al. 2011. *Expanded High-Level Waste Glass Property Data Development: Phase I*. Pacific Northwest National Laboratory, PNNL-17950. Richland, WA.

Skidmore, C. H., J. D. Vienna, T. Jin, D. S. Kim, B. A. Stanfill, K. M. Fox, and A. A. Kruger. 2019. “Sulfur solubility in low activity waste glass and its correlation to melter tolerance.” *International Journal of Applied Glass Science* 10 (4): 558-568. https://doi.org/10.1111/ijag.13272

Staples, B. A., B. A. Scholes, D. K. Peeler, L. L. Torres, J. D. Vienna, C. A. Musick, and B. R. Boyle. 2000. *The Preparation and Characterization of INTEC Phase 2b Composition Variation Study Glasses*. Idaho National Engineering and Environmental Laboratory, INEEL/EXT-99-01322. Idaho Falls, ID.

Staples, B. A., D. K. Peeler, J. D. Vienna, B. A. Scholes, and C. A. Musick. 1999. *The Preparation and Characterization of INTEC HAW Phase 1 Composition Variation Study Glasses*. Idaho National Engineering and Environmental Laboratory, INEEL/EXT-98-00970. Idaho Falls, ID.

US District Court of Eastern Washington. 2025. *Order Amending Consent Decree Between U.S. Department of Energy and State of Washington*, 2:08-CV-5085-RMP, ECF No. 269, Richland, WA.

Vienna, J. D., A. Heredia-Langner, S. K. Cooley, A. E. Holmes, D. S. Kim, and N. A. Lumetta. 2022b. *Glass Property-Composition Models for Support of Hanford WTP LAW Facility Operation*. Pacific Northwest National Laboratory, PNNL-30932, Rev. 2. Richland, WA.

Vienna, J. D., and D. S. Kim. 2014. *Preliminary IHLW Formulation Algorithm Description*. River Protection Project, Waste Treatment Plant, 24590-HLW-RPT-RT-05-001, Rev. 1. Richland, WA.

Vienna, J. D., and J. V. Crum. 2018. “Non-linear effects of alumina concentration on Product Consistency Test response of waste glasses.” *Journal of Nuclear Materials* 511:396-405. https://doi.org/10.1016/j.jnucmat.2018.09.040

Vienna, J. D., D. K. Peeler, R. L. Plaisted, et al. 2000. *Glass Formulation for Idaho National Engineering and Environmental Laboratory Zirconia Calcine High-Activity Waste*. Pacific Northwest National Laboratory, PNNL-12202. Richland, WA.

Vienna, J. D., D. S. Kim, D. C. Skorski, and J. Matyas. 2013. *Glass Property Models and Constraints for Estimating the Glass to be Produced at Hanford by Implementing Current Advanced Glass Formulation Efforts*. Pacific Northwest National Laboratory, PNNL-22631, Rev. 1; ORP-58289. Richland, WA.

Vienna, J. D., D. S. Kim, I. S. Muller, G. F. Piepel, and A. A. Kruger. 2014. “Toward understanding the effect of low-activity waste glass composition on sulfur solubility.” *Journal of the American Ceramic Society* 97 (10): 3135-3142. https://doi.org/10.1111/jace.13125

Vienna, J. D., G. F. Piepel, D. S. Kim, J. V. Crum, C. E. Lonergan, B. A. Stanfill, B. J. Riley, S. K. Cooley, and T. Jin. 2016. *Update of Hanford Glass Property Models and Constraints for Use in Estimating the Glass Mass to be Produced at Hanford by Implementing Current Enhanced Glass Formulation Efforts*. Pacific Northwest National Laboratory, PNNL-25835. Richland, WA.

Vienna, J. D., H. D. Smith, M. J. Schweiger, J. V. Crum, D. E. Smith, D. K. Peeler, I. A. Reamer, C. A. Musick, and R. D. Tillotson. 1999. *Glass Formulation Development for INEEL Sodium-Bearing Waste*. Pacific Northwest National Laboratory, PNNL-12234. Richland, WA.

Vienna, J. D., P. R. Hrma, M. J. Schweiger, et al. 1996. *Effect of Composition and Temperature on the Properties of High-Level Waste (HLW) Glass Melting Above 1200 degrees Celsius*. Pacific Northwest National Laboratory, PNNL-10987. Richland, WA.

Vienna, J. D., W. C. Buchmiller, J. V. Crum, et al. 2002. *Glass Formulation Development for INEEL Sodium-Bearing Waste*. Pacific Northwest National Laboratory, PNNL-14050. Richland, WA.

Vienna, J. D., S. K. Cooley, J. V. Crum, T. B. Edwards, J. Matyas, D. K. Peeler, G. F. Piepel, and D. E. Smith. 2003. *Liquidus Temperature Testing and Model Evaluation Results*. Pacific Northwest Division, PNWD3369 (WTP-RPT-085), Rev. 0, Richland, WA.

Vienna, J. D., X. Lu, P. Ferkl, D. Kim, J. Marcial, J. Bai, and J.V. Crum, et al. 2025. *Glass Property-Composition Models Update for use in Direct Feed High-Level Waste Flowsheet Development: EWG2.6*. Pacific Northwest National Laboratory, PNNL-37762. Richland, WA.

Vienna, J. D., X. Lu, P. Ferkl, J. Marcial, M. S. Fountain, and C. L. Bottenus. 2022a. *Initial Evaluation of Direct-Feed High-Level Waste Glass Formulations and Processing Rates*. Pacific Northwest National Laboratory, PNNL-32866, Rev. 1. Richland, WA.

Vienna, J. D., X. Lu, P. Ferkl, J. Marcial, M. S. Fountain, M. Trenidad, R. Hanson, M. D. Britton, L. Cree, and W. Abdul. 2023. “High-Level Waste Glass Processing over Broad Range of Alternative Feed Compositions.” In *Proceedings of the 2023 Waste Management Symposia*, Phoenix, AZ.

Vienna, J. D., X. Lu, P. Ferkl, L. L. Gunnell, A. Heredia-Langner, N. A. Lumetta, T. Jin, et al. 2024. *Glass Property-Composition Models Update for use in Direct Feed High-Level Waste Flowsheet Development*. Pacific Northwest National Laboratory, PNNL-35884. Richland, WA.

Westesen, A. M., E. L. Campbell, S. K. Fiskum, A. M. Carney, T. T. Trang-Le, and R. A. Peterson. 2022. “Impact of feed variability on cesium removal with multiple actual waste samples from the Hanford site.” *Separation Science and Technology* 57(15). https://doi.org/10.1080/01496395.2022.2059378

Wilson, B. K., P. Hrma, J. Alton, T. J. Plaisted, and J. D. Vienna. 2002. “The effect of composition on spinel equilibrium and crystal size in high-level waste glass.” *Journal of Materials Science* 37:5327-5331. https://doi.org/10.1023/A:1021081126162

Appendix A – Variance-Covariance Matrices

Table A.1. Variance-covariance table for PCT model (part 1).

	Al_2O_3	B_2O_3	CaO	Fe_2O_3	K_2O	Li_2O	MgO	Na_2O	NiO	P_2O_5
Al_2O_3	14.591079	-0.366347	-0.284203	-0.348157	-0.269928	-0.222833	0.056963	-0.311510	-0.568327	0.473437
B_2O_3	-0.366347	0.937181	-0.012874	-0.064391	-0.075912	-0.083127	-0.089785	-0.022073	0.209621	0.599344
CaO	-0.284203	-0.012874	0.171148	-0.001324	0.024116	0.026101	-0.004851	-0.000879	-0.003179	0.106547
Fe_2O_3	-0.348157	-0.064391	-0.001324	0.504888	-0.011069	-0.007883	-0.039397	0.000356	-0.085967	-0.066231
K_2O	-0.269928	-0.075912	0.024116	-0.011069	1.784898	0.092303	-0.013832	0.071976	-0.027326	-0.331175
Li_2O	-0.222833	-0.083127	0.026101	-0.007883	0.092303	0.134068	-0.007888	0.052143	-0.171090	0.123633
MgO	0.056963	-0.089785	-0.004851	-0.039397	-0.013832	-0.007888	0.459080	0.004120	0.034384	0.136877
Na_2O	-0.311510	-0.022073	-0.000879	0.000356	0.071976	0.052143	0.004120	0.097021	-0.087299	-0.109565
NiO	-0.568327	0.209621	-0.003179	-0.085967	-0.027326	-0.171090	0.034384	-0.087299	5.680101	-0.517892
P_2O_5	0.473437	0.599344	0.106547	-0.066231	-0.331175	0.123633	0.136877	-0.109565	-0.517892	14.116808
SiO_2	-0.269782	-0.029914	0.001602	-0.011298	-0.014856	-0.017188	-0.007831	-0.017843	0.010469	-0.069709
ZrO_2	-0.047714	-0.036336	0.005218	0.122553	-0.144869	-0.086552	0.085749	-0.043312	0.235346	-0.389374
BaO	-42.728518	-2.939936	0.845840	-5.365929	-30.458735	-1.368349	1.599539	0.067363	0.556080	-36.05667
CdO	14.176315	-1.640557	-0.085892	0.345277	3.476029	-0.006914	-1.119788	0.041560	-4.766647	3.020399
Cl	-0.416934	-0.649154	-0.058149	0.426004	-1.080995	0.242243	-0.224215	-0.098493	0.317363	0.799928
F	-0.245530	0.013320	-0.097874	0.028742	-0.004323	-0.043994	0.004462	0.004680	0.150894	-0.586770
MnO	-0.159407	0.026299	0.005529	-0.300558	0.035695	-0.035409	-0.021525	-0.025993	-1.014139	0.225360
SO_3	-3.414889	0.048759	-0.322201	0.387983	-0.040711	0.050608	0.170593	0.001689	-0.853765	0.217935
TiO_2	-0.137823	0.058021	0.006622	-0.054053	-0.112574	-0.046456	0.103054	-0.011163	0.258638	0.503193
V_2O_5	1.588760	-0.257914	-0.221336	0.022169	-0.392895	-0.078308	-0.144924	-0.092321	0.484477	-1.491511
ZnO	-0.620242	-0.195927	-0.046576	0.148719	0.040181	0.016816	-0.130407	-0.126731	0.022100	-0.829618
Ln_2O_3	-0.881312	0.740259	0.022888	-0.003037	0.644720	0.114899	-0.085982	0.216170	-1.778719	-0.270788
Others	0.095261	-0.217417	0.020851	-0.003242	-0.170518	-0.019931	0.018707	-0.026310	0.648053	0.259629
$Al_2O_3 \times Al_2O_3$	-232.01910	4.227880	4.336355	6.470838	3.311286	3.447504	0.237016	3.848130	12.008887	-8.217297
$Al_2O_3 \times B_2O_3$	-6.616951	-0.486482	0.599847	-0.110828	0.211465	-0.277715	0.174673	-0.027606	-0.248571	-2.778997
$B_2O_3 \times B_2O_3$	3.953249	-4.331189	-0.136791	0.277714	0.242808	0.498307	0.291188	0.151204	-0.796737	-1.911277
$(Al_2O_3)^3$	1334.7846	-9.6681	-29.3585	-37.7236	-16.0585	-18.4063	-5.2379	-18.7276	-74.1590	41.3602
$(Al_2O_3)^4$	-2404.3858	-2.7680	58.8490	66.0926	27.9391	33.4327	12.7141	31.8707	131.8580	-53.1998

Table A.2. Variance-covariance table for PCT model (part 2).

	SiO_2	ZrO_2	BaO	CdO	Cl	F	MnO	SO_3	TiO_2
Al_2O_3	-0.269782	-0.047714	-42.728518	14.176315	-0.416934	-0.245530	-0.159407	-3.414889	-0.137823
B_2O_3	-0.029914	-0.036336	-2.939936	-1.640557	-0.649154	0.013320	0.026299	0.048759	0.058021
CaO	0.001602	0.005218	0.845840	-0.085892	-0.058149	-0.097874	0.005529	-0.322201	0.006622
Fe_2O_3	-0.011298	0.122553	-5.365929	0.345277	0.426004	0.028742	-0.300558	0.387983	-0.054053
K_2O	-0.014856	-0.144869	-30.458735	3.476029	-1.080995	-0.004323	0.035695	-0.040711	-0.112574
Li_2O	-0.017188	-0.086552	-1.368349	-0.006914	0.242243	-0.043994	-0.035409	0.050608	-0.046456
MgO	-0.007831	0.085749	1.599539	-1.119788	-0.224215	0.004462	-0.021525	0.170593	0.103054
Na_2O	-0.017843	-0.043312	0.067363	0.041560	-0.098493	0.004680	-0.025993	0.001689	-0.011163
NiO	0.010469	0.235346	0.556080	-4.766647	0.317363	0.150894	-1.014139	-0.853765	0.258638
P_2O_5	-0.069709	-0.389374	-36.056666	3.020399	0.799928	-0.586770	0.225360	0.217935	0.503193
SiO_2	0.019943	-0.001615	1.470745	-0.362846	0.004424	0.012291	0.017223	0.016906	-0.005522
ZrO_2	-0.001615	0.815686	6.215105	-1.539287	0.142871	-0.053977	0.032724	0.488235	0.042501
BaO	1.470745	6.215105	5787.869673	-494.16240	45.222970	3.875482	0.221151	-18.98617	-18.51352
CdO	-0.362846	-1.539287	-494.162400	171.04659	2.270526	-0.594376	2.186182	-6.048882	1.990141
Cl	0.004424	0.142871	45.222970	2.270526	21.868393	-0.078405	0.334580	-0.878126	-0.144924
F	0.012291	-0.053977	3.875482	-0.594376	-0.078405	0.456081	0.050570	-0.843064	0.021003
MnO	0.017223	0.032724	0.221151	2.186182	0.334580	0.050570	1.482794	0.040965	0.017135
SO_3	0.016906	0.488235	-18.986175	-6.048882	-0.878126	-0.843064	0.040965	29.46311	0.044749
TiO_2	-0.005522	0.042501	-18.513522	1.990141	-0.144924	0.021003	0.017135	0.044749	0.940438
V_2O_5	0.005495	0.107471	28.567893	2.490209	0.207219	0.173663	0.183463	-8.002920	0.041250
ZnO	0.060007	-0.286560	9.059494	0.462538	-1.189881	0.170663	0.198071	-1.064289	-0.108899
Ln_2O_3	-0.069248	-0.436226	29.319836	-2.182322	-3.956089	0.018961	1.136335	-0.368174	-0.256800
Others	0.016459	0.167257	-16.793898	0.867586	-0.414461	-0.031936	-0.555611	0.431981	0.110743
$Al_2O_3 \times Al_2O_3$	4.145679	2.171604	685.39531	-227.65987	5.271976	3.687882	-0.574703	44.25080	3.504843
$Al_2O_3 \times B_2O_3$	0.324266	1.081794	84.883885	-2.371368	-0.863799	-0.279342	0.613793	2.945768	-0.679606
$B_2O_3 \times B_2O_3$	0.020564	-0.344918	-27.731814	7.954519	3.409823	0.064045	-0.196321	-1.184884	0.060173
$(Al_2O_3)^3$	-24.27166	-19.92051	-4229.58835	1274.55512	-19.14813	-17.51192	6.80957	-219.05495	-20.17824
$(Al_2O_3)^4$	43.98464	40.97047	7763.67630	-2215.36293	20.83727	27.06739	-13.95138	341.74272	35.46239

Table A.3. Variance-covariance table for PCT model (part 3).

	V_2O_5	ZnO	Ln_2O_3	Others	$Al_2O_3 \times Al_2O_3$	$Al_2O_3 \times B_2O_3$	$B_2O_3 \times B_2O_3$	$(Al_2O_3)^3$	$(Al_2O_3)^4$
Al_2O_3	1.588760	-0.620242	-0.881312	0.095261	-232.01910	-6.616951	3.953249	1334.78464	-2404.38580
B_2O_3	-0.257914	-0.195927	0.740259	-0.217417	4.227880	-0.486482	-4.331189	-9.668093	-2.768041
CaO	-0.221336	-0.046576	0.022888	0.020851	4.336355	0.599847	-0.136791	-29.358523	58.849047
Fe_2O_3	0.022169	0.148719	-0.003037	-0.003242	6.470838	-0.110828	0.277714	-37.723633	66.092626
K_2O	-0.392895	0.040181	0.644720	-0.170518	3.311286	0.211465	0.242808	-16.058520	27.939079
Li_2O	-0.078308	0.016816	0.114899	-0.019931	3.447504	-0.277715	0.498307	-18.406257	33.432724
MgO	-0.144924	-0.130407	-0.085982	0.018707	0.237016	0.174673	0.291188	-5.237909	12.714123
Na_2O	-0.092321	-0.126731	0.216170	-0.026310	3.848130	-0.027606	0.151204	-18.727635	31.870744
NiO	0.484477	0.022100	-1.778719	0.648053	12.008887	-0.248571	-0.796737	-74.159039	131.857980
P_2O_5	-1.491511	-0.829618	-0.270788	0.259629	-8.217297	-2.778997	-1.911277	41.360159	-53.199838
SiO_2	0.005495	0.060007	-0.069248	0.016459	4.145679	0.324266	0.020564	-24.271661	43.984637
ZrO_2	0.107471	-0.286560	-0.436226	0.167257	2.171604	1.081794	-0.344918	-19.920511	40.970472
BaO	28.56789	9.05949	29.31984	-16.79390	685.39531	84.88388	-27.73181	-4229.58835	7763.67630
CdO	2.490209	0.462538	-2.182322	0.867586	-227.65987	-2.371368	7.954519	1274.55512	-2215.36293
Cl	0.207219	-1.189881	-3.956089	-0.414461	5.271976	-0.863799	3.409823	-19.148135	20.837265
F	0.173663	0.170663	0.018961	-0.031936	3.687882	-0.279342	0.064045	-17.511924	27.067388
MnO	0.183463	0.198071	1.136335	-0.555611	-0.574703	0.613793	-0.196321	6.809567	-13.951378
SO_3	-8.002920	-1.064289	-0.368174	0.431981	44.250802	2.945768	-1.184884	-219.054950	341.742720
TiO_2	0.041250	-0.108899	-0.256800	0.110743	3.504843	-0.679606	0.060173	-20.178240	35.462388
V_2O_5	20.080491	-2.083577	0.232252	-0.127924	-17.025420	-3.261402	1.768538	82.127882	-129.439882
ZnO	-2.083577	3.915722	1.159787	-0.400989	11.128367	-0.501781	0.723402	-60.716104	102.166090
Ln_2O_3	0.232252	1.159787	9.613440	-3.678692	11.076314	-0.594251	-3.818898	-45.485663	58.817063
Others	-0.127924	-0.400989	-3.678692	1.785592	-2.264114	0.372979	0.886611	12.745120	-20.005363
$Al_2O_3 \times Al_2O_3$	-17.02542	11.12837	11.07631	-2.26411	3951.15689	67.53120	-44.50619	-23514.14769	43242.83320
$Al_2O_3 \times B_2O_3$	-3.261402	-0.501781	-0.594251	0.372979	67.531198	53.442913	-16.542487	-602.614851	1404.103657
$B_2O_3 \times B_2O_3$	1.768538	0.723402	-3.818898	0.886611	-44.506195	-16.542487	28.756850	241.994194	-413.254944
$(Al_2O_3)^3$	82.12788	-60.71610	-45.48566	12.74512	-23514.14769	-602.61485	241.99419	146171.00498	-277657.96324
$(Al_2O_3)^4$	-129.43988	102.16609	58.81706	-20.00536	43242.83320	1404.10366	-413.25494	-277657.96324	541577.42488

Table A.4. Variance-covariance table for the SO_3 solubility model (part 1).

	Al_2O_3	B_2O_3	CaO	Cl	Cr_2O_3	F	Fe_2O_3	K_2O	Li_2O	MgO	MnO	Na_2O
Al_2O_3	1.308898	-0.224021	-0.221076	-0.302422	0.262828	-0.149846	-0.096743	-0.083178	-0.096922	-0.176198	-4.247983	0.129642
B_2O_3	-0.224021	0.098338	0.030006	0.013145	-0.054722	0.086738	0.013444	0.013699	0.039370	0.043602	0.302167	0.000852
CaO	-0.221076	0.030006	0.228950	-0.073714	0.097026	0.043913	0.035600	0.047931	0.049058	0.135745	1.150918	0.000768
Cl	-0.302422	0.013145	-0.073714	9.193908	-0.051677	0.135028	0.015319	-0.421462	-0.765083	0.268213	3.121026	-0.407649
Cr_2O_3	0.262828	-0.054722	0.097026	-0.051677	5.062532	-0.800794	-0.047810	-0.041268	-0.063131	0.003272	-2.930743	-0.058402
F	-0.149846	0.086738	0.043913	0.135028	-0.800794	1.962343	-0.022779	0.045818	-0.101017	0.051604	-4.097390	0.029618
Fe_2O_3	-0.096743	0.013444	0.035600	0.015319	-0.047810	-0.022779	0.278039	0.033304	-0.021707	-0.033325	-1.855246	-0.027965
K_2O	-0.083178	0.013699	0.047931	-0.421462	-0.041268	0.045818	0.033304	0.477620	0.013730	-0.110855	1.375067	-0.006182
Li_2O	-0.096922	0.039370	0.049058	-0.765083	-0.063131	-0.101017	-0.021707	0.013730	0.891480	-0.096713	0.741545	0.212341
MgO	-0.176198	0.043602	0.135745	0.268213	0.003272	0.051604	-0.033325	-0.110855	-0.096713	1.513376	3.076612	-0.053967
MnO	-4.247983	0.302167	1.150918	3.121026	-2.930743	-4.097390	-1.855246	1.375067	0.741545	3.076612	155.202170	-0.215002
Na_2O	0.129642	0.000852	0.000768	-0.407649	-0.058402	0.029618	-0.027965	-0.006182	0.212341	-0.053967	-0.215002	0.232184
P_2O_5	-0.209538	0.020894	0.026201	0.118990	-0.362579	-0.159141	-0.053034	0.033826	-0.083293	0.217472	0.493584	-0.054291
SiO_2	0.116127	-0.031840	-0.056230	0.101580	0.021244	-0.060040	-0.004999	-0.013194	-0.094878	-0.021052	-0.409208	-0.080468
SnO_2	-0.136839	0.017276	0.038524	0.103670	0.214590	0.122712	0.002711	-0.024094	-0.179582	-0.045359	1.890714	-0.104913
V_2O_5	-0.084337	-0.008165	-0.030485	0.078620	0.002468	-0.088246	-0.023482	-0.024258	-0.041897	-0.048370	0.445898	-0.004749
ZnO	-0.274292	0.024426	0.296047	0.193198	-0.016278	0.048402	0.041226	0.045163	0.003408	-0.232994	1.087049	-0.064501
ZrO_2	-0.042870	-0.010736	-0.020145	-0.162524	-0.066147	-0.065981	0.031613	-0.036641	-0.039660	0.083986	-0.028894	-0.048252
Others	-0.155114	-0.007437	0.021912	-1.263750	0.139877	0.188397	-0.044943	-0.219966	-0.004134	-0.313170	-3.900713	-0.018091
CaO×MgO	0.897084	-0.261122	-2.707956	2.415745	-1.261890	-0.383895	0.253283	1.005255	-0.996555	-15.097377	-19.562743	-0.524005
Al_2O_3×Na_2O	-2.831421	0.289904	0.353188	2.558120	0.208828	0.014294	0.274228	0.234963	-0.338081	0.420773	9.386948	-1.778519
Al_2O_3×SiO_2	-2.563667	0.405115	0.495993	0.165384	-0.938337	0.442967	0.168010	0.120306	0.140187	0.258294	6.557234	0.331180
CaO×ZnO	1.928006	0.021259	-5.057425	1.890893	-2.924292	-0.142764	-0.712040	-1.736073	-1.244221	3.052821	-12.887240	-0.633155

Table A.5. Variance-covariance table for the SO_3 solubility model (part 2).

	P_2O_5	SiO_2	SnO_2	V_2O_5	ZnO	ZrO_2	Others	CaO×MgO	Al_2O_3×Na_2O	Al_2O_3×SiO_2	CaO×ZnO
Al_2O_3	-0.209538	0.116127	-0.136839	-0.084337	-0.274292	-0.042870	-0.155114	0.897084	-2.831421	-2.563667	1.928006
B_2O_3	0.020894	-0.031840	0.017276	-0.008165	0.024426	-0.010736	-0.007437	-0.261122	0.289904	0.405115	0.021259
CaO	0.026201	-0.056230	0.038524	-0.030485	0.296047	-0.020145	0.021912	-2.707956	0.353188	0.495993	-5.057425
Cl	0.118990	0.101580	0.103670	0.078620	0.193198	-0.162524	-1.263750	2.415745	2.558120	0.165384	1.890893
Cr_2O_3	-0.362579	0.021244	0.214590	0.002468	-0.016278	-0.066147	0.139877	-1.261890	0.208828	-0.938337	-2.924292
F	-0.159141	-0.060040	0.122712	-0.088246	0.048402	-0.065981	0.188397	-0.383895	0.014294	0.442967	-0.142764
Fe_2O_3	-0.053034	-0.004999	0.002711	-0.023482	0.041226	0.031613	-0.044943	0.253283	0.274228	0.168010	-0.712040
K_2O	0.033826	-0.013194	-0.024094	-0.024258	0.045163	-0.036641	-0.219966	1.005255	0.234963	0.120306	-1.736073
Li_2O	-0.083293	-0.094878	-0.179582	-0.041897	0.003408	-0.039660	-0.004134	-0.996555	-0.338081	0.140187	-1.244221
MgO	0.217472	-0.021052	-0.045359	-0.048370	-0.232994	0.083986	-0.313170	-15.097377	0.420773	0.258294	3.052821
MnO	0.493584	-0.409208	1.890714	0.445898	1.087049	-0.028894	-3.900713	-19.562743	9.386948	6.557234	-12.887240
Na_2O	-0.054291	-0.080468	-0.104913	-0.004749	-0.064501	-0.048252	-0.018091	-0.524005	-1.778519	0.331180	-0.633155
P_2O_5	1.053595	-0.005027	0.020798	0.018941	-0.042594	0.025270	-0.001362	-1.911941	0.648506	0.204129	0.799722
SiO_2	-0.005027	0.060215	0.006382	-0.020770	-0.046521	0.003013	-0.020595	0.688656	0.433506	-0.528603	1.071044
SnO_2	0.020798	0.006382	0.532978	0.045620	0.011715	-0.025060	-0.005292	0.051242	0.730414	0.164472	-0.472785
V_2O_5	0.018941	-0.020770	0.045620	0.373046	-0.062682	0.044653	-0.023926	0.611055	0.087945	0.303653	0.790737
ZnO	-0.042594	-0.046521	0.011715	-0.062682	1.163199	-0.062705	0.195318	1.979941	0.757207	0.446884	-13.706928
ZrO_2	0.025270	0.003013	-0.025060	0.044653	-0.062705	0.230820	0.093207	-0.465688	0.218071	0.101313	1.192759
Others	-0.001362	-0.020595	-0.005292	-0.023926	0.195318	0.093207	2.141448	0.874916	-0.013912	0.499502	0.968828
CaO×MgO	-1.911941	0.688656	0.051242	0.611055	1.979941	-0.465688	0.874916	271.599283	2.460486	-2.635203	-27.830619
Al_2O_3×Na_2O	0.648506	0.433506	0.730414	0.087945	0.757207	0.218071	-0.013912	2.460486	21.756404	-1.590093	-0.328408
Al_2O_3×SiO_2	0.204129	-0.528603	0.164472	0.303653	0.446884	0.101313	0.499502	-2.635203	-1.590093	9.086456	-5.582159
CaO×ZnO	0.799722	1.071044	-0.472785	0.790737	-13.706928	1.192759	0.968828	-27.830619	-0.328408	-5.582159	268.741363

Table A.6. Variance-covariance table for the K-3 1200 only model (part 1).

	Stat, 1200	Al_2O_3	B_2O_3	CaO	Cr_2O_3	Fe_2O_3	K_2O	Li_2O	Na_2O	P_2O_5
Stat, 1200	0.006042	-0.023355	-0.011185	-0.019289	-0.224569	-0.086275	0.011041	0.017356	0.009396	-0.231382
Al_2O_3	-0.023355	2.253401	-0.857766	-0.080248	-0.294638	-1.920242	0.118554	-0.787302	-0.688181	7.377924
B_2O_3	-0.011185	-0.857766	1.191839	1.261148	-0.927524	-3.207562	-0.004361	-0.023808	0.152154	0.516607
CaO	-0.019289	-0.080248	1.261148	3.688700	0.565958	-4.505613	0.082246	-0.803008	-0.195859	1.052980
Cr_2O_3	-0.224569	-0.294638	-0.927524	0.565958	296.05381	-3.474976	-2.456302	4.575284	0.308660	-59.881081
Fe_2O_3	-0.086275	-1.920242	-3.207562	-4.505613	-3.474976	195.98474	-3.116646	-3.243230	-2.633234	-2.278386
K_2O	0.011041	0.118554	-0.004361	0.082246	-2.456302	-3.116646	3.980086	0.383051	0.059750	2.605348
Li_2O	0.017356	-0.787302	-0.023808	-0.803008	4.575284	-3.243230	0.383051	1.981685	0.849167	-2.867175
Na_2O	0.009396	-0.688181	0.152154	-0.195859	0.308660	-2.633234	0.059750	0.849167	0.606127	-2.290406
P_2O_5	-0.231382	7.377924	0.516607	1.052980	-59.88108	-2.278386	2.605348	-2.867175	-2.290406	207.71170
SiO_2	-0.005137	0.249889	-0.266426	-0.365525	0.009451	3.240921	-0.121381	-0.300473	-0.242705	-0.163409
V_2O_5	-0.050562	-0.003251	0.235785	0.458405	-4.939136	-2.745988	0.890697	-0.832215	-0.531980	-4.342372
ZnO	0.079719	-0.517686	0.081672	0.767772	-4.628725	2.390875	-0.492627	-0.398922	0.073820	-1.744137
ZrO_2	0.034562	0.720955	0.229319	1.319477	-4.492238	-6.610580	0.116037	-0.640275	-0.697167	7.099306
Others	-0.017464	-0.104171	0.114113	0.042043	-0.802007	-1.394335	-0.159864	-0.050974	0.110241	-1.055425
B_2O_3×CaO	0.181236	1.077954	-11.401019	-29.996402	-3.182927	22.353781	1.192103	6.387509	2.178634	-0.328175
Cr_2O_3×Li_2O	-1.734443	-9.254962	51.515716	78.097873	-3956.05185	177.56471	6.686621	-211.015612	-27.341990	363.76459
Al_2O_3×P_2O_5	1.106875	-84.25172	-3.908617	0.571249	436.28036	-111.78684	-17.441483	27.095953	23.115733	-1833.65852
Fe_2O_3×SiO_2	0.197604	4.221398	7.915807	12.578172	16.985853	-447.49509	5.630967	7.019598	6.067497	3.774003

Table A.7. Variance-covariance table for the K-3 1200 only model (part 2).

	SiO_2	V_2O_5	ZnO	ZrO_2	Others	B_2O_3×CaO	Cr_2O_3×Li_2O	Al_2O_3×P_2O_5	Fe_2O_3×SiO_2
Stat, 1200	-0.005137	-0.050562	0.079719	0.034562	-0.017464	0.181236	-1.734443	1.106875	0.197604
Al_2O_3	0.249889	-0.003251	-0.517686	0.720955	-0.104171	1.077954	-9.254962	-84.251720	4.221398
B_2O_3	-0.266426	0.235785	0.081672	0.229319	0.114113	-11.401019	51.515716	-3.908617	7.915807
CaO	-0.365525	0.458405	0.767772	1.319477	0.042043	-29.996402	78.097873	0.571249	12.578172
Cr_2O_3	0.009451	-4.939136	-4.628725	-4.492238	-0.802007	-3.182927	-3956.05185	436.280364	16.985853
Fe_2O_3	3.240921	-2.745988	2.390875	-6.610580	-1.394335	22.353781	177.56471	-111.78684	-447.49509
K_2O	-0.121381	0.890697	-0.492627	0.116037	-0.159864	1.192103	6.686621	-17.441483	5.630967
Li_2O	-0.300473	-0.832215	-0.398922	-0.640275	-0.050974	6.387509	-211.01561	27.095953	7.019598
Na_2O	-0.242705	-0.531980	0.073820	-0.697167	0.110241	2.178634	-27.341990	23.115733	6.067497
P_2O_5	-0.163409	-4.342372	-1.744137	7.099306	-1.055425	-0.328175	363.76459	-1833.65852	3.774003
SiO_2	0.206765	0.092176	-0.235527	-0.165927	-0.084845	2.382073	6.048752	0.925219	-7.965889
V_2O_5	0.092176	24.115250	-0.364751	1.849425	-0.940873	-7.940158	13.947659	39.412020	10.087151
ZnO	-0.235527	-0.364751	6.285194	-0.691718	-0.208311	-7.936314	109.92206	19.274973	-6.216768
ZrO_2	-0.165927	1.849425	-0.691718	7.254537	-0.554838	-9.564654	-21.056429	-47.651809	19.300874
Others	-0.084845	-0.940873	-0.208311	-0.554838	0.900706	0.063401	29.592451	9.357618	2.339850
B_2O_3×CaO	2.382073	-7.940158	-7.936314	-9.564654	0.063401	281.06380	-613.717112	-80.598186	-63.638030
Cr_2O_3×Li_2O	6.048752	13.947659	109.92206	-21.056429	29.592451	-613.71711	139672.5996	-2773.89409	-425.98289
Al_2O_3×P_2O_5	0.925219	39.412020	19.274973	-47.651809	9.357618	-80.598186	-2773.89409	19804.6079	231.22411
Fe_2O_3×SiO_2	-7.965889	10.087151	-6.216768	19.300874	2.339850	-63.638030	-425.98289	231.22411	1044.86920

Table A.8. Variance-covariance table for the viscosity model (part 1).

	A	B_SiO_2	B_Na_2O	B_B_2O_3	B_Al_2O_3	B_Fe_2O_3	B_CaO	B_ZrO_2	B_Li_2O	B_ZnO
A	0.003010	-7.239407	-1.129922	-1.931521	-8.234353	-4.324211	-2.115779	-6.693929	6.754728	-3.591885
B_SiO_2	-7.239407	17648.0269	2529.3900	4598.5087	20013.8236	10403.4915	5001.2415	16218.1614	-16825.8691	8696.4090
B_Na_2O	-1.129922	2529.3900	955.1975	755.9788	2839.5398	1608.0217	918.4368	2267.5548	-1643.3401	1309.4745
B_B_2O_3	-1.931521	4598.5087	755.9788	1815.8951	5060.1549	2706.0127	1360.8693	4170.0915	-4375.3125	2244.7221
B_Al_2O_3	-8.234353	20013.8236	2839.5398	5060.1549	23234.1372	11919.8289	5641.9668	18673.2905	-19146.4035	9955.9018
B_Fe_2O_3	-4.324211	10403.4915	1608.0217	2706.0127	11919.8289	6936.4062	3088.3158	9903.8634	-9829.4352	5048.1876
B_CaO	-2.115779	5001.2415	918.4368	1360.8693	5641.9668	3088.3158	2431.4239	4685.4162	-4571.3815	2337.0912
B_ZrO_2	-6.693929	16218.1614	2267.5548	4170.0915	18673.2905	9903.8634	4685.4162	16531.8175	-15730.0745	7536.6850
B_Li_2O	6.754728	-16825.8691	-1643.3401	-4375.3125	-19146.4035	-9829.4352	-4571.3815	-15730.0745	19155.3465	-7967.6414
B_ZnO	-3.591885	8696.4090	1309.4745	2244.7221	9955.9018	5048.1876	2337.0912	7536.6850	-7967.6414	9543.2313
B_K_2O	-3.024172	7225.3518	1203.7008	1999.0798	8262.3740	4368.7589	2199.4085	6627.8604	-6822.2637	3883.3771
B_MgO	-3.417471	8149.0967	1502.5112	2153.9751	9426.5925	4743.7971	2252.4151	7771.3731	-7871.3248	3080.1242
B_P_2O_5	-6.325772	15239.9505	2350.2202	4133.9904	17130.8787	9172.0162	4601.4186	13944.3361	-14524.1998	7966.8801
B_LN_2O_3	-4.252376	10112.3487	1735.4620	2934.3239	11724.7102	6408.3963	2839.1223	9310.8901	-9733.7424	5871.2798
B_V_2O_5	-3.441398	8373.2558	972.6752	1986.7557	9526.0989	5184.0263	2221.2530	7946.3988	-7978.6411	4339.9218
B_TiO_2	-3.553221	8537.5837	1321.6540	2065.4237	9964.3284	4874.1298	2779.7476	8427.6626	-7828.0575	2493.9422
B_F	-0.119995	143.3057	120.7786	307.6399	15.9687	173.5231	-152.6237	-396.5223	-169.2977	742.4212
B_SO_3	-6.164872	14735.2896	1946.6237	3568.0366	17577.9359	9722.6095	924.2577	14572.4251	-14224.0079	3114.8598
B_SnO_2	-6.239830	15232.0896	1820.0805	4073.2921	17294.1449	9332.1081	4333.3067	13662.6143	-14505.2141	7053.7026
B_MnO	-2.281697	5388.4274	954.7803	1507.0782	6352.2318	2642.1028	2026.8929	5114.9554	-5284.6463	2227.3135
B_SrO	-2.758152	6656.2133	1117.3528	1797.3008	7485.6200	3918.5646	1914.9705	5857.9856	-6290.7713	3291.8892
B_Cr_2O_3	-6.361165	15540.5719	1610.7089	2956.4125	17109.7890	9479.4789	4884.1502	15671.3639	-15021.8468	7454.5862
B_NiO	-4.550872	10949.9852	1469.1582	2986.0544	11695.7856	4413.4431	3384.8416	8328.2963	-10240.6660	9431.6762
B_UO_3	-5.372948	12981.4880	2009.3197	3534.3105	14808.3587	7428.1861	3748.8926	11566.2398	-11926.5179	6578.6691
B_Cl	-8.590258	21486.5149	258.6445	6377.5918	23629.1409	11947.8254	5510.6074	18825.8955	-17291.5121	6122.1938
B_Others	-3.854538	9287.9885	1515.6462	2432.3537	10560.8314	5322.3007	2772.8139	8785.3209	-8650.2729	4926.8919
T_0	0.639824	-1558.7358	-237.1639	-413.7236	-1773.7346	-928.0789	-448.6851	-1442.7785	1465.3016	-781.8780

Table A.9. Variance-covariance table for the viscosity model (part 2).

	B_K_2O	B_MgO	B_P_2O_5	B_LN_2O_3	B_V_2O_5	B_TiO_2	B_F	B_SO_3	B_SnO_2
A	-3.024172	-3.417471	-6.325772	-4.252376	-3.441398	-3.553221	-0.119995	-6.164872	-6.239830
B_SiO_2	7225.3518	8149.0967	15239.9505	10112.3487	8373.2558	8537.5837	143.3057	14735.2896	15232.0896
B_Na_2O	1203.7008	1502.5112	2350.2202	1735.4620	972.6752	1321.6540	120.7786	1946.6237	1820.0805
B_B_2O_3	1999.0798	2153.9751	4133.9904	2934.3239	1986.7557	2065.4237	307.6399	3568.0366	4073.2921
B_Al_2O_3	8262.3740	9426.5925	17130.8787	11724.7102	9526.0989	9964.3284	15.9687	17577.9359	17294.1449
B_Fe_2O_3	4368.7589	4743.7971	9172.0162	6408.3963	5184.0263	4874.1298	173.5231	9722.6095	9332.1081
B_CaO	2199.4085	2252.4151	4601.4186	2839.1223	2221.2530	2779.7476	-152.6237	924.2577	4333.3067
B_ZrO_2	6627.8604	7771.3731	13944.3361	9310.8901	7946.3988	8427.6626	-396.5223	14572.4251	13662.6143
B_Li_2O	-6822.2637	-7871.3248	-14524.1998	-9733.7424	-7978.6411	-7828.0575	-169.2977	-14224.0079	-14505.2141
B_ZnO	3883.3771	3080.1242	7966.8801	5871.2798	4339.9218	2493.9422	742.4212	3114.8598	7053.7026
B_K_2O	5249.8461	3662.4100	5791.9598	4283.8515	3643.7291	2926.7425	-252.5440	6856.6289	5441.2266
B_MgO	3662.4100	10510.4400	7138.4531	4247.6599	3608.5398	1957.5918	772.3219	6164.2359	6212.0373
B_P_2O_5	5791.9598	7138.4531	18337.2205	9496.4894	7111.5200	7939.6983	-21.1263	12696.9561	13556.9574
B_LN_2O_3	4283.8515	4247.6599	9496.4894	9768.1587	4696.4055	4471.1074	1008.6748	11016.7980	8933.6349
B_V_2O_5	3643.7291	3608.5398	7111.5200	4696.4055	13250.7903	4967.4899	-713.1972	-2996.4687	5837.7182
B_TiO_2	2926.7425	1957.5918	7939.6983	4471.1074	4967.4899	20312.5577	612.0082	8980.5060	8264.0569
B_F	-252.5440	772.3219	-21.1263	1008.6748	-713.1972	612.0082	15481.2430	-100.4510	1061.7932
B_SO_3	6856.6289	6164.2359	12696.9561	11016.7980	-2996.4687	8980.5060	-100.4510	106371.5995	13605.0523
B_SnO_2	5441.2266	6212.0373	13556.9574	8933.6349	5837.7182	8264.0569	1061.7932	13605.0523	23375.4849
B_MnO	2645.4954	3405.0929	5306.0961	3800.9977	1911.2359	3861.8243	1463.8833	5932.8978	4451.0808
B_SrO	2929.6229	3439.7176	6055.6828	4123.0673	3244.9156	3480.2808	-640.7644	6275.6437	5593.1639
B_Cr_2O_3	5584.7542	8477.3696	12327.3499	6793.7239	6931.8248	10891.3931	-2501.2324	10301.2230	10766.9605
B_NiO	5671.3509	6036.0834	7532.3901	-1661.4893	5813.7145	6304.8381	-8076.3060	7614.2287	9755.8425
B_UO_3	5563.9243	6425.8601	11180.4447	7970.6693	5955.5167	5867.9375	439.4048	10171.2754	11028.4260
B_Cl	6492.6268	4780.4772	18553.2310	6298.7534	9535.9957	-2264.2709	-1705.0939	21318.6842	19150.7524
B_Others	3829.4765	4527.4053	7670.7677	4350.7018	4805.2894	5008.9490	625.4585	6906.2417	8017.7384
T_0	-648.1993	-734.4161	-1353.4587	-904.2279	-730.0535	-765.4779	-15.9623	-1335.5882	-1340.0679

Table A.10. Variance-covariance table for the viscosity model (part 3).

	B_MnO	B_SrO	B_Cr_2O_3	B_NiO	B_UO_3	B_Cl	B_Others	T_0
A	-2.281697	-2.758152	-6.361165	-4.550872	-5.372948	-8.590258	-3.854538	0.639824
B_SiO_2	5388.4274	6656.2133	15540.5719	10949.9852	12981.4880	21486.5149	9287.9885	-1558.7358
B_Na_2O	954.7803	1117.3528	1610.7089	1469.1582	2009.3197	258.6445	1515.6462	-237.1639
B_B_2O_3	1507.0782	1797.3008	2956.4125	2986.0544	3534.3105	6377.5918	2432.3537	-413.7236
B_Al_2O_3	6352.2318	7485.6200	17109.7890	11695.7856	14808.3587	23629.1409	10560.8314	-1773.7346
B_Fe_2O_3	2642.1028	3918.5646	9479.4789	4413.4431	7428.1861	11947.8254	5322.3007	-928.0789
B_CaO	2026.8929	1914.9705	4884.1502	3384.8416	3748.8926	5510.6074	2772.8139	-448.6851
B_ZrO_2	5114.9554	5857.9856	15671.3639	8328.2963	11566.2398	18825.8955	8785.3209	-1442.7785
B_Li_2O	-5284.6463	-6290.7713	-15021.8468	-10240.6660	-11926.5179	-17291.5121	-8650.2729	1465.3016
B_ZnO	2227.3135	3291.8892	7454.5862	9431.6762	6578.6691	6122.1938	4926.8919	-781.8780
B_K_2O	2645.4954	2929.6229	5584.7542	5671.3509	5563.9243	6492.6268	3829.4765	-648.1993
B_MgO	3405.0929	3439.7176	8477.3696	6036.0834	6425.8601	4780.4772	4527.4053	-734.4161
B_P_2O_5	5306.0961	6055.6828	12327.3499	7532.3901	11180.4447	18553.2310	7670.7677	-1353.4587
B_LN_2O_3	3800.9977	4123.0673	6793.7239	-1661.4893	7970.6693	6298.7534	4350.7018	-904.2279
B_V_2O_5	1911.2359	3244.9156	6931.8248	5813.7145	5955.5167	9535.9957	4805.2894	-730.0535
B_TiO_2	3861.8243	3480.2808	10891.3931	6304.8381	5867.9375	-2264.2709	5008.9490	-765.4779
B_F	1463.8833	-640.7644	-2501.2324	-8076.3060	439.4048	-1705.0939	625.4585	-15.9623
B_SO_3	5932.8978	6275.6437	10301.2230	7614.2287	10171.2754	21318.6842	6906.2417	-1335.5882
B_SnO_2	4451.0808	5593.1639	10766.9605	9755.8425	11028.4260	19150.7524	8017.7384	-1340.0679
B_MnO	14343.2555	-1588.9386	3048.4168	62.8585	3178.7562	5353.5431	2056.6556	-485.8839
B_SrO	-1588.9386	10011.7946	7307.1848	3087.4504	3271.2885	5786.9464	3190.1261	-590.8155
B_Cr_2O_3	3048.4168	7307.1848	86361.7724	4966.4686	10147.4791	17357.3583	7721.4488	-1362.8192
B_NiO	62.8585	3087.4504	4966.4686	133040.3207	8127.3795	40141.9268	583.5518	-971.6096
B_UO_3	3178.7562	3271.2885	10147.4791	8127.3795	20657.6284	17107.1090	4959.4146	-1147.6252
B_Cl	5353.5431	5786.9464	17357.3583	40141.9268	17107.1090	223815.0570	9465.2881	-1889.5809
B_Others	2056.6556	3190.1261	7721.4488	583.5518	4959.4146	9465.2881	10153.4910	-828.2414
T_0	-485.8839	-590.8155	-1362.8192	-971.6096	-1147.6252	-1889.5809	-828.2414	139.1140

Table A.11. Variance-covariance table for the EC model (part 1).

	A	B_SiO_2	B_Na_2O	B_B_2O_3	B_Al_2O_3	B_CaO	B_Fe_2O_3	B_ZrO_2	B_ZnO	B_Li_2O	B_K_2O
A	0.002739	-6.506405	1.437424	-5.468533	-6.566065	-6.630074	-5.313695	-6.315783	-4.370150	6.720440	-4.411657
B_SiO_2	-6.506405	15770.7046	-3748.5477	12967.7010	15865.2299	15778.2370	12587.9886	15110.6068	10240.0112	-16806.5760	10468.4662
B_Na_2O	1.437424	-3748.5477	1453.6553	-2928.6626	-3846.5178	-3493.8682	-2854.6012	-3738.5425	-2386.0059	5266.8612	-2285.5687
B_B_2O_3	-5.468533	12967.7010	-2928.6626	11875.5970	12794.8547	13354.9220	10567.3835	12689.6028	8776.6527	-13594.5727	8789.9771
B_Al_2O_3	-6.566065	15865.2299	-3846.5178	12794.8547	16512.1559	15930.9618	12842.8829	15330.7946	10528.9785	-17160.5468	10655.6520
B_CaO	-6.630074	15778.2370	-3493.8682	13354.9220	15930.9618	17117.2774	13114.6806	15388.1522	10713.3022	-16594.9394	10952.7964
B_Fe_2O_3	-5.313695	12587.9886	-2854.6012	10567.3835	12842.8829	13114.6806	11314.2437	12622.0007	8659.7437	-13491.7674	8593.2789
B_ZrO_2	-6.315783	15110.6068	-3738.5425	12689.6028	15330.7946	15388.1522	12622.0007	16836.4375	9449.3044	-16262.2603	10236.3043
B_ZnO	-4.370150	10240.0112	-2386.0059	8776.6527	10528.9785	10713.3022	8659.7437	9449.3044	11904.0917	-10987.1183	7069.1500
B_Li_2O	6.720440	-16806.5760	5266.8612	-13594.5727	-17160.5468	-16594.9394	-13491.7674	-16262.2603	-10987.1183	23385.2271	-10545.3954
B_K_2O	-4.411657	10468.4662	-2285.5687	8789.9771	10655.6520	10952.7964	8593.2789	10236.3043	7069.1500	-10545.3954	10026.5730
B_MgO	-4.693690	11049.1974	-2375.5752	9503.1581	11288.5656	11361.8611	9206.9635	11040.3616	5786.5315	-12174.3269	7464.4349
B_V_2O_5	-4.431409	10687.7186	-2685.7824	8837.0034	10732.1303	10690.2995	8860.7562	10696.1924	7373.2704	-11407.5195	7158.7386
B_SnO_2	-7.960797	19195.1833	-4828.1515	16241.6187	19392.9219	19411.0919	15952.2730	18024.4244	13252.3244	-21036.1963	11891.7837
B_TiO_2	-4.911569	11558.3764	-2798.8310	9994.8049	11850.5010	12337.8119	9289.6905	11828.2949	7426.7721	-12046.2962	6789.1749
B_P_2O_5	-5.074192	12092.4499	-2516.7900	9903.7057	11749.1903	12410.6888	9829.8433	12289.8814	8481.0324	-11908.8060	8675.5729
B_SO_3	-6.262113	14644.7212	-4135.6978	11924.8786	15988.6411	12510.6624	14372.8434	15236.7798	9037.6316	-18426.1154	10308.5134
B_MnO	-5.642719	13465.9044	-3159.3273	11309.1994	13860.0129	14081.4234	10390.1403	13097.3455	9143.8931	-14879.3888	9530.1307
B_SrO	-6.177553	14745.0494	-3233.7878	12592.9778	14834.8057	15202.6595	12055.5624	14168.9297	10004.9176	-15298.9721	10051.0847
B_Cr_2O_3	-4.329108	10121.5363	-3372.8378	7745.6261	10551.6316	11182.2096	9846.5108	11990.5247	9512.7938	-14096.5534	3180.1160
B_Others	-4.835247	11490.9608	-2600.5861	9839.2630	11603.9499	11986.9747	9249.7522	10691.9611	8398.1591	-12364.0862	7915.2636
T_0	-1.575565	3796.5622	-871.9518	3185.2648	3830.4610	3870.1359	3092.0498	3685.1664	2541.1774	-3975.4692	2565.7120

Table A.12. Variance-covariance table for the EC model (part 2).

	B_MgO	B_V_2O_5	B_SnO_2	B_TiO_2	B_P_2O_5	B_SO_3	B_MnO	B_SrO	B_Cr_2O_3	B_Others	T_0
A	-4.693690	-4.431409	-7.960797	-4.911569	-5.074192	-6.262113	-5.642719	-6.177553	-4.329108	-4.835247	-1.575565
B_SiO_2	11049.1974	10687.7186	19195.1833	11558.3764	12092.4499	14644.7212	13465.9044	14745.0494	10121.5363	11490.9608	3796.5622
B_Na_2O	-2375.5752	-2685.7824	-4828.1515	-2798.8310	-2516.7900	-4135.6978	-3159.3273	-3233.7878	-3372.8378	-2600.5861	-871.9518
B_B_2O_3	9503.1581	8837.0034	16241.6187	9994.8049	9903.7057	11924.8786	11309.1994	12592.9778	7745.6261	9839.2630	3185.2648
B_Al_2O_3	11288.5656	10732.1303	19392.9219	11850.5010	11749.1903	15988.6411	13860.0129	14834.8057	10551.6316	11603.9499	3830.4610
B_CaO	11361.8611	10690.2995	19411.0919	12337.8119	12410.6888	12510.6624	14081.4234	15202.6595	11182.2096	11986.9747	3870.1359
B_Fe_2O_3	9206.9635	8860.7562	15952.2730	9289.6905	9829.8433	14372.8434	10390.1403	12055.5624	9846.5108	9249.7522	3092.0498
B_ZrO_2	11040.3616	10696.1924	18024.4244	11828.2949	12289.8814	15236.7798	13097.3455	14168.9297	11990.5247	10691.9611	3685.1664
B_ZnO	5786.5315	7373.2704	13252.3244	7426.7721	8481.0324	9037.6316	9143.8931	10004.9176	9512.7938	8398.1591	2541.1774
B_Li_2O	-12174.3269	-11407.5195	-21036.1963	-12046.2962	-11908.8060	-18426.1154	-14879.3888	-15298.9721	-14096.5534	-12364.0862	-3975.4692
B_K_2O	7464.4349	7158.7386	11891.7837	6789.1749	8675.5729	10308.5134	9530.1307	10051.0847	3180.1160	7915.2636	2565.7120
B_MgO	17488.2377	6877.0595	12823.6625	4666.1627	8078.2974	11580.3115	10383.5116	10695.9377	10532.2375	8976.6273	2730.6194
B_V_2O_5	6877.0595	13056.7619	12291.6239	8984.5155	7732.4968	3263.2683	8912.9873	10101.5341	7514.7166	7684.2018	2577.2979
B_SnO_2	12823.6625	12291.6239	29451.9887	15275.0707	14033.0283	20713.0727	16356.1154	18028.3966	13615.7432	14535.8348	4653.6543
B_TiO_2	4666.1627	8984.5155	15275.0707	21818.8859	8874.2364	12365.3180	11600.0261	11195.3770	13084.4003	8925.8918	2843.2616
B_P_2O_5	8078.2974	7732.4968	14033.0283	8874.2364	20214.0233	10738.9365	11264.1197	12241.3809	4697.0122	7449.2568	2947.2400
B_SO_3	11580.3115	3263.2683	20713.0727	12365.3180	10738.9365	93115.6386	14623.1723	13476.3072	16196.0754	12007.1151	3660.9152
B_MnO	10383.5116	8912.9873	16356.1154	11600.0261	11264.1197	14623.1723	20361.9728	10399.6351	9753.9249	9455.7648	3288.5526
B_SrO	10695.9377	10101.5341	18028.3966	11195.3770	12241.3809	13476.3072	10399.6351	20082.7648	10204.0242	9864.3734	3602.6408
B_Cr_2O_3	10532.2375	7514.7166	13615.7432	13084.4003	4697.0122	16196.0754	9753.9249	10204.0242	66486.6546	7506.5144	2523.0902
B_Others	8976.6273	7684.2018	14535.8348	8925.8918	7449.2568	12007.1151	9455.7648	9864.3734	7506.5144	11187.0993	2816.7036
T_0	2730.6194	2577.2979	4653.6543	2843.2616	2947.2400	3660.9152	3288.5526	3602.6408	2523.0902	2816.7036	926.8281

Table A.13. Variance-covariance table for the TL-P model.

Var-covar	Al_2O_3	B_2O_3	CaO	Cr_2O_3	Li_2O	Na_2O	P_2O_5	SiO_2	ZrO_2	Others	CaO×CaO	Li_2O×Li_2O	CaO×Na_2O	CaO×SiO_2
Al_2O_3	14694.38	-7560.25	-53244.67	-207.72	-32099.11	-7716.89	474.14	1691.07	7746.55	90.03522	137411.17	299120.10	105933.20	72655.51
B_2O_3	-7560.25	13906.74	-40404.52	8467.96	22661.22	9.57703	-6815.01	-2831.96	-165.44	1365.33	141394.96	-141998.43	81876.64	50458.56
CaO	-53244.67	-40404.52	1440098.97	7444.99	-203562.40	33011.43	12225.88	30084.66	-60694.32	-45557.81	-5618802.87	1890906.93	-2510238.62	-1792036.51
Cr_2O_3	-207.72	8467.96	7444.99	810590.97	-91204.20	-33463.28	-44606.82	14614.27	17917.89	-14151.59	222840.20	1032830.42	-356561.84	-125923.22
Li_2O	-32099.11	22661.22	-203562.40	-91204.20	661341.18	28256.57	2760.87	-21608.36	-1523.91	4254.39	1303349.59	-9992267.02	57654.55	218937.55
Na_2O	-7716.89	9.57703	33011.43	-33463.28	28256.57	53738.59	-3518.82	-17950.42	-3165.81	3648.23	-192520.53	166881.37	-722215.34	187863.09
P_2O_5	474.14	-6815.01	12225.88	-44606.82	2760.87	-3518.82	67896.04	-951.79	-4275.52	-4692.44	-131850.45	-284133.22	45508.60	21262.43
SiO_2	1691.07	-2831.96	30084.66	14614.27	-21608.36	-17950.42	-951.79	9110.60	-3223.42	-3507.57	-42758.74	3149.95	173688.56	-136722.02
ZrO_2	7746.55	-165.44	-60694.32	17917.89	-1523.91	-3165.81	-4275.52	-3223.42	40839.79	2355.55	173444.98	-166804.94	29796.64	111269.36
Others	90.03522	1365.33	-45557.81	-14151.59	4254.39	3648.23	-4692.44	-3507.57	2355.55	6370.75	181565.41	138882.08	55337.59	65495.79
CaO×CaO	137411.17	141394.96	-5618802.87	222840.20	1303349.59	-192520.53	-131850.45	-42758.74	173444.98	181565.41	29165718.71	-17433251.72	11660842.00	4469320.56
Li_2O×Li_2O	299120.10	-141998.43	1890906.93	1032830.42	-9992267.02	166881.37	-284133.22	3149.95	-166804.94	138882.08	-17433251.72	184482119.59	-2568008.77	356528.09
CaO×Na_2O	105933.20	81876.64	-2510238.62	-356561.84	57654.55	-722215.34	45508.60	173688.56	29796.64	55337.59	11660842.00	-2568008.77	19652189.01	-1713737.11
CaO×SiO_2	72655.51	50458.56	-1792036.51	-125923.22	218937.55	187863.09	21262.43	-136722.02	111269.36	65495.79	4469320.56	356528.09	-1713737.11	4495221.57

Table A.14. Variance-covariance table for the TL-Zr model (part 1).

Var covar	Al_2O_3	B_2O_3	Cr_2O_3	F	Fe_2O_3	K_2O	Li_2O	MgO	MnO
Al_2O_3	25721.976	-11839.818	-77414.995	14568.492	4848.799	-39885.120	-22526.737	16347.517	23076.626
B_2O_3	-11839.818	23270.177	-56216.791	-20430.376	3980.273	93561.135	7438.036	-13523.165	27112.419
Cr_2O_3	-77414.995	-56216.791	7731830.356	-151369.467	-122551.569	347981.229	-105906.916	370744.705	-704553.874
F	14568.492	-20430.376	-151369.467	768880.461	5643.831	-268582.886	38103.956	-97453.982	96313.533
Fe_2O_3	4848.799	3980.273	-122551.569	5643.831	44699.711	44390.938	8974.546	-21605.799	4802.839
K_2O	-39885.120	93561.135	347981.229	-268582.886	44390.938	1502318.658	-26908.152	-16590.828	60905.631
Li_2O	-22526.737	7438.036	-105906.916	38103.956	8974.546	-26908.152	138928.622	-55817.132	52434.045
MgO	16347.517	-13523.165	370744.705	-97453.982	-21605.799	-16590.828	-55817.132	422461.876	-23304.053
MnO	23076.626	27112.419	-704553.874	96313.533	4802.839	60905.631	52434.045	-23304.053	511973.666
Na_2O	-27918.593	-9775.777	-328108.190	161418.624	-15985.590	-118175.955	28659.405	-95725.343	-34594.758
SiO_2	4511.897	-2397.770	17032.656	9355.146	-3887.424	-3180.459	-15079.184	-7752.749	2327.888
ThO_2	-3871.655	-19611.224	521554.201	-59120.554	878.470	18282.188	-53388.542	56531.912	-364230.676
UO_3	-3655.944	6396.616	-8115.886	187954.922	-41751.383	-91207.073	1874.080	-53808.783	127958.164
ZrO_2	13709.963	-6878.435	173977.246	-81256.755	10099.424	7325.870	-36122.495	94788.690	-47069.059
Others	-4243.066	-4448.170	127.765	-62958.393	-6889.437	-34472.748	13818.085	17253.729	-50587.059
B_2O_3×K_2O	257856.827	-940531.923	-451451.834	1813649.417	-531602.041	-13982822.531	362740.939	792415.065	-661318.582
Na_2O×Na_2O	46604.694	83994.948	1025973.830	-925637.866	65573.014	601715.075	-29737.417	348038.473	142167.819

Table A.15. Variance-covariance table for the TL-Zr model (part 2).

Var covar	Na_2O	SiO_2	ThO_2	UO_3	ZrO_2	Others	$B_2O_3 \times K_2O$	$Na_2O \times Na_2O$
Al_2O_3	-27918.593	4511.897	-3871.655	-3655.944	13709.963	-4243.066	257856.827	46604.694
B_2O_3	-9775.777	-2397.770	-19611.224	6396.616	-6878.435	-4448.170	-940531.923	83994.948
Cr_2O_3	-328108.190	17032.656	521554.201	-8115.886	173977.246	127.765	-451451.834	1025973.830
F	161418.624	9355.146	-59120.554	187954.922	-81256.755	-62958.393	1813649.417	-925637.866
Fe_2O_3	-15985.590	-3887.424	878.470	-41751.383	10099.424	-6889.437	-531602.041	65573.014
K_2O	-118175.955	-3180.459	18282.188	-91207.073	7325.870	-34472.748	-13982822.531	601715.075
Li_2O	28659.405	-15079.184	-53388.542	1874.080	-36122.495	13818.085	362740.939	-29737.417
MgO	-95725.343	-7752.749	56531.912	-53808.783	94788.690	17253.729	792415.065	348038.473
MnO	-34594.758	2327.888	-364230.676	127958.164	-47069.059	-50587.059	-661318.582	142167.819
Na_2O	297031.671	-13198.701	-71688.341	87470.494	-64464.865	-23315.197	789321.377	-1170514.571
SiO_2	-13198.701	7346.212	5671.930	14354.664	-10579.904	-4724.852	-33785.951	30605.597
ThO_2	-71688.341	5671.930	965659.216	-261347.931	49388.797	46053.293	81546.345	215422.027
UO_3	87470.494	14354.664	-261347.931	443491.893	-78185.243	-54165.371	566555.431	-397299.084
ZrO_2	-64464.865	-10579.904	49388.797	-78185.243	84535.987	16922.498	152757.307	233111.559
Others	-23315.197	-4724.852	46053.293	-54165.371	16922.498	30758.472	481494.745	117398.627
$B_2O_3 \times K_2O$	789321.377	-33785.951	81546.345	566555.431	152757.307	481494.745	149723875.843	-3920182.207
$Na_2O \times Na_2O$	-1170514.571	30605.597	215422.027	-397299.084	233111.559	117398.627	-3920182.207	5064721.785

Table A.16. Variance-covariance table for the SP C950 model (part 1).

Var covar	Al_2O_3	B_2O_3	CaO	Cr_2O_3	Fe_2O_3	K_2O	Li_2O	MgO	MnO	Na_2O
Al_2O_3	1.078002	-0.260753	-0.238559	1.448259	0.348666	-0.108272	-0.315060	1.144764	-1.788899	-2.014087
B_2O_3	-0.260753	1.298694	0.140947	-0.684792	0.079992	0.634599	0.884202	1.579778	-0.924594	-1.908463
CaO	-0.238559	0.140947	2.171909	-2.627720	-0.153285	-0.016150	0.173344	-1.846113	0.652290	-0.541539
Cr_2O_3	1.448259	-0.684792	-2.627720	105.926371	2.959108	-1.968747	-3.478241	7.569931	-8.090611	-4.680115
Fe_2O_3	0.348666	0.079992	-0.153285	2.959108	3.417201	-1.154280	-0.404495	3.186729	-7.280897	-1.236466
K_2O	-0.108272	0.634599	-0.016150	-1.968747	-1.154280	7.460634	0.708580	3.948613	-17.113108	0.152121
Li_2O	-0.315060	0.884202	0.173344	-3.478241	-0.404495	0.708580	8.174164	-2.897102	-10.420095	-0.904021
MgO	1.144764	1.579778	-1.846113	7.569931	3.186729	3.948613	-2.897102	102.308912	-28.721746	-3.165485
MnO	-1.788899	-0.924594	0.652290	-8.090611	-7.280897	-17.113108	-10.420095	-28.721746	294.528316	-6.905310
Na_2O	-2.014087	-1.908463	-0.541539	-4.680115	-1.236466	0.152121	-0.904021	-3.165485	-6.905310	12.082804
NiO	0.330417	-6.159231	-2.933830	-1.400380	39.971077	-24.969627	-10.963909	7.288079	-13.780206	10.836095
P_2O_5	-0.210209	0.265438	-0.285251	-4.710696	-0.837782	-0.489806	3.309150	-2.281589	-2.796469	-2.538570
SiO_2	-0.523660	-0.755976	-0.126635	-1.528716	-1.070560	-0.131204	-1.201720	-3.147930	6.152113	3.164119
SrO	0.361436	0.960152	0.039280	4.142811	-0.533137	0.045519	2.658944	-0.263283	-10.758714	-3.331002
ZnO	0.728399	-0.521638	-0.064213	1.901497	2.591056	-1.839901	-0.076973	-2.481733	7.922067	-3.791516
Other	0.607870	0.382207	0.009869	0.322960	-0.157665	-0.445452	0.178203	2.056668	-3.108256	-2.986842
Fe_2O_3×NiO	7.615190	57.209668	28.972143	4.239981	-375.615366	225.025689	79.102101	42.677336	201.684536	-115.087313
MnO×SiO_2	6.284298	5.346870	0.552071	6.545767	17.655531	42.954416	27.042961	98.492747	-753.007781	8.862706
Na_2O×SiO_2	5.577378	6.828399	2.348814	10.861072	3.692739	1.247200	5.965032	9.268075	7.106110	-37.274315

Table A.17. Variance-covariance table for the SP C950 model (part 2).

Var covar	NiO	P_2O_5	SiO_2	SrO	ZnO	Other	Fe_2O_3×NiO	MnO×SiO_2	Na_2O×SiO_2
Al_2O_3	0.330417	-0.210209	-0.523660	0.361436	0.728399	0.607870	7.615190	6.284298	5.577378
B_2O_3	-6.159231	0.265438	-0.755976	0.960152	-0.521638	0.382207	57.209668	5.346870	6.828399
CaO	-2.933830	-0.285251	-0.126635	0.039280	-0.064213	0.009869	28.972143	0.552071	2.348814
Cr_2O_3	-1.400380	-4.710696	-1.528716	4.142811	1.901497	0.322960	4.239981	6.545767	10.861072
Fe_2O_3	39.971077	-0.837782	-1.070560	-0.533137	2.591056	-0.157665	-375.615366	17.655531	3.692739
K_2O	-24.969627	-0.489806	-0.131204	0.045519	-1.839901	-0.445452	225.025689	42.954416	1.247200
Li_2O	-10.963909	3.309150	-1.201720	2.658944	-0.076973	0.178203	79.102101	27.042961	5.965032
MgO	7.288079	-2.281589	-3.147930	-0.263283	-2.481733	2.056668	42.677336	98.492747	9.268075
MnO	-13.780206	-2.796469	6.152113	-10.758714	7.922067	-3.108256	201.684536	-753.007781	7.106110
Na_2O	10.836095	-2.538570	3.164119	-3.331002	-3.791516	-2.986842	-115.087313	8.862706	-37.274315
NiO	770.329901	-22.914705	-4.265794	-15.683606	28.094764	-10.791699	-6743.898101	-18.914681	-40.145100
P_2O_5	-22.914705	14.022410	-0.756080	2.800617	-0.452339	1.331475	195.798379	5.888495	8.835129
SiO_2	-4.265794	-0.756080	1.406235	-1.128535	-1.027597	-0.917747	35.168080	-19.477097	-10.884848
SrO	-15.683606	2.800617	-1.128535	6.484157	-1.223325	1.660329	156.635116	24.705882	10.664012
ZnO	28.094764	-0.452339	-1.027597	-1.223325	13.134594	-0.728420	-225.754118	-20.898272	11.042896
Other	-10.791699	1.331475	-0.917747	1.660329	-0.728420	2.570784	90.308784	11.565605	9.311282
Fe_2O_3×NiO	-6743.898101	195.798379	35.168080	156.635116	-225.754118	90.308784	63980.237951	-28.608421	366.410273
MnO×SiO_2	-18.914681	5.888495	-19.477097	24.705882	-20.898272	11.565605	-28.608421	1998.641059	12.893412
Na_2O×SiO_2	-40.145100	8.835129	-10.884848	10.664012	11.042896	9.311282	366.410273	12.893412	120.892421

Table A.18. Variance-covariance table for the TCLP model (part 1).

	Al_2O_3	B_2O_3	CaO	Fe_2O_3	K_2O	Li_2O	LN_2O_3	MgO
Al_2O_3	0.715622	-0.218964	0.009780	0.110116	0.201613	-0.453509	-0.129882	-0.079029
B_2O_3	-0.218964	0.335782	-0.033667	-0.033846	-0.066474	-0.411678	0.211319	0.031309
CaO	0.009780	-0.033667	0.438920	0.193647	0.044850	-0.230121	-0.193762	-0.104604
Fe_2O_3	0.110116	-0.033846	0.193647	2.118844	0.506340	-0.579965	1.154077	-0.022839
K_2O	0.201613	-0.066474	0.044850	0.506340	6.651289	-1.181897	-3.553591	-1.148210
Li_2O	-0.453509	-0.411678	-0.230121	-0.579965	-1.181897	6.995956	-0.038430	-0.524590
LN_2O_3	-0.129882	0.211319	-0.193762	1.154077	-3.553591	-0.038430	24.753463	1.121033
MgO	-0.079029	0.031309	-0.104604	-0.022839	-1.148210	-0.524590	1.121033	2.247112
Na_2O	-0.236931	0.041822	0.024595	-0.000414	-0.003260	-0.304340	0.222422	0.312847
P_2O_5	-0.764535	-0.492293	-0.100533	0.317884	-0.166010	0.313860	0.292585	-0.264137
SiO_2	0.027829	-0.062172	-0.058841	-0.163559	-0.130556	0.468804	-0.261014	-0.113635
ZnO	0.306646	-0.448822	0.148309	-0.519561	0.693778	-0.271048	2.773819	0.476311
ZrO_2	0.431771	-0.082704	0.132236	0.271522	0.390567	-0.561462	-0.638132	0.100342
Others	-0.013820	0.075967	-0.000863	0.046448	-0.015707	-0.618547	-0.039882	0.105469
$Li_2O \times SiO_2$	0.639286	1.060287	0.679447	1.149025	2.630803	-15.361605	-0.214254	1.106122
$MgO \times Na_2O$	1.963898	-0.463882	-0.217330	1.721636	7.344477	-0.382383	-9.559349	-16.850768

Table A.19. Variance-covariance table for the TCLP model (part 2).

	Na_2O	P_2O_5	SiO_2	ZnO	ZrO_2	Others	$Li_2O \times SiO_2$	$MgO \times Na_2O$
Al_2O_3	-0.236931	-0.764535	0.027829	0.306646	0.431771	-0.013820	0.639286	1.963898
B_2O_3	0.041822	-0.492293	-0.062172	-0.448822	-0.082704	0.075967	1.060287	-0.463882
CaO	0.024595	-0.100533	-0.058841	0.148309	0.132236	-0.000863	0.679447	-0.217330
Fe_2O_3	-0.000414	0.317884	-0.163559	-0.519561	0.271522	0.046448	1.149025	1.721636
K_2O	-0.003260	-0.166010	-0.130556	0.693778	0.390567	-0.015707	2.630803	7.344477
Li_2O	-0.304340	0.313860	0.468804	-0.271048	-0.561462	-0.618547	-15.361605	-0.382383
LN_2O_3	0.222422	0.292585	-0.261014	2.773819	-0.638132	-0.039882	-0.214254	-9.559349
MgO	0.312847	-0.264137	-0.113635	0.476311	0.100342	0.105469	1.106122	-16.850768
Na_2O	0.427412	-0.999044	-0.130588	0.010715	-0.295075	0.036424	1.183315	-3.081621
P_2O_5	-0.999044	34.462294	0.260644	0.159700	0.015907	-0.173302	-1.465679	7.794435
SiO_2	-0.130588	0.260644	0.103639	-0.119968	-0.036227	-0.060727	-1.314515	0.280848
ZnO	0.010715	0.159700	-0.119968	10.035608	0.111739	-0.726595	0.421965	-0.363728
ZrO_2	-0.295075	0.015907	-0.036227	0.111739	3.019465	-0.155062	0.642994	2.119509
Others	0.036424	-0.173302	-0.060727	-0.726595	-0.155062	0.432597	1.359926	-0.305467
$Li_2O \times SiO_2$	1.183315	-1.465679	-1.314515	0.421965	0.642994	1.359926	36.085460	1.800079
$MgO \times Na_2O$	-3.081621	7.794435	0.280848	-0.363728	2.119509	-0.305467	1.800079	212.320613

Appendix B – Waste Compositions

Table B.1. Waste compositions (mg or mCi per L waste) used in the example calculations.

Example #	Unit	1	2	3	4	5	6
Ac	mg/L	0.000E+00	0.000E+00	0.000E+00	0.000E+00	0.000E+00	0.000E+00
Ag	mg/L	1.073E+01	1.095E+02	3.313E+00	0.000E+00	0.000E+00	1.643E+00
Al	mg/L	3.678E+04	4.625E+03	1.391E+04	1.595E+04	1.336E+04	2.924E+04
Am	mg/L	0.000E+00	0.000E+00	0.000E+00	0.000E+00	0.000E+00	0.000E+00
As	mg/L	3.935E+01	4.342E+00	9.814E+01	0.000E+00	0.000E+00	7.685E+01
B	mg/L	1.015E+02	2.489E+02	4.500E+01	0.000E+00	0.000E+00	3.405E+01
Ba	mg/L	1.965E+01	1.293E+01	2.162E+01	2.400E-08	5.009E-08	1.297E+01
Be	mg/L	1.966E+00	1.219E+01	1.488E+00	0.000E+00	0.000E+00	6.148E-01
Bi	mg/L	9.607E+00	8.738E+01	9.317E+00	2.533E+03	6.623E+00	7.411E+00
Ca	mg/L	8.858E+01	1.465E+02	2.399E+02	4.009E+02	7.559E+02	8.372E+02
Cd	mg/L	6.908E+00	8.045E+00	3.104E+01	1.863E-06	7.792E-06	2.603E+01
Ce	mg/L	3.935E+01	1.252E+00	7.336E+01	0.000E+00	0.000E+00	5.379E+01
Cl	mg/L	4.675E+02	6.551E+02	1.734E+03	4.237E+02	4.035E+02	1.181E+03
Cm	mg/L	0.000E+00	0.000E+00	0.000E+00	0.000E+00	0.000E+00	0.000E+00
Co	mg/L	3.390E+01	4.908E-01	6.698E+00	3.379E-07	1.915E-06	3.377E+00
Cr	mg/L	2.960E+02	1.397E+03	4.417E+02	2.630E+02	4.632E+02	6.985E+02
Cs	mg/L	4.120E-01	4.757E-01	2.234E+00	8.836E-01	1.849E+00	2.235E+00
Cu	mg/L	3.938E+00	1.399E+00	1.647E+01	0.000E+00	0.000E+00	1.335E+01
Eu	mg/L	0.000E+00	0.000E+00	0.000E+00	0.000E+00	0.000E+00	0.000E+00
F	mg/L	3.963E+02	2.819E+04	7.240E+02	2.296E+03	1.014E+04	1.682E+04
Fe	mg/L	3.264E+01	3.104E+02	4.392E+03	2.570E+04	1.837E+04	9.554E+03
Gd	mg/L	0.000E+00	0.000E+00	0.000E+00	0.000E+00	0.000E+00	0.000E+00
Hg	mg/L	2.804E-01	9.683E-02	2.299E-01	1.570E+01	1.441E+01	1.163E+01
I	mg/L	0.000E+00	0.000E+00	0.000E+00	0.000E+00	0.000E+00	0.000E+00
K	mg/L	7.472E+02	2.623E+03	6.452E+02	1.771E+02	5.336E+02	8.547E+02
La	mg/L	2.283E-04	8.055E+01	2.084E+01	6.735E+01	1.047E+03	2.904E+01
Li	mg/L	1.366E+01	1.392E+00	1.342E+01	0.000E+00	0.000E+00	1.085E+01
Mg	mg/L	3.940E+01	2.087E+02	1.243E+02	0.000E+00	0.000E+00	9.942E+01
Mn	mg/L	3.927E+00	2.006E+01	4.846E+02	1.254E+03	1.438E+03	1.835E+03
Mo	mg/L	2.584E+01	2.523E+00	2.613E+01	0.000E+00	0.000E+00	1.609E+01
Na	mg/L	2.767E+04	7.433E+04	1.201E+05	4.053E+04	5.772E+04	1.380E+05
Nb	mg/L	0.000E+00	0.000E+00	0.000E+00	0.000E+00	0.000E+00	0.000E+00
Nd	mg/L	3.940E+01	2.655E+01	1.482E+02	0.000E+00	0.000E+00	1.215E+02
Ni	mg/L	7.809E+00	2.409E+01	1.094E+02	7.757E+02	8.937E+02	6.281E+02
Np	mg/L	0.000E+00	0.000E+00	0.000E+00	0.000E+00	0.000E+00	0.000E+00
P	mg/L	1.394E+02	1.037E+03	1.224E+03	6.058E+03	9.063E+02	1.550E+03
Pa	mg/L	0.000E+00	0.000E+00	0.000E+00	0.000E+00	0.000E+00	0.000E+00
Pb	mg/L	3.932E+01	1.738E+01	2.401E+02	2.531E+03	4.789E+02	3.860E+02
Pd	mg/L	0.000E+00	0.000E+00	0.000E+00	0.000E+00	0.000E+00	0.000E+00
Pr	mg/L	0.000E+00	0.000E+00	0.000E+00	0.000E+00	0.000E+00	0.000E+00
Pu	mg/L	0.000E+00	0.000E+00	0.000E+00	0.000E+00	0.000E+00	0.000E+00
Ra	mg/L	0.000E+00	0.000E+00	0.000E+00	0.000E+00	0.000E+00	0.000E+00
Rb	mg/L	0.000E+00	0.000E+00	0.000E+00	0.000E+00	0.000E+00	0.000E+00

Example #	Unit	1	2	3	4	5	6
Rh	mg/L	0.000E+00	0.000E+00	0.000E+00	0.000E+00	0.000E+00	0.000E+00
Ru	mg/L	1.125E-19	4.335E-19	2.115E+01	7.943E-20	6.682E-19	1.960E+01
S	mg/L	1.501E+02	3.000E+03	1.167E+03	7.042E+02	3.000E+03	3.500E+03
Sb	mg/L	2.361E+01	5.772E-01	1.021E+01	3.812E-09	1.724E-08	2.017E-09
Se	mg/L	3.940E+01	1.670E+00	5.288E+01	2.874E-03	9.503E-03	8.437E-02
Si	mg/L	2.391E+02	4.796E+02	8.795E+01	5.786E+02	1.250E+02	2.109E+03
Sm	mg/L	0.000E+00	0.000E+00	0.000E+00	0.000E+00	0.000E+00	0.000E+00
Sn	mg/L	0.000E+00	0.000E+00	0.000E+00	0.000E+00	0.000E+00	0.000E+00
Sr	mg/L	2.669E-02	3.486E-01	6.202E+00	6.340E+01	6.148E+01	2.325E+01
Ta	mg/L	0.000E+00	0.000E+00	0.000E+00	0.000E+00	0.000E+00	0.000E+00
Tc	mg/L	0.000E+00	0.000E+00	0.000E+00	0.000E+00	0.000E+00	0.000E+00
Te	mg/L	0.000E+00	0.000E+00	0.000E+00	0.000E+00	0.000E+00	0.000E+00
Th	mg/L	2.610E-01	1.628E+00	2.824E+01	1.634E+02	2.668E+02	7.182E+03
Ti	mg/L	3.940E+00	1.694E+00	1.700E+00	0.000E+00	0.000E+00	0.000E+00
Tl	mg/L	0.000E+00	7.960E-01	3.390E+01	0.000E+00	0.000E+00	0.000E+00
U	mg/L	2.989E+01	2.633E+03	1.357E+02	2.288E+03	4.337E+02	5.922E+03
V	mg/L	1.967E+01	6.894E+00	8.502E+00	0.000E+00	0.000E+00	0.000E+00
W	mg/L	0.000E+00	0.000E+00	1.550E+02	0.000E+00	0.000E+00	1.436E+02
Y	mg/L	1.082E-07	5.914E+00	4.706E+01	4.053E-04	9.459E-04	4.203E+01
Zn	mg/L	2.362E+01	2.964E+00	3.268E+01	0.000E+00	0.000E+00	2.853E+01
Zr	mg/L	3.623E+00	2.603E+04	1.174E+02	2.135E+01	5.327E+02	1.294E+04
NO_2	mg/L	1.412E+04	1.648E+04	4.375E+04	1.718E+04	1.408E+04	3.371E+04
NO_3	mg/L	2.065E+04	2.618E+04	4.828E+04	2.257E+04	2.121E+04	3.411E+04
TOC	mg/L	8.030E+02	2.054E+03	1.400E+04	8.581E+02	2.388E+03	1.562E+04
^{59}Ni	mCi/L	3.311E-03	1.096E-03	1.893E-03	1.212E-03	1.350E-02	2.590E-03
^{60}Co	mCi/L	3.166E-05	7.043E-05	3.456E-05	3.821E-04	2.166E-03	3.429E-04
^{63}Ni	mCi/L	2.459E-01	8.098E-02	2.181E-01	8.960E-02	7.845E-01	2.633E-01
^{79}Se	mCi/L	4.229E-04	2.398E-04	2.945E-04	2.003E-04	6.623E-04	5.879E-03
^{90}Sr	mCi/L	5.916E-02	1.818E+00	2.063E+01	2.217E+02	5.174E+02	5.779E+01
^{90}Y	mCi/L	5.880E-02	1.807E+00	2.050E+01	2.204E+02	5.143E+02	5.743E+01
^{93m}Nb	mCi/L	8.927E-03	3.653E-03	8.355E-03	2.603E-03	9.913E-02	6.578E-03
^{93}Zr	mCi/L	9.113E-03	3.848E-03	1.013E-02	2.764E-03	1.036E-01	8.437E-03
^{99}Tc	mCi/L	7.100E-02	1.642E-02	6.096E-03	1.405E-02	1.897E-02	1.819E-02
^{106}Ru	mCi/L	3.767E-16	1.452E-15	3.601E-16	2.660E-16	2.238E-15	3.585E-16
^{113m}Cd	mCi/L	1.656E-03	9.350E-04	7.097E-04	4.307E-04	1.801E-03	8.476E-04
^{125}Sb	mCi/L	3.634E-07	4.364E-06	3.827E-07	3.953E-06	1.788E-05	2.092E-06
^{126}Sn	mCi/L	1.923E-03	7.827E-04	1.537E-03	4.311E-04	2.642E-02	1.185E-03
^{129}I	mCi/L	8.452E-06	1.569E-05	2.424E-05	1.691E-04	3.315E-05	1.571E-04
^{134}Cs	mCi/L	6.825E-10	5.947E-09	2.914E-09	1.281E-09	8.032E-09	2.523E-09
^{137m}Ba	mCi/L	6.025E+00	6.931E+00	3.252E+01	1.291E+01	2.696E+01	3.255E+01
^{137}Cs	mCi/L	6.347E+00	7.328E+00	3.442E+01	1.361E+01	2.849E+01	3.443E+01
^{151}Sm	mCi/L	3.986E+00	1.249E+00	6.675E+01	3.943E+01	1.076E+02	6.899E+01
^{152}Eu	mCi/L	9.641E-05	3.203E-05	1.322E-03	7.324E-04	6.601E-03	1.643E-03
^{154}Eu	mCi/L	1.611E-03	8.382E-04	3.171E-02	1.782E-02	1.521E-01	3.834E-02
^{155}Eu	mCi/L	8.299E-05	3.682E-05	1.138E-03	8.550E-04	4.581E-03	1.486E-03
^{226}Ra	mCi/L	1.490E-08	6.467E-09	1.020E-08	4.461E-09	1.326E-08	3.508E-08
^{227}Ac	mCi/L	1.461E-05	5.588E-06	1.270E-05	2.554E-06	8.848E-06	1.629E-04

Example #	Unit	1	2	3	4	5	6
^{228}Ra	mCi/L	2.703E-08	1.719E-07	1.996E-06	1.803E-05	2.742E-05	7.903E-04
^{229}Th	mCi/L	6.376E-09	3.986E-09	7.891E-09	3.712E-06	1.784E-07	1.129E-04
^{231}Pa	mCi/L	1.602E-05	6.967E-06	1.985E-05	3.214E-06	1.156E-05	4.964E-05
^{232}Th	mCi/L	2.281E-08	1.753E-07	3.084E-06	1.792E-05	2.782E-05	7.873E-04
^{232}U	mCi/L	2.046E-07	1.621E-05	9.297E-07	1.364E-05	1.249E-06	4.964E-04
^{233}U	mCi/L	1.795E-05	1.423E-03	8.154E-05	1.204E-03	1.100E-03	6.713E-02
^{234}U	mCi/L	1.274E-05	1.194E-03	5.777E-05	7.775E-04	1.766E-04	3.470E-03
^{235}U	mCi/L	5.018E-07	4.641E-05	2.514E-06	3.333E-05	7.020E-06	9.117E-05
^{236}U	mCi/L	8.619E-07	9.679E-05	3.912E-06	1.344E-05	1.418E-05	1.175E-04
^{237}Np	mCi/L	1.070E-04	8.274E-05	8.197E-04	3.213E-05	1.228E-03	1.457E-03
^{238}Pu	mCi/L	5.340E-05	5.087E-03	1.707E-02	8.911E-03	6.016E-02	8.338E-02
^{238}U	mCi/L	9.964E-06	8.772E-04	4.519E-05	7.636E-04	1.445E-04	1.973E-03
^{239}Pu	mCi/L	9.750E-04	7.225E-02	7.565E-02	5.432E-01	3.496E-01	7.052E-01
^{240}Pu	mCi/L	2.535E-04	1.991E-02	1.952E-02	8.901E-02	1.074E-01	1.807E-01
^{241}Am	mCi/L	2.475E-03	4.118E-02	5.036E-01	1.583E+00	4.297E+00	1.357E+00
^{241}Pu	mCi/L	7.842E-04	8.453E-02	3.311E-02	8.078E-02	6.049E-01	4.054E-01
^{242}Cm	mCi/L	2.935E-07	4.208E-06	2.916E-03	5.496E-04	1.823E-02	2.982E-03
^{242}Pu	mCi/L	2.693E-08	2.469E-06	2.208E-04	4.208E-06	4.079E-05	2.196E-04
^{243}Am	mCi/L	1.648E-06	6.822E-06	2.545E-03	4.727E-04	8.979E-03	2.577E-03
^{243}Cm	mCi/L	7.976E-09	1.021E-07	2.621E-04	1.599E-05	9.777E-04	2.548E-04
^{244}Cm	mCi/L	1.155E-07	1.491E-06	3.802E-03	2.278E-04	1.401E-02	3.696E-03

Appendix C – Glass-Forming Chemical Compositions

Table C.1. Nominal glass-forming chemical composition in mass fractions.

Oxide	Kyanite	Boric acid	Wollastonite	Na_2CO_3	Li_2CO_3	Cr_2O_3	Silica	Zincite	Zircon	V_2O_5
Al_2O_3	0.570223	0	0.002003	0	0	0	0.001657	0	0.002502	0
B_2O_3	0	0.565221	0	0	0	0	0	0	0	0
CaO	0.000267	0	0.475099	$1.29´10^{-5}$	0.003657	0	0.0001	0	0	0
CdO	0	0	0	0	0	0	0	0.0001	0	0
Cl	0	0	0	0.000174	$8.32´10^{-5}$	0	0	0	0	0
Cr_2O_3	0	0	0	$7.77´10^{-5}$	0.0001	0.990223	0	0	0	0
Fe_2O_3	0.007568	0	0.004003	$1.3´10^{-5}$	$1.67´10^{-5}$	$3.88´10^{-5}$	0.000217	$1.66´10^{-5}$	0.000783	0.000074
K_2O	0.000116	0	0	0	$1.66´10^{-5}$	0	$3.35´10^{-5}$	0	0	$2.34´10^{-5}$
Li_2O	0	0	0	0	0.402062	0	0	0	0	0
MgO	0.000133	0	0.000835	$1.3´10^{-5}$	$9.99´10^{-5}$	0	$8.33´10^{-5}$	0	0	0
MnO	0	0	0.001	0	0	0	0	$1.66´10^{-5}$	0	0
Na_2O	0.003495	0	0	0.58376	0.000716	0	0.000167	0	0	$4.36´10^{-5}$
NiO	0	0	0	0	0	0	0	0	0	0
P_2O_5	0	0	0	0	0	0	0	0	0	0
PbO	0	0	0	0	0	0	0	$1.66´10^{-5}$	0	0
SO_3	0	$4.98´10^{-5}$	0	0.0001	0.000266	0	0	0	0	0
SiO_2	0.406079	0	0.508207	0	0	0	0.996506	0	0.322526	$2.77´10^{-5}$
TiO_2	0.008769	0	0.0002	0	0	0	0.00015	0	0.001017	0
UO_3	0	0	0	0	0	0	0	0	0.00045	0
V_2O_5	0	0	0	0	0	0	0	0	0	0.994
ZnO	0	0	0	0	0	0	0	0.998145	0	0
ZrO_2	0	0	0	0	0	0	0	0	0.660036	0

Table C.2. Minimum glass-forming chemical composition in mass fractions.

Min	Kyanite	Boric acid	Wollastonite	Na_2CO_3	Li_2CO_3	Cr_2O_3	Silica	Zincite	Zircon	V_2O_5
Al_2O_3	0.54	0	0.0013	0	0	0	0.0004	0	0.001	0
B_2O_3	0	0.5625	0	0	0	0	0	0	0	0
CaO	0	0	0.4477	0	0	0	0	0	0	0
Cr_2O_3	0	0	0	0	0	0.985	0	0	0	0
Fe_2O_3	0.0042	0	0.0029	0	0	0	0.0001	0	0.0006	0
Li_2O	0	0	0	0	0.4	0	0	0	0	0
MnO	0	0	0.0009	0	0	0	0	0	0	0
Na_2O	0	0	0	0.5831	0	0	0	0	0	0
SiO_2	0.39	0	0.48	0	0	0	0.992	0	0.32	0
TiO_2	0.005	0	0.0001	0	0	0	0	0	0.0007	0
UO_3	0	0	0	0	0	0	0	0	0.0003	0
V_2O_5	0	0	0	0	0	0	0	0	0	0.992
ZnO	0	0	0	0	0	0	0	0.993	0	0
ZrO_2	0	0	0	0	0	0	0	0	0.65	0

Table C.3. Maximum glass-forming chemical composition in mass fractions.

Max	Kyanite	Boric acid	Wollastonite	Na_2CO_3	Li_2CO_3	Cr_2O_3	Silica	Zincite	Zircon	V_2O_5
Al_2O_3	0.6	0	0.0027	0	0	0	0.004	0	0.004	0
B_2O_3	0	0.568	0	0	0	0	0	0	0	0
CaO	0.0004	0	0.5023	0.0001	0.022	0	0.0002	0	0	0
CdO	0	0	0	0	0	0	0	0.0002	0	0
Cl	0	0	0	0.0002	0.0001	0	0	0	0	0
Cr_2O_3	0	0	0	0.0006	0.0002	0.991	0	0	0	0
Fe_2O_3	0.01	0	0.0051	0.0001	0.0001	0.0003	0.0004	0.0001	0.0009	0.0006
K_2O	0.0007	0	0	0	0.0001	0	0.0002	0	0	0.0002
Li_2O	0	0	0	0	0.4044	0	0	0	0	0
MgO	0.0004	0	0.001	0.0001	0.0002	0	0.0001	0	0	0
MnO	0	0	0.0011	0	0	0	0	0.0001	0	0
Na_2O	0.0042	0	0	0.5848	0.0011	0	0.0002	0	0	0.0003
PbO	0	0	0	0	0	0	0	0.0001	0	0
SO_3	0	0.0003	0	0.0002	0.0004	0	0	0	0	0
SiO_2	0.42	0	0.53	0	0	0	0.999	0	0.325	0.0002
TiO_2	0.016	0	0.0003	0	0	0	0.0005	0	0.0014	0
UO_3	0	0	0	0	0	0	0	0	0.0008	0
V_2O_5	0	0	0	0	0	0	0	0	0	**0.996**
ZnO	0	0	0	0	0	0	0	0.9999	0	0
ZrO_2	0	0	0	0	0	0	0	0	0.67	0

Table C.4. Most likely glass-forming chemical composition in mass fractions.

Most likely	Kyanite	Boric acid	Wollastonite	Na_2CO_3	Li_2CO_3	Cr_2O_3	Silica	Zincite	Zircon	V_2O_5
Al_2O_3	0.5703	0	0.002	0	0	0	0.0014	0	0.0025	0
B_2O_3	0	0.5652	0	0	0	0	0	0	0	0
CaO	0.0003	0	0.475	0	0	0	0.0001	0	0	0
CdO	0	0	0	0	0	0	0	0.0001	0	0
Cl	0	0	0	0.0002	0.0001	0	0	0	0	0
Cr_2O_3	0	0	0	0	0.0001	0.991	0	0	0	0
Fe_2O_3	0.0078	0	0.004	0	0	0	0.0002	0	0.0008	0
Li_2O	0	0	0	0	0.402	0	0	0	0	0
MgO	0.0001	0	0.001	0	0.0001	0	0.0001	0	0	0
MnO	0	0	0.001	0	0	0	0	0	0	0
Na_2O	0.0042	0	0	0.5837	0.0008	0	0.0002	0	0	0
SO_3	0	0	0	0.0001	0.0003	0	0	0	0	0
SiO_2	0.4067	0	0.51	0	0	0	0.997	0	0.3225	0
TiO_2	0.0079	0	0.0002	0	0	0	0.0001	0	0.001	0
UO_3	0	0	0	0	0	0	0	0	0.0004	0
V_2O_5	0	0	0	0	0	0	0	0	0	**0.994**
ZnO	0	0	0	0	0	0	0	0.999	0	0
ZrO_2	0	0	0	0	0	0	0	0	0.66	0

Appendix D – Non-Linear Viscosity and EC Models

To explore the potential to increase the precision of viscosity and electrical conductivity (EC) models, non-linear partial quadratic models were developed that included selected second-order terms for parameter *B* in the Vogel-Fulcher-Tammann (VFT) equation as:

$$B = \sum_{i=1}^{n} g_i B_i + Selected\left\{\sum_{i=1}^{n} B_{ii} g_i^2 + \sum_{i=1}^{n}\sum_{j\neq i}^{n-1} B_{ij} g_i g_j\right\} \quad \text{(D.1)}$$

The parameters *A* and T_0 were still considered as composition independent. The number of components was the same as in the models presented in Section 2.1. The quadratic terms were manually chosen primarily from major components to increase the R^2 in training, testing, and direct feed high-level waste (DFHLW) subsets.

The results are presented in Figure D.1, Figure D.2, Table D.1, and Table D.2. Compared to the linear models, the non-linear models generally achieved higher R^2 for all tested subsets. However, their ability to predict property values for composition regions outside of the covered region is questionable and should be tested when new DFHLW data becomes available. The component effects shown in Figure D.3 and Figure D.4 indicate most non-linear effects for SiO_2, Li_2O, and B_2O_3 in the viscosity model and Na_2O and Li_2O in the EC model. However, this could be partially affected by the selection of quadratic terms and should be investigated in more detail in the future.

Table D.1. Viscosity model coefficients and summary statistics.

Term	Coefficient	Unit	Statistic	Value
A	-2.6912	log(Pa·s)	# glass components	25
B_SiO_2	7560.6	K	# model parameters	41
B_Na_2O	612.28	K	# model features	26
B_B_2O_3	-1640.2	K	R^2, all	0.961
B_Al_2O_3	7680.1	K	R^2, train	0.970
B_Fe_2O_3	2598.5	K	R^2, test	0.961
B_CaO	293.82	K	R^2, excluded	0.880
B_ZrO_2	4145.2	K	RMSE, all	0.114
B_Li_2O	-9103.6	K	RMSE, train	0.098
B_ZnO	675.59	K	RMSE, test	0.100
B_K_2O	-263.9	K	RMSE, excluded	0.592
B_MgO	92.219	K	MdAE, all	0.050
B_P_2O_5	3404.6	K	MdAE, train	0.049
B_LN_2O_3	1319.3	K	MdAE, test	0.056
B_V_2O_5	317.14	K	MdAE, excluded	0.432
B_TiO_2	769.58	K	# points, all	13013
B_F	-3630.7	K	# points, train	11783
B_SO_3	5135.7	K	# points, test	1097
B_SnO_2	3770.5	K	# points, excluded	133
B_MnO	-693.26	K		
B_SrO	-495.04	K		
B_Cr_2O_3	4773.1	K		
B_NiO	-1194.5	K		
B_UO_3	2395.2	K		
B_Cl	5260.6	K		
B_Others	802.16	K		
B_SiO_2xSiO_2	-581.08	K		
B_SiO_2xNa_2O	-7794.8	K		
B_SiO_2xB_2O_3	-3232.6	K		
B_SiO_2xAl_2O_3	-897.99	K		
B_SiO_2xFe_2O_3	-3283.8	K		
B_SiO_2xLi_2O	-20960	K		
B_SiO_2xCaO	-3372.0	K		
B_Na_2OxB_2O_3	-6135.0	K		
B_Na_2OxLi_2O	20499.0	K		
B_B_2O_3xB_2O_3	12832	K		
B_B_2O_3xAl_2O_3	-6003.3	K		
B_Al_2O_3xLi_2O	-20693	K		
B_Al_2O_3xCaO	-4461.6	K		
B_Li_2OxLi_2O	80114	K		
T_0	554.71	K		

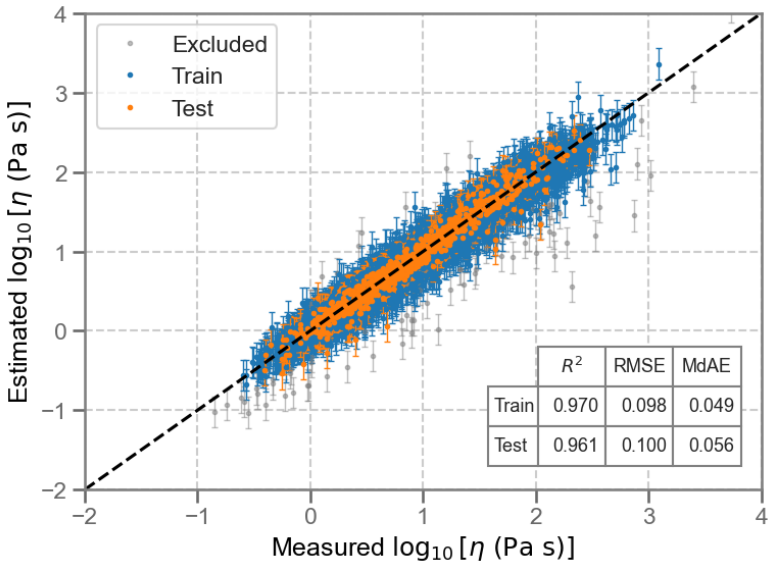

Figure D.1. Measured vs. estimated viscosity.

Table D.2. EC model coefficients and summary statistics.

Term	Coefficient	Unit	Statistic	Value
A	2.8849	log(S/m)	# glass components	20
B_SiO_2	-3257.6	K	# model parameters	31
B_Na_2O	6457.8	K	# model features	21
B_B_2O_3	-2035.3	K	R^2, all	0.880
B_Al_2O_3	-2499.9	K	R^2, train	0.914
B_CaO	-2546.9	K	R^2, test	0.853
B_Fe_2O_3	-1747.8	K	R^2, excluded	0.558
B_ZrO_2	-1859.9	K	RMSE, all	0.092
B_ZnO	-1450.3	K	RMSE, train	0.073
B_Li_2O	15285	K	RMSE, test	0.093
B_K_2O	-1237.6	K	RMSE, excluded	0.317
B_MgO	-1568.8	K	MdAE, all	0.044
B_V_2O_5	-1102.1	K	MdAE, train	0.042
B_SnO_2	-3152.9	K	MdAE, test	0.051
B_TiO_2	-1723.9	K	MdAE, excluded	0.271
B_P_2O_5	-1663.0	K	# points, all	7584
B_SO_3	-2003.8	K	# points, train	6867
B_MnO	-1892.7	K	# points, test	492
B_SrO	-2316.3	K	# points, excluded	225
B_Cr_2O_3	-959.06	K		
B_Others	-1511.8	K		
B_SiO_2xSiO_2	983.31	K		
B_SiO_2xNa_2O	-526.23	K		
B_SiO_2xB_2O_3	1069.2	K		
B_Na_2OxB_2O_3	-3620.4	K		
B_Na_2OxLi_2O	-60990	K		
B_Na_2OxNa_2O	-9373.0	K		
B_Na_2OxZrO_2	-3057.1	K		
B_B_2O_3xB_2O_3	1427.2	K		
B_Li_2OxLi_2O	-40869	K		
T_0	523.51	K		

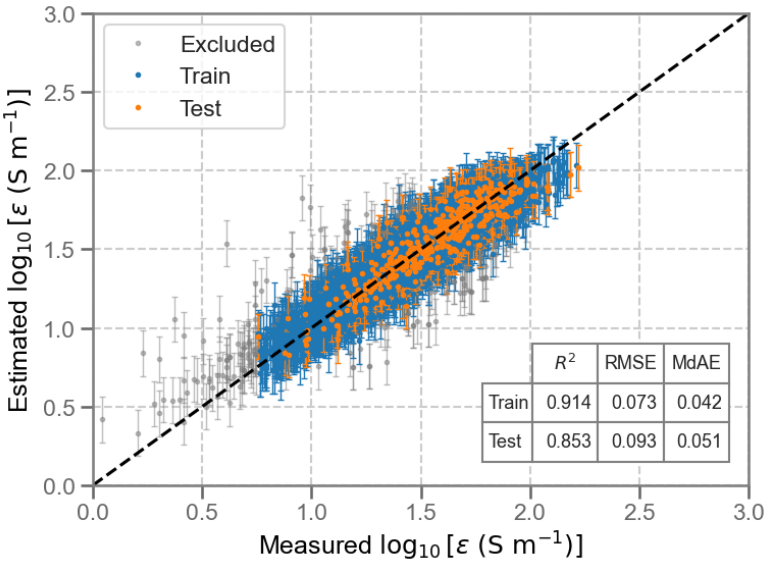

Figure D.2. Measured vs. estimated electrical conductivity.

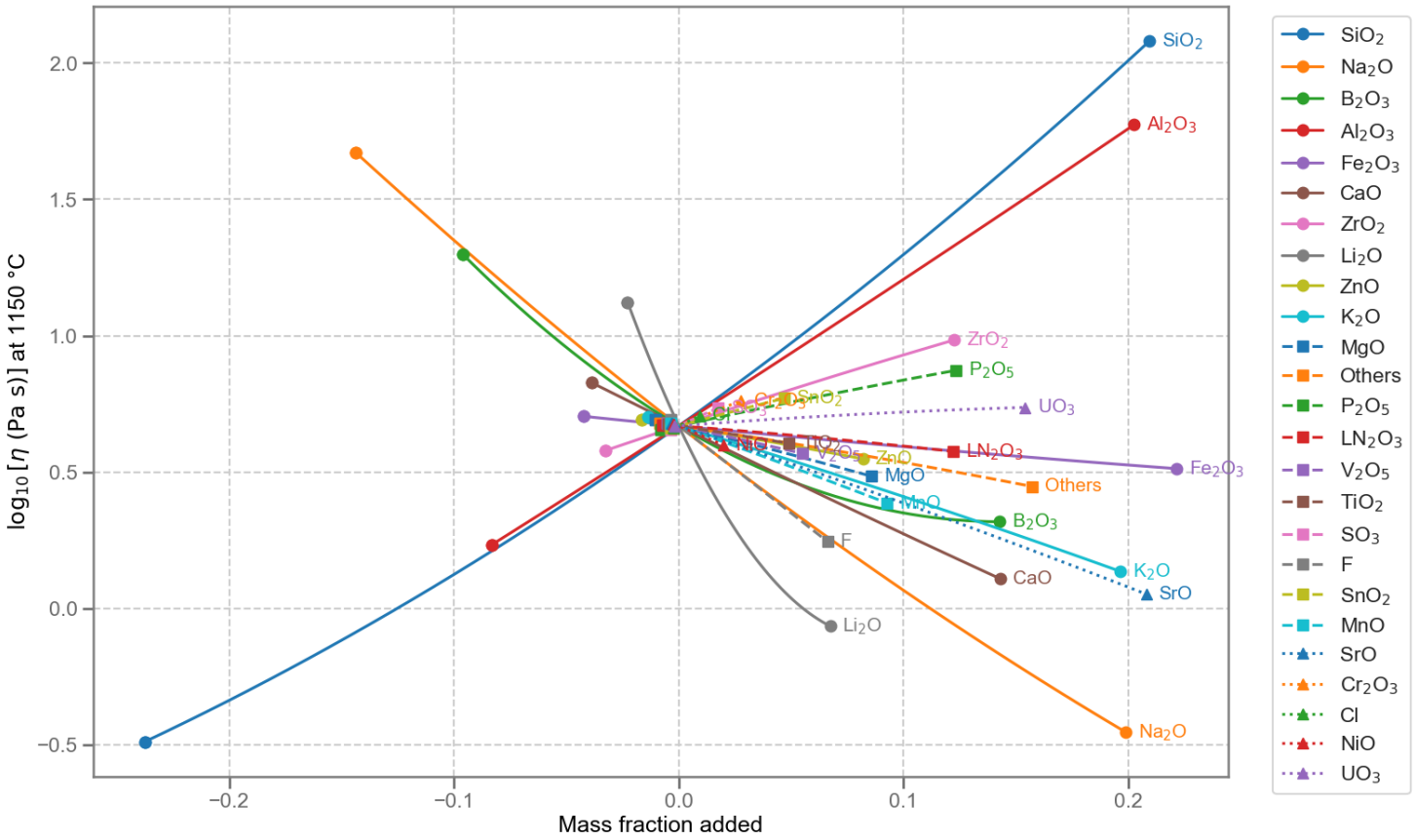

Figure D.3. Component effects on $\log_{10}(\eta_{1150}$, Pa·s).

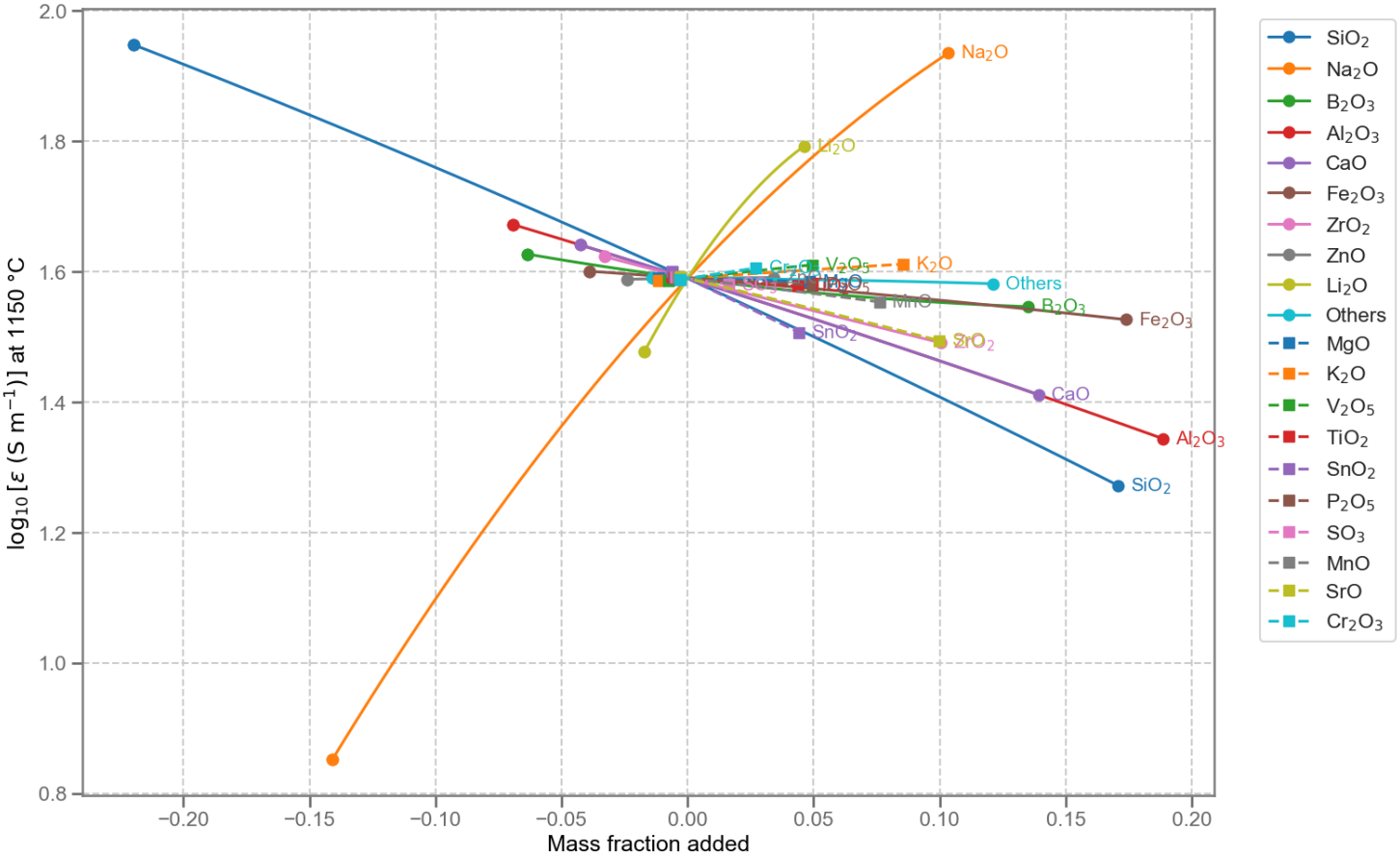

Figure D.4. Component effects on $\log_{10}(\varepsilon_{1150}$, S/m).

Appendix E – Temperature Dependent K-3 model

Section 2.3 discusses the model for natural logarithm of K-3 neck corrosion at 1200 to 1208 °C for 6 to 7 days. Additional data for other test conditions were also modeled using the following equation:

$$ln[k] = k_{s1150-3}S_{1150-3} + k_{s1150-7}S_{1150-7} + k_{s1200-3}S_{1200-3} + k_{s1200}S_{1200} + \sum_{i=1}^{q} k_i x_i + Selected\left\{\sum_{i=1}^{q} k_{ii}x_i^2 + \sum_{i=1}^{q}\sum_{j\neq i}^{q-1} k_{ij}x_i x_j\right\}, \quad (E.1)$$

where k_{s1200} = an offset coefficient for data measured under static conditions at 1200 °C for 6 or 7 d
$k_{s1150-3}$ = an offset coefficient for data measured under static conditions at 1150 °C for 3 d
$k_{s1150-7}$ = an offset coefficient for data measured under static conditions at 1150 °C for 7 d
$k_{s1200-3}$ = an offset coefficient for data measured under static conditions at 1200 °C for 3 d
S_{1200} = a static method counter = 1 for static at 1200 °C and 6 or 7 d and = 0 for other conditions
S_{1150-3} = a static method counter = 1 for static at 1150 °C and 3 d and = 0 for other conditions
S_{1150-7} = a static method counter = 1 for static at 1150 °C and 7 d and = 0 for other conditions
S_{1200-3} = a static method counter = 1 for static at 1200 °C and 3 d and = 0 for other conditions
k_i = the i^{th} component coefficient for ln[*k*]
k_{ii} = the i^{th} component quadratic coefficient for ln[*k*]
k_{ij} = the i^{th} and j^{th} components crossproduct coefficient for ln[*k*]
x_i = the i^{th} component mole fraction in glass
q = the number of components in the model

The data sources used for this model are described in Section 2.3.1. A total of 677 datapoints were available for modeling; 20 of those points were removed because of k ⩽ 0.002 in. and an additional 11 data points were excluded from model fitting as summarized in Table E.1, leaving 646 modeled points. The range of glass component concentrations are listed Table E.2.

Table E.1. List of glasses excluded from K-3 model development

Glass	Reason
LAWC34S2	Erroneous SO_3 content
LAWC36S2	Erroneous SO_3 content
HAL24M2-17	Studentized residual > Bonferroni 95% limit
HAL24M1-22	Studentized residual > Bonferroni 95% limit
HAL24M2-06-1150, 7d	Studentized residual > Bonferroni 95% limit
HAL24M2-06-1200, 7d	Studentized residual > Bonferroni 95% limit
HAL24M2-13	Studentized residual > Bonferroni 95% limit
HAL24M2-11	Studentized residual > Bonferroni 95% limit
HAL24M2-16	Studentized residual > Bonferroni 95% limit
HAL24M2-20	Studentized residual > Bonferroni 95% limit
HS24-39	Studentized residual > Bonferroni 95% limit
Total	11

Table E.2. Component concentration ranges in ln[*k*] dataset, molar fractions.

Component	Min	Mean	Median	Max
Al_2O_3	0.0172	0.0714	0.0621	0.1840
B_2O_3	0.0335	0.1140	0.0977	0.2370
CaO	0.0000	0.0514	0.0427	0.1396
Cr_2O_3	0.0000	0.0014	0.0005	0.0109
Fe_2O_3	0.0000	0.0116	0.0044	0.0633
K_2O	0.0000	0.0075	0.0032	0.0589
Li_2O	0.0000	0.0231	0.0020	0.1199
MgO	0.0000	0.0157	0.0155	0.0819
MnO	0.0000	0.0012	0.0000	0.0213
Na_2O	0.0248	0.1967	0.2138	0.2877
P_2O_5	0.0000	0.0034	0.0007	0.0206
SiO_2	0.2726	0.4329	0.4464	0.6009
V_2O_5	0.0000	0.0043	0.0023	0.0210
ZnO	0.0000	0.0201	0.0240	0.0411
ZrO_2	0.0000	0.0173	0.0165	0.0532
Others	0.0002	0.0279	0.0176	0.1456

A first-order model was fitted to the data to determine which components had significant effects on ln[*k*]. Al_2O_3, B_2O_3, Cr_2O_3, Fe_2O_3, K_2O, Li_2O, MgO, MnO, Na_2O, P_2O_5, SiO_2, V_2O_5, ZnO, and ZrO_2 were found to have significant effects. The two components added compared to the model in Section 2.3 were MgO and MnO. A partial quadratic model was developed using stepwise regression, where the following second-order terms were found to improve the model statistics: $Al_2O_3 \times Cr_2O_3$, $B_2O_3 \times Na_2O$, $Cr_2O_3 \times Li_2O$, $V_2O_5 \times V_2O_5$. This model was found to have the best fit statistics without overfitting with an $R^2 = 0.7825$.

The model coefficients are reported in Table E.3. The predicted values are compared to measured values in Figure E.1. Component concentration effects are presented in Figure E.2. Notable differences between the model in Section 2.3 and this temperature dependent model is the V_2O_5 effect on the model response. This model shows a quadratic effect rather than a monotonic negative effect.

Table E.3. Coefficients and summary statistics for ln[k_{neck}, inch] model with composition in normalized mass fractions.

Term	Coefficient		Statistic	Value
Stat, 1150/3d	-0.4215254		# of data	646
Stat, 1150/7d	-0.0094300		# of terms	24
Stat, 1200/3d	0.1891415		Mean ln[k_{neck}, inch]	-3.8711
Stat, 1200	0.2459776		R^2_{fit}	0.7825
Al_2O_3	-25.43959		R^2_{Adj}	0.7744
B_2O_3	7.29013		R^2_{press}	0.7601
CaO	3.78022		R^2_{kfold}	0.7509
Cr_2O_3	-275.32545		$RMSE_{fit}$	0.4815
Fe_2O_3	-10.21363		$RMSE_{press}$	0.4965
K_2O	13.36208		Pooled SD ln[k], static only	0.3976
Li_2O	12.74355		Pooled SD ln[k], bubbled only	0.3311
MgO	-9.12250		Pooled SD ln[k], static + bubbled	0.3401
MnO	-23.45059			
Na_2O	18.86116			
P_2O_5	-18.78438			
SiO_2	-10.34968			
V_2O_5	-81.45114			
ZnO	-20.96781			
ZrO_2	-17.95386			
Others	-4.44701			
$Al_2O_3 \times Cr_2O_3$	1637.05107			
$Cr_2O_3 \times Li_2O$	-2411.12615			
$B_2O_3 \times Na_2O$	-51.24392			
$V_2O_5 \times V_2O_5$	4071.75274			

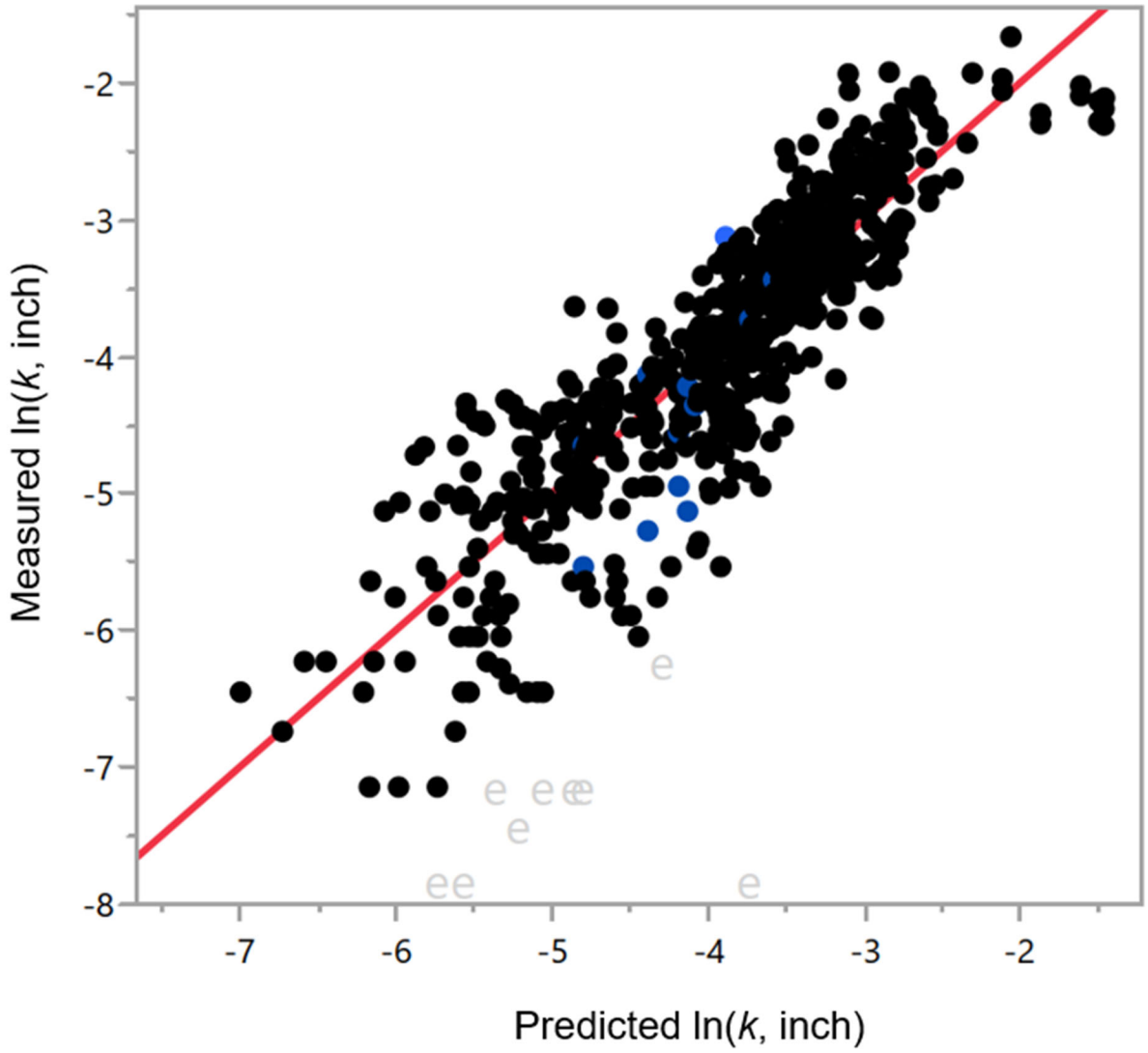

Figure E.1. Predicted vs. measured ln(k, inch) for all data modelled. Blue dots represent composition extreme included in the modeling dataset, letter e represent outliers

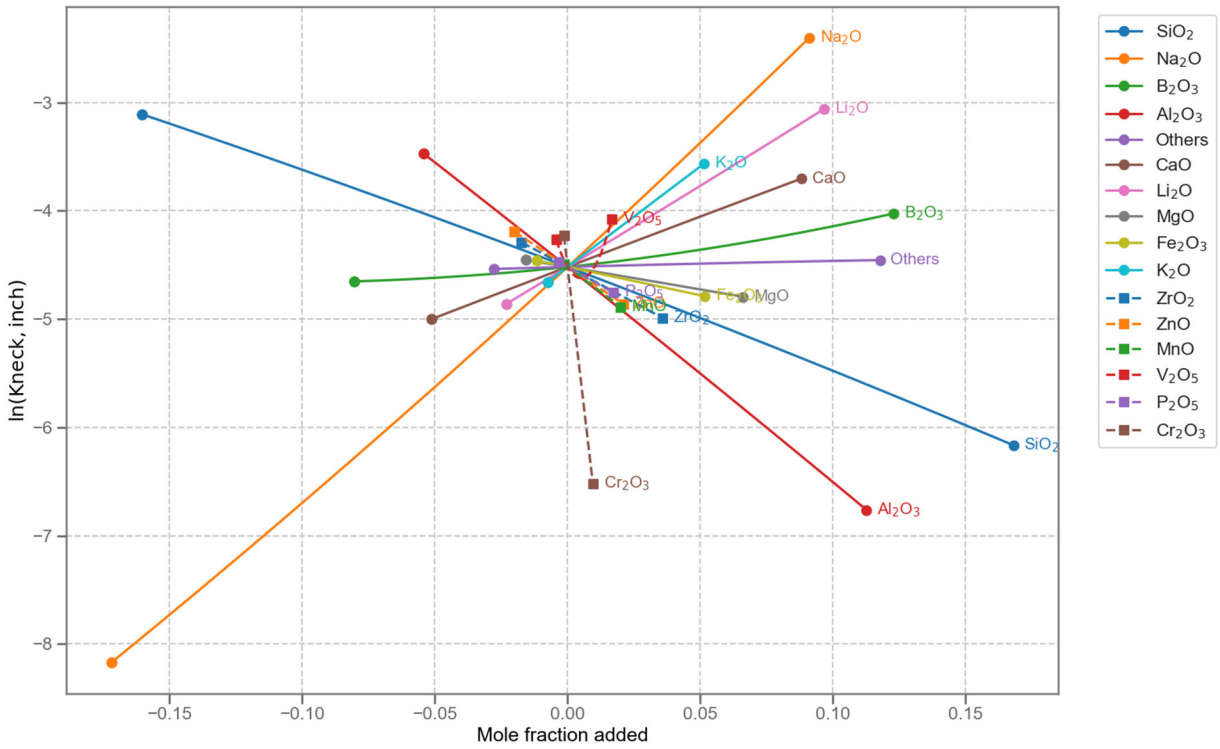

Figure E.2. Component impact of the ln(k_{neck}, inch) for all data modelled.

Appendix F – Retention Factors

Table F.1. Retention factors and decontamination factors (DFs) in ln(DF) for minimum, most likely, and maximum values.

Oxide	Retention Factor	ln(DF) Minimum	ln(DF) Most Likely	ln(DF) Maximum
Ac_2O_3	0.99721	2.6027	6.1079	11.1239
Ag_2O	0.97803	1.8563	4.1638	6.9256
Al_2O_3	0.99888	4.3656	6.6733	8.8901
Am_2O_3	0.97803	1.8563	4.1638	6.9256
As_2O_5	0.77121	1.8405	2.4844	3.989
B_2O_3	0.98968	3.3726	4.4967	5.8519
BaO	0.99721	4.1109	5.0163	5.5413
BeO	0.99721	2.6027	6.1079	11.1239
Bi_2O_3	0.97803	1.8563	4.1638	6.9256
CaO	0.99892	3.7126	6.8385	8.6034
CdO	0.99721	3.619	4.7221	5.6218
Ce_2O_3	0.99721	2.6027	6.1079	11.1239
Cl	0.54407	0.0979	0.7583	1.9095
Cm_2O_3	0.99721	2.6027	6.1079	11.1239
CoO	0.99721	2.6027	6.1079	11.1239
Cr_2O_3	0.95261	1.8563	3.2542	6.9256
Cs_2O	0.87902	0.47	2.4423	4.237
CuO	0.99721	4.1927	5.1008	5.7141
Eu_2O_3	0.99721	2.6027	6.1079	11.1239
F	0.72984	0.0643	1.2953	2.8649
Fe_2O_3	0.99848	3.9608	6.4321	8.8984
Gd_2O_3	0.99721	2.6027	6.1079	11.1239
HgO	0	0	0	0
I	0.50961	0.0945	0.5463	2.266
K_2O	0.96423	2.0669	3.3844	5.5607
La_2O_3	0.99721	2.6027	6.1079	11.1239
Li_2O	0.99601	3.4689	5.806	7.2894
MgO	0.99984	3.381	8.6802	11.0268
MnO	0.99721	4.5799	5.5721	6.6107
MoO_3	0.97803	1.8563	4.1638	6.9256
Na_2O	0.99136	3.4874	4.792	6.4944
Nb_2O_5	0.99721	2.6027	6.1079	11.1239
Nd_2O_3	0.99721	2.6027	6.1079	11.1239
NiO	0.99187	3.9299	4.7875	6.3835
NpO_2	0.99721	2.6027	6.1079	11.1239
P_2O_5	0.99169	2.9601	4.9154	6.7822
Pa_2O_5	0.99721	2.6027	6.1079	11.1239

Oxide	Retention Factor	ln(DF) Minimum	ln(DF) Most Likely	ln(DF) Maximum
PbO	0.98796	3.2426	4.382	6.2971
PdO	0.99721	2.6027	6.1079	11.1239
Pr_2O_3	0.99721	2.6027	6.1079	11.1239
PuO_2	0.99721	2.6027	6.1079	11.1239
RaO	0.77121	0.0643	1.4803	5.591
Rb_2O	0.97803	1.8563	4.1638	6.9256
Rh_2O_3	0.99721	2.6027	6.1079	11.1239
RuO_2	0.97803	1.8563	4.1638	6.9256
SO_3	0.84032	0.3219	1.8469	3.2089
Sb_2O_3	0.77121	3.9532	4.9125	5.591
SeO_2	0.77121	0.1205	0.4547	1.2187
SiO_2	0.99926	4.6597	7.3324	9.7527
Sm_2O_3	0.99721	2.6027	6.1079	11.1239
SnO_2	0.99721	2.6027	6.1079	11.1239
SrO	0.99721	3.7773	4.7158	5.6595
Ta_2O_5	0.99721	2.6027	6.1079	11.1239
Tc_2O_7	0.43049	0.0953	0.47	1.6094
TeO_2	0.77121	0.0643	1.4803	5.591
ThO_2	0.99721	2.6027	6.1079	11.1239
TiO_2	0.99752	2.6027	6.0313	8.074
Tl_2O	0.77121	0.0643	1.4803	5.591
UO_3	0.99721	2.6027	6.1079	11.1239
V_2O_5	0.97803	1.8563	4.1638	6.9256
WO_3	0.99721	2.6027	6.1079	11.1239
Y_2O_3	0.99721	2.6027	6.1079	11.1239
ZnO	0.99773	4.0656	5.9819	7.8709
ZrO_2	0.99982	4.2121	8.6115	11.1239

Pacific Northwest National Laboratory

902 Battelle Boulevard
P.O. Box 999
Richland, WA 99354

1-888-375-PNNL (7665)

www.pnnl.gov